GEOLOGICAL SURVEY OF DENMARK AND GREENLAND BULLETIN 38 • 2017

Review of Survey activities 2016

Edited by
Adam A. Garde and Ole Bennike

GEOLOGICAL SURVEY OF DENMARK AND GREENLAND
DANISH MINISTRY OF ENERGY, UTILITIES AND CLIMATE

Geological Survey of Denmark and Greenland Bulletin 38

Keywords
Geological Survey of Denmark and Greenland, survey organisations, current research, Denmark, Greenland.

Cover photographs from left to right

1. The traditional spear auger remains a principal tool in mapping Danish quaternary deposits, but can now be combined with short-range electromagnetic methods for specific purposes such as 3D delineation of contaminated landfill sites. Photograph: Jakob Lautrup
2. Elevation map around the stream of Hagens Møllebæk in north-west Jylland with the positions of measuring stations to determine the nitrate runoff from agricultural fields at different times of the year.
3. The monitoring of the surface conditions of the Greenland ice sheet by GEUS is an important tool fo understanding global climate change. Photograph: Baptiste Vandecrux.
4. Rescuing primary seismic data from the North Sea obtained by private exploration companies to a national electronic database at GEUS. Photograph: Peter Warna-Moors.

Frontispiece: facing page

Surface of Qagssimiut ice lobe ablation area, southern Greenland ice sheet, after a period of extended clear sky conditions that enabled a strong dark ice algal bloom registered in satellite imagery presented in Box *et al.* (2017, this volume). Aerial oblique photo near 61°11.006′N, 46°42.333′W, 820 m elevation. Photo: Jason E. Box, 23 August 2014.

Chief editor of this series: Adam A. Garde
Editorial board of this series: John A. Korstgård, Department of Geoscience, Aarhus University; Minik Rosing, Geological Museum, University of Copenhagen; Finn Surlyk, Department of Geosciences and Natural Resource Management, University of Copenhagen
Scientific editors: Adam A. Garde and Ole Bennike
Editorial secretary: Jane Holst
Referees (numbers refer to first page of reviewed article): Nicolaj K. Larsen & Lars Nielsen, DK (9); Anonymous & Ole Silkjær, DK (13); Peter K. Engesgaard & Bo V. Iversen, DK (17); John Korstgård & Lars Nielsen, DK (21); Thomas Balstrøm & Nicolaj K. Larsen, DK (25), Niels Balling & Reinhard Kirsch, DK (29); Anonymous & Allan Mahler, DK (33); Mikael Erlström, SE & Maciej I. Kotarba, PL (37); Jakob Keiding, NO & Vesa Nykänen, FI (41); Christopher Harrison, CA & Martin Sønderholm, DK (45); Michael K. Engkilde & Ida L. Fabricius, DK (49); Xavier Fettwis, BE & Teruo Aoki, JP (53); James H. Lever, US & Christopher J. Ries, DK (57); Anonymous & Jacob C. Yde, NO (61); Asger K. Pedersen, DK & Daniel Sopher, SE (65); Christian Holmegaard, DK & Martin L. Nayembil, UK (69); Jens Havskov, NO & Christopher J. Ries, DK (73).
Illustrations: Benny M. Schark, Allan Lindy, Stefan Sølberg and Susanne Rømer
Layout and graphic production: Jane Holst and Carsten E. Thuesen
Printer: Rosendahls-Schultz Grafisk A/S, Albertslund, Denmark
Manuscripts received: 12 January – 28 March 2017
Final versions approved: 15 March – 19 May 2017
Printed: 31 July 2017

ISSN (print) 1604-8156, ISBN (print) 978-87-7871-469-5
ISSN (online) 1904-4666, ISBN (online) 978-87-7871-470-1

Citation of the name of this series

It is recommended that the name of this series is cited in full, viz. *Geological Survey of Denmark and Greenland Bulletin*.
If abbreviation of this volume is necessary, the following form is suggested: *Geol. Surv. Den. Green. Bull.* 38, 76 pp.

Available from

Geological Survey of Denmark and Greenland (GEUS), Øster Voldgade 10, DK-1350 Copenhagen K, Denmark
Phone: +45 38 14 20 00, fax: +45 38 14 20 50, e-mail: *geus@geus.dk* and at *www.geus.dk/publications/bull*

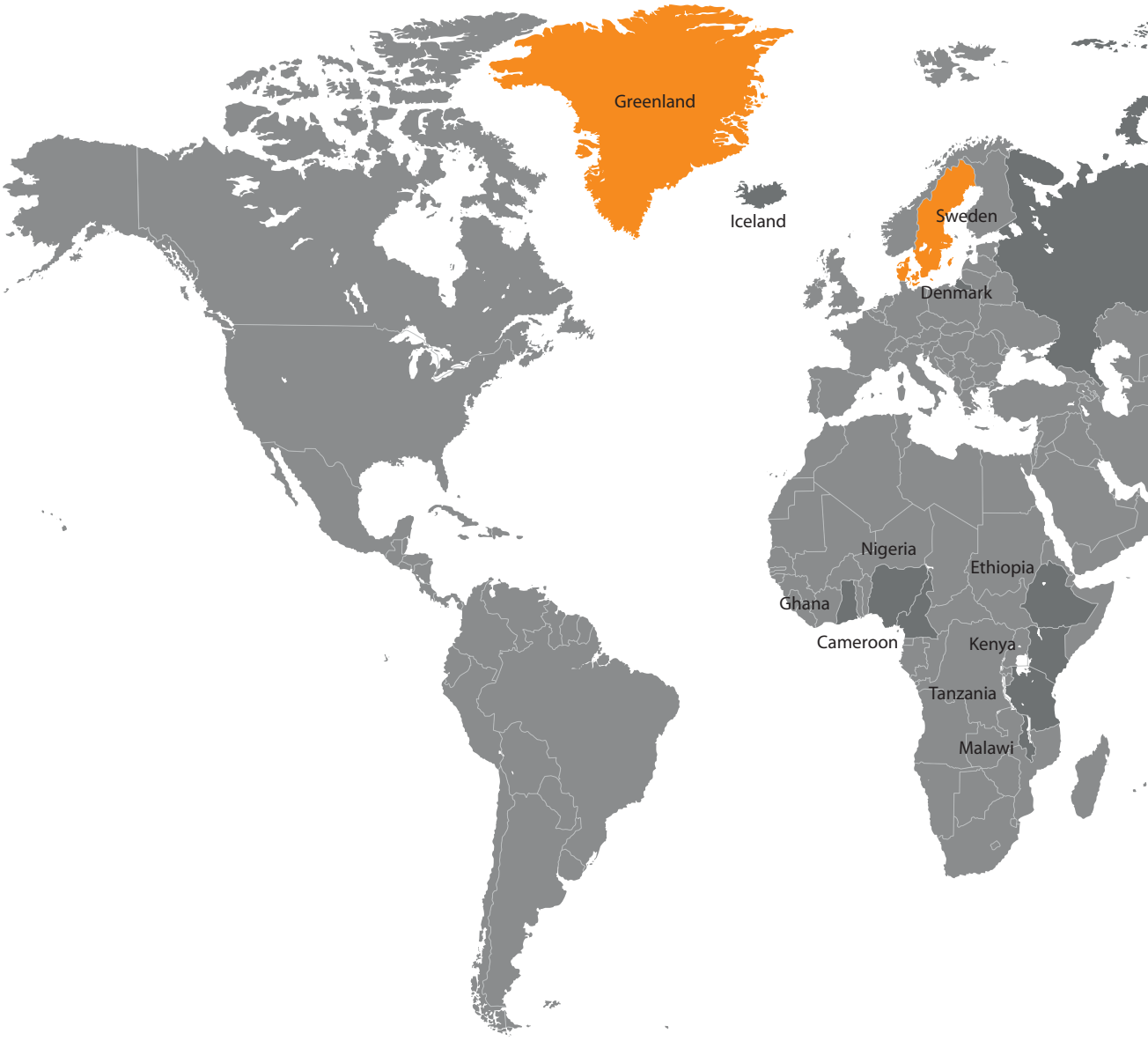

Dark grey indicates countries where GEUS has ongoing or recently completed projects.

Orange indicates countries with GEUS projects described in this volume.

Review of Survey activities 2016

Flemming G. Christiansen
Deputy Director

2016 was a year of transition in the international geological society. Like previous years, it was still a period with lots of reorganisation and cut-backs in the energy and mineral industry but also with obvious signs of an even more complex business pattern where well-organised geological data and easy access to geological knowledge will be strongly needed. Compared to the industry, and also to some of the authorities that are regulating the use of natural resources, GEUS has a high degree of continuity of both activities and personnel; in these years with strong focus on key strategic goals. This creates and develops a corporate memory that can be easily applied even with sudden shifts of a political or business agenda. This also establishes GEUS as the starting point for getting access to geological information from Denmark and Greenland, and makes GEUS a natural collaboration partner nationally as well as internationally.

Publication of results, both internationally and in our own series is a key factor for keeping a high scientific standard and for documentation of this towards society, authorities and industry. This issue of GEUS' Review of Survey activities shows like in previous years a broad spectrum with a total of 17 papers covering many different activities. The papers give a good overview in their own right but with systematic references to background reports and other papers, they also provide an easy way to dig deep into the important work that GEUS is carrying out. Eight papers are on Denmark, six on Greenland and three on other themes.

Activities in Denmark

GEUS works on many different – and often closely interrelated – topics in Denmark such as the use of water, energy, and mineral resources, protection of nature under significant climatic changes, and by making up-to-date geological and geophysical data and information easily available for all sorts of purposes.

The use of groundwater is very important for Denmark, and GEUS carries out many studies on water resources and their protection in connection with climate changes, environmental impact and domestic use. Systematic geological and geophysical studies provide not only specific water data, but also give a much better understanding of the geological models that can be used to predict resources and regulate their use. One paper with a case study from Samsø describes how traditional geological mapping can be optimised by using high-resolution electromagnetic induction data. Another paper gives an overview of buried valleys in Denmark, their geological architecture and very significant length, which has great implications for the groundwater resources in many parts of Denmark. A third paper gives a detailed description of nitrate transport pathways in one catchment area in northern Jylland where results from year-around monitoring can be used for planning and regulating to meet the demands of the EU Water Framework Directive.

In many areas in Denmark, chalk and limestone are directly exposed or found near terrain surface with only a thin cover of Quaternary deposits. Such deposits are important as a mineral resource for many different purposes and due to their groundwater resources and they may also control structures in overlying sediments. One paper documents the structures and stratigraphy of Danian limestone on eastern Sjælland, whereas another study uses GIS and digital terrain models to map karst sinkholes in areas of Jylland and to interpret the geological and climatic conditions and anthropogenic activities that influence their development.

Denmark has a large potential for subsurface geothermal energy and for heat and energy storage. Following the recent launching of the Geothermal WebGIS portal with all geological and geophysical data relevant for geothermal exploration, GEUS has continued with more detailed studies of specific areas and on specific parameters. One paper gives a summary of a EUDP-supported project on the planning of exploration in urban areas of Copenhagen by targeting on shallower reservoirs in the Gassum Formation and by using smaller drilling rigs. Another paper has focus on the porosity and permeability variation of the Bunter Sandstone Formation that is a potential geothermal reservoir in large onshore areas of southern Denmark.

Shale-gas production has been a major game changer in the energy sector for quite some years, and we have seen

many studies of the resource potential and some exploration in Europe, including Denmark and southern Sweden. One paper gives a detailed description of the gas composition and discuss biogenic versus thermogenic origin of gas in Lower Palaeozoic shales from scientific core holes in southern Sweden.

Activities in Greenland

Once again there was a high level of geological and glaciological activities in Greenland in 2016, both traditional studies with focus on the mineral and petroleum potential and exploration studies as well as monitoring and research related to climate changes and their effect.

GEUS has been active with regional mapping and research in South-East Greenland for quite some years, and some of the geo-datasets are important for identifying exploration targets. One paper argues for the possibility of orogenic gold deposits by using aeromagnetic and stream sediment geochemistry data in a minerals systems model. A large number of data and proxies maps have been applied to construct a final prospectivity map pointing towards the most interesting possibilities in the Tasiilaq area.

The Nuussuaq Basin in West Greenland has served as an analogue geological model for offshore petroleum exploration for decades but there may also be an onshore potential. As preparation for both off- and onshore licensing rounds, GEUS has compiled key data in a GIS model and re-studied especially the large-scale structures in more detail using photogrammetric mapping. One paper describes a very large inversion anticline on central Nuussuaq that could be an interesting drilling target. A revised migration pathway model is proposed; this could explain distribution of both oil and gas seeps outside the traditional area with common seepage. Another paper describes the reservoir properties of quite a number of sedimentary and volcanic successions of Aptian to Paleocene age in the Nuussuaq basin.

Monitoring programmes of the Greenland ice sheet and research based on local ground truth data from stations on the ice – and from fjords and nearby offshore areas – are very important contributions from GEUS to global climate models. One paper gives an example of albedo grids measured from satellite and checked with local data to give a much better de-noising and bias correlation. Another paper outlines a new climate monitoring and radar mapping programme in the Camp Century area in northern Greenland that will be managed by GEUS; some historical information and background models are also presented. A third paper describes the ice-sheet development along the central East Greenland margin in late Miocene to recent time where thick and different types of glacigenic deposits are interpreted using seismic data.

Other themes

As the national geological data center GEUS has a strong obligation to make all data available to authorities, educational and research institutes and to private enterprises. The ever accelerating changes in technology make this a great challenge in terms of competence, capacity and economic resources, both for collection and quality control of the actual data and for the database and distribution systems. The value for society is, however, very high and there is a strong focus on digitalisation strategy in Denmark these years.

One paper describes the tremendous effort that was made to rescue most of the seismic field data from exploration activities in the 1980s and 1990s in the Danish North Sea and how successfully this worked in collaboration with the operators. Another paper introduces Jupiter, the integrated public database for geology, groundwater and drinking water in Denmark, and describes the data systems, agreements and management behind it.

Finally, the last paper presents the early history of earthquake monitoring in Denmark and Greenland, and discusses how this was as geopolitically important more than a century ago as it is today.

Optimising geological mapping of glacial deposits using high-resolution electromagnetic induction data

Knud Erik S. Klint, Ingelise Møller, Pradip K. Maurya, and Anders V. Christiansen

There is a growing demand in modern society for detailed, localised geological maps and 3D models in connection with e.g. planning of major construction works, study of subsurface drainage systems, infiltration of storm water or risk assessment of contaminated waste dumps and pollution plumes. This demand is difficult to meet in Denmark as the surficial glacial deposits that cover most of the country are notoriously very heterogeneous. Standard geological maps are based on regional data collection, and their resolution is far from sufficient to identify structural elements on the 10–20 m scale needed in the above-mentioned applications.

Geophysical mapping for geological characterisation of the upper *c.* 5 m of the subsurface can be carried out using for instance direct-current geoelectrical methods (e.g. Loke *et al.* 2013), induced polarisation (e.g. Revil *et al.* 2012) set up with 1–2 m electrode spacing, electromagnetic induction (EMI; e.g. Christiansen *et al.* 2016; Doolittle & Brevik 2014), ground penetrating radar (GPR; e.g. Neal 2004) or seismic refraction tomography using a multicomponent landstreamer (e.g. Brodic *et al.* 2015). The resulting geophysical maps show the distribution of the measured parameter, for instance electric resistivity or seismic velocity. To construct *geological* maps using geophysical methods, the data must be verified and calibrated with geological field observations. GPR imaging of geological structures require laborious interpretation before a geological map can be constructed, and the method is limited to low-loss materials such as sandy sediments (Neal 2004).

A new approach, using a combination of shallow, high-resolution EMI surveying and traditional spear-auger soil sampling along the same transects, was tested in an area of *c.* 2 km^2 around the contaminated, former landfill site at Pillemark on Samsø (Fig. 1). The resistivity recorded using the EMI method is strongly related to the clay content, and this parameter is therefore well suited for geological mapping. The EMI method is also robust, data acquisition is 5–50 times faster than with other geophysical methods and the processing and inversion scheme is well defined (Christiansen *et al.* 2016).

Methodology

Spear-auger mapping

In the past almost 130 years, the geological mapping of the surficial cover of Denmark has largely been based on simple collection of pristine samples of the local sediment below the mull horizon using a specially designed sampling device, the so-called *spear auger*. This is a 1 m long steel rod with a diameter of 12 mm, a handle bar, and a 15–25 cm long, single or double slit at its tip. When the spear is pushed into the ground and turned, the slit captures a small soil sample (Fig. 2). The mapping geologist interprets the nature and origin of the sample and adds a soil-type symbol to a field map currently using the terminology described by Jakobsen *et al.* (2011). To map the boundaries between different soil types, samples are collected with a distance of 100–200 m depending on the local geological complexity. The symbols are then transferred to a master

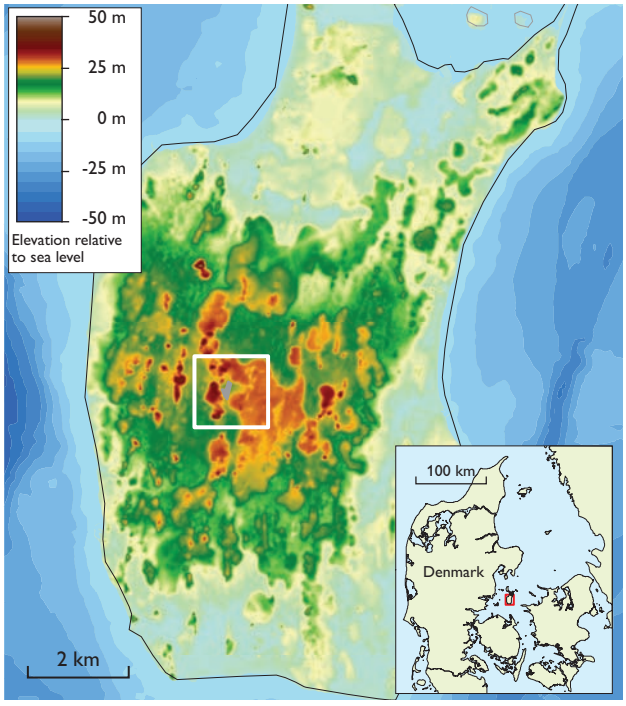

Fig. 1. The location of the study area on the island of Samsø is shown on the digital terrain model.

Fig. 2. Traditional geological mapping using the spear auger.

Fig. 3. The EMI survey system towed behind a vehicle. The *c.* 4 m long sensor is located inside a white tube on two sleds. The GPS sensor is mounted in the front of the tube above the transmitter coil. A data logger and a computer controlling the data acquisition are placed on the vehicle.

map sheet on a scale of 1:25 000; the resolution of the resulting geological map is about ±100 m.

Geophysical mapping by electromagnetic induction

EMI methods are commonly used for soil mapping (e.g. Doolittle & Brevik 2014). During the last decade the development of multi-coil sensors, integration with GPS and use of inversion algorithms for data interpretation (e.g. Christiansen *et al.* 2016; Doolittle & Brevik 2014), have made EMI a very fast technique for mapping the resistivity of the upper 4–8 m of the subsurface (Fig. 3). The multi-coil DUALEM-421S sensor used in our study transmits an electromagnetic wave at 9 KHz from a horizontal coil and samples the total signal in horizontal and vertical receiver coils 1, 2 and 4 m from the transmitter coil. A signal is received 10 × per second, making the equipment suitable for towing behind a motorised vehicle (Fig. 3).

Acquisition of field data in the study area

The EMI survey of the study area comprised *c.* 85 line-km mainly by towing; in difficult terrain and vegetation the sensor was carried manually. The EMI data were (1) averaged using a running mean filter of 2 m, (2) outliers manually culled and (3) inverted using a full-solution 1D algorithm (Auken *et al.* 2015), where the models are linked by 3D constraints to obtain a pseudo-3D resistivity model (Viezzoli *et al.* 2008). The resistivity models were discretised in 10 layers covering the upper 10 m of the subsurface; the mean depth of investigation was *c.* 6 m (Christiansen & Auken 2012). The interval resistivity at 1–2 m below surface was calculated (Fig. 4) and used together with the spear-auger mapping.

The EMI survey was conducted prior to the spear-auger mapping, and the selection of soil sampling points was adjusted to the interval resistivity map so that areas with highly variable resistivity were mapped at a resolution of 10–20 m between the sampling points and areas with more homogeneous resistivity were mapped at a lower resolution. In Fig. 4 soil symbols and transitions of polygons with similar soil types based primarily on the spear-auger mapping are shown as an overlay on the geophysical mapping. The final interpretation of the soil type distribution is shown in Fig. 5, where it is seen that the soil type boundaries could be drawn with much higher accuracy than with traditional spear-auger mapping.

Results

The Pillemark study area (Fig. 1) has a hummocky topography. The geological map (Fig. 5) shows that a large variety of soil types is present. Clayey deposits such as clay till partly overlying meltwater clay dominates the hills, whereas sandier deposits such as sandy tills, meltwater sand/gravel occur along the fringes of the hills and on the highest hilltops. Extramarginal sand predominates in the low-lying areas, in the lowermost areas and in local depressions partly covered with postglacial sediments such as freshwater sand, clay and peat.

Based on the combined mapping techniques, the depositional history of the soil types could be outlined. The hills are interpreted to consist of mainly layered lacustrine deposits, which were overridden by a glacier that deposited tills and potentially deformed the lake sediments before

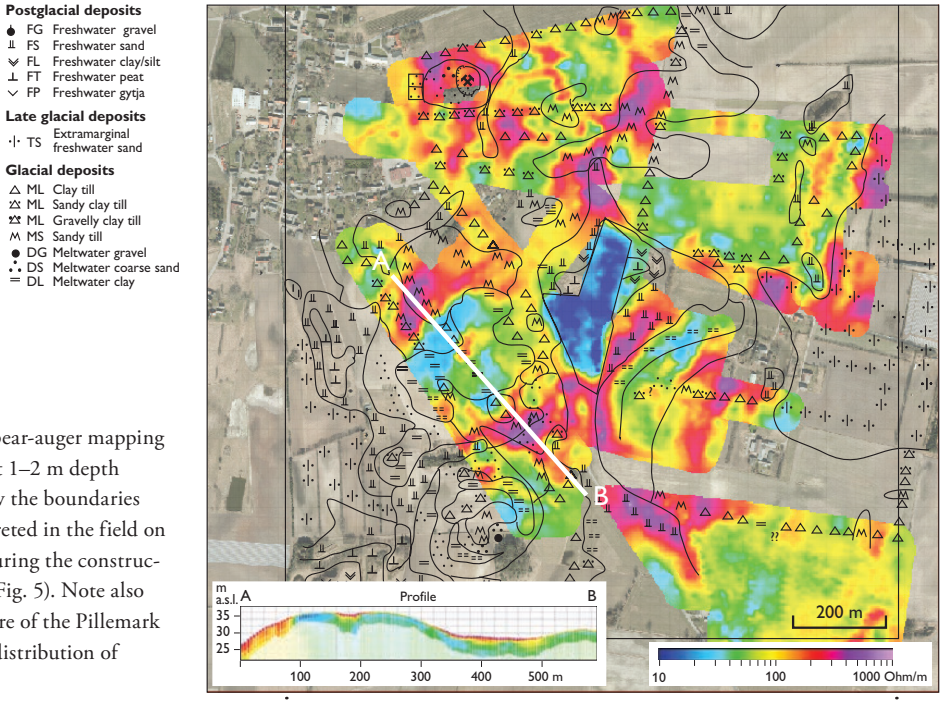

Fig. 4. Raw data from the spear-auger mapping and the interval resistivity at 1–2 m depth in the survey area. Note how the boundaries between soil types as interpreted in the field on this figure were modified during the construction of the geological map (Fig. 5). Note also the strong dark blue signature of the Pillemark landfill site, indicating the distribution of contaminated soil.

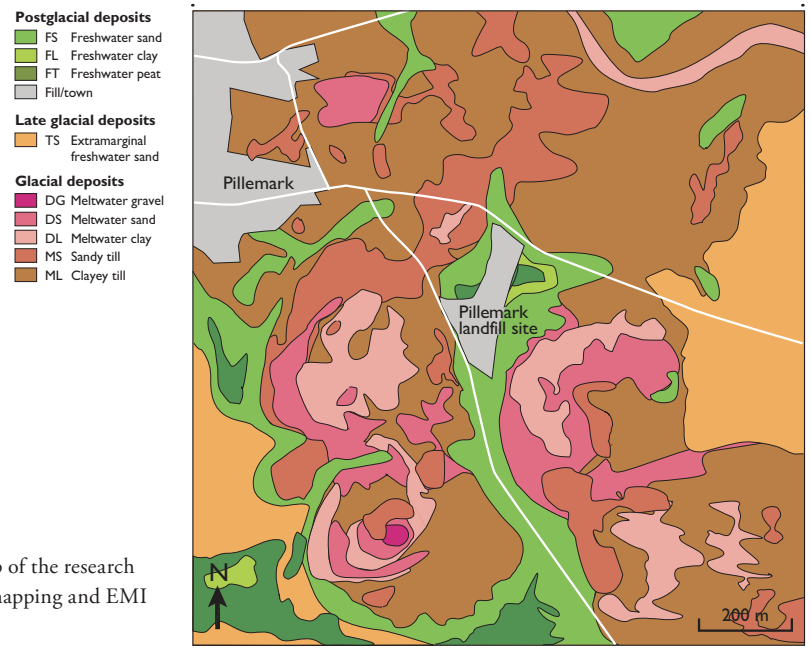

Fig. 5. High-resolution geological map of the research area based on combined spear-auger mapping and EMI surveying.

stagnating and melting. Lakes in local depressions were then slowly filled with postglacial freshwater sand, silt/clay and organic matter, slowly transforming into peat bogs. The landfill site was covered with anthropogenic soil and fill material; the outline of the contaminated soil is clearly apparent in Fig. 4.

Summary and perspectives

Compared to traditional spear-auger mapping, the combined EMI and spear-auger mapping makes it possible to produce high-resolution geological maps in highly heterogeneous glacial landscapes. It efficiently outlined the contaminated area at the landfill site. The method is considered solid and very cost-effective, since the total mapping of the area was carried out in three days plus another three days' work for processing the geophysical data and correlation with the spear-auger mapping.

Unfortunately, local disturbance from buried pipes, electrical wires etc. influences the quality of the geophysical data within a distance of 10–15 m from the instrument, making the technique less applicable in densely urbanised areas. Moreover, without using a GPS, the precision of spear-auger mapping is low on a 10-metre scale. A dedicated mapping exercise coordinating GPS positioning of all sampling points with geophysical measurements would increase the overall resolution. Finally, spear-auger mapping requires a well-trained geologist for interpreting the very small soil samples correctly.

The combined EMI and spear-auger mapping also has great potential for site characterisation, from general surveys on a scale of *c.* 10 km to local studies on a scale of *c.* 100 m. The methodology can easily be adapted to, or combined with, more dedicated soil sampling e.g. for detection of contaminated soil. There is also an obvious potential in other situations where high-resolution geological maps are needed, for example for identification of efficient infiltration areas in connection with establishment of suburban drainage systems (Bockhorn *et al.* 2015).

Acknowledgements

This study was supported by the research project GEOCON – advancing Geological, geophysical and Contaminant monitoring technologies for contaminated site investigation (contract 1305-00004B). Funding for this is provided by The Danish Council for Strategic Research under the Programme commission on sustainable energy and environment.

References

Auken, E. *et al.* 2015: An overview of a highly versatile forward and stable inverse algorithm for airborne, ground-based and borehole electromagnetic and electric data. Exploration Geophysics **46**, 223–235, *http://dx.doi.org/10.1071/EG13097*

Bockhorn, B., Klint, K.E.S., Jensen, M.B. & Møller, I. 2015: Use of geological mapping tools to improve the hydraulic performance of SuDS. Water Science and Technology **71**, 1492–1499, *http://dx.doi.org/10.2166/wst.2015.125*

Brodic, B., Malehmir, A., Juhlin, C., Dynesius, L., Bastani, M. & Palm, H. 2015: Multicomponent broadband digital-based seismic landstreamer for near-surface applications. Journal of Applied Geophysics **123**, 227–241, *http://dx.doi.org/10.1016/j.jappgeo.2015.10.009*

Christiansen, A.V., Pedersen, J.B., Auken, E., Søe, N.E., Holst, M.H. & Kristiansen, S.M. 2016: Improved geoarchaeological mapping with electromagnetic induction instruments from dedicated processing and inversion. Remote Sensing **8**, 1022, *http://dx.doi.org/10.3390/rs8121022*

Christiansen, A.V. & Auken, E. 2012: A global measure for depth of investigation. Geophysics **77**, WB171–177, *http://dx.doi.org/10.1190/geo2011-0393.1*

Doolittle, J.A. & Brevik, E.C. 2014: The use of electromagnetic induction techniques in soils studies. Geoderma **223–225**, 33–45, *http://dx.doi.org/10.1016/j.geoderma.2014.01.027*

Jakobsen, P.R., Hermansen, B. & Tougaard, L. 2011: Danmarks digitale jordartskort 1:25 000 Version 3.1. Danmarks og Grønlands Geologiske Undersøgelse Rapport **2011/40**. Copenhagen: Geological Survey of Denmark and Greenland.

Loke, M.H., Chambers, J.E., Rucker, D.F., Kuras, O. & Wilkinson, P.B. 2013: Recent developments in the direct-current geoelectrical imaging method. Journal of Applied Geophysics **95**, 135–156, *http://dx.doi.org/10.1016/j.jappgeo.2013.02.017*

Neal, A. 2004: Ground-penetrating radar and its use in sedimentology: Principles, problems and progress. Earth-Science Reiew **66**, 261–330, *http://dx.doi.org/10.1016/j.earscirev.2004.01.004*

Revil, A., Karaoulis, M., Johnson, T. & Kemna, A. 2012: Review: Some low-frequency electrical methods for subsurface characterization and monitoring in hydrogeology. Hydrogeology Journal **20**, 617–658, *http://dx.doi.org/10.1007/s10040-011-0819-x*

Viezzoli, A., Christiansen, A.V., Auken, E. & Sørensen, K. 2008: Quasi-3D modeling of airborne TEM data by spatially constrained inversion. Geophysics **73**, F105–113, *http://dx.doi.org/10.1190/1.2895521*

Authors' addresses

K.E.S.K., *GEO, Maglebjergvej 1, DK-2800 Kgs. Lyngby, Denmark;* E-mail *kek@geo.dk*.

I.M., *Geological Survey of Denmark and Greenland (GEUS), Øster Voldgade 10, DK-1350 Copenhagen K, Denmark*

P.K.M & A.V.C., *Hydrogeophysics Group, Department of Geoscience, Aarhus University, C.F. Møllers Allé 4, DK-8000 Aarhus C, Denmark.*

Buried tunnel valleys in Denmark and their impact on the geological architecture of the subsurface

Peter B.E. Sandersen and Flemming Jørgensen

Buried valleys are elongate erosional structures in the Danish subsurface now partly or completely filled and covered with younger sediments. The majority was formed by meltwater underneath ice sheets. The number of buried-valley structures in Denmark is large, and because the valley-infill in many areas hosts significant groundwater resources, knowledge of them and their formation is important. This was the starting point of the buried-valley mapping project, which was initiated in the late 1990s and continued until the end of 2015 (Sandersen & Jørgensen 2016). This project became part of the National Groundwater Mapping Programme which was set up with the purpose of mapping the groundwater resources within areas of specific groundwater interest (Thomsen *et al.* 2004). The areas of specific groundwater interest encompass existing catchment areas and cover around 40% of the country. Within these areas, high-density electromagnetic surveys have typically been performed together with exploration drilling and supplementary geophysical measurements. The mapping of the buried valleys has been based on these newly collected data as well as existing data in the national databases. In some instances, it has also been possible to map buried valleys in less data-dense areas outside the surveyed areas, mainly on the basis of borehole data.

The groundwater resource and its vulnerability have been important in the mapping of the buried valleys. The valleys also constitute an important part of the subsurface geological architecture, and it is obvious that a thorough knowledge of them is critical for the general understand-

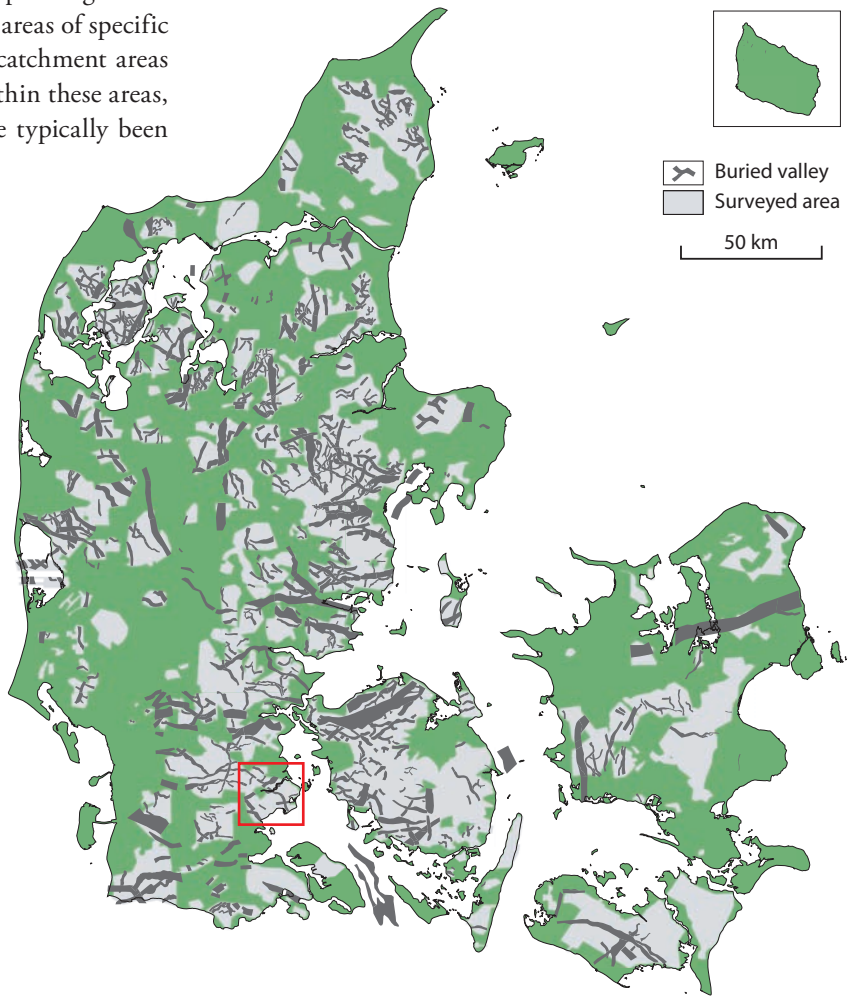

Fig. 1. Mapped buried valleys in Denmark as of end 2015. The mapped valleys are shown as dark grey polygons and the TEM-surveyed areas are shown in light grey. The Haderslev area covered by Fig. 2 is highlighted with a red rectangle.

ing of the geology of the uppermost 100–400 m of the Danish subsurface. In this paper we present an overview of the buried-valley mapping project and an updated buried-valley map (Fig. 1).

Mapping of the buried-valley structures

All relevant geophysical and lithological data from primarily onshore areas have been used to map and describe the buried valleys. The transient electromagnetic method (TEM; Sørensen & Auken 2004) has proven especially valuable because such surveys usually provide a spatially dense data grid that can be combined with borehole data and other geophysical data (Jørgensen & Sandersen 2009). The valleys have been delineated from an integrated interpretation of the data, and their outlines and extensions within the mapped areas were drawn as polygons using simple signatures (Fig. 2). In order to obtain a high degree of certainty and objectivity in the delineation of the valleys, the lateral extent and orientation of the valleys were to be unambiguously expressed in the data. Therefore, no interpolations outside and between the local mapped areas have been made, and accordingly the map in Fig. 1 represents the minimum occurrence of buried valleys in Denmark rather than their true distribution and density. The advantage of this approach is an un-biased picture of the valleys based on the data available and not on secondary data and assumptions. In addition to this, the approach gives an opportunity to get a valuable insight into the formation history and age of the valleys.

The highest valley densities are found in areas where TEM data have been collected and the conditions for the chosen methods were ideal. The map in Fig. 1 only shows the location of the valley structures where they can be outlined by interpretation of the data. The grey areas indicate the areas where TEM data are available and many additional buried valleys must be expected outside these areas.

Although many buried valleys have been mapped, even more are expected to exist, because not all valleys can be identified with the used methods. For instance, very narrow valleys or channels can be difficult to resolve, and valleys with low lithological and/or electrical resistivity contrast compared to the surroundings can be difficult to outline.

Occurrence and subsurface architecture

The depth of the mapped buried valleys is variable, with the deepest structures sometimes exceeding 400 m. Their width is generally between 0.5 and 1.5 km, but widths of more than 3.5 km occur. Their lengths are difficult to assess because many of the surveyed areas are small, but some exceed 25–30 km. They commonly terminate abruptly and are highly irregular, with depressions and thresholds along the valley floors. Buried valleys appear both as single valleys and in dense cross-cutting networks. Their internal structure is typically complex due to repeated erosional and depositional events.

The majority of the buried valleys were formed during the Pleistocene as tunnel valleys eroded by high-pressure meltwater underneath the ice sheets (Jørgensen & Sandersen 2006). With respect to morphology and dimensions,

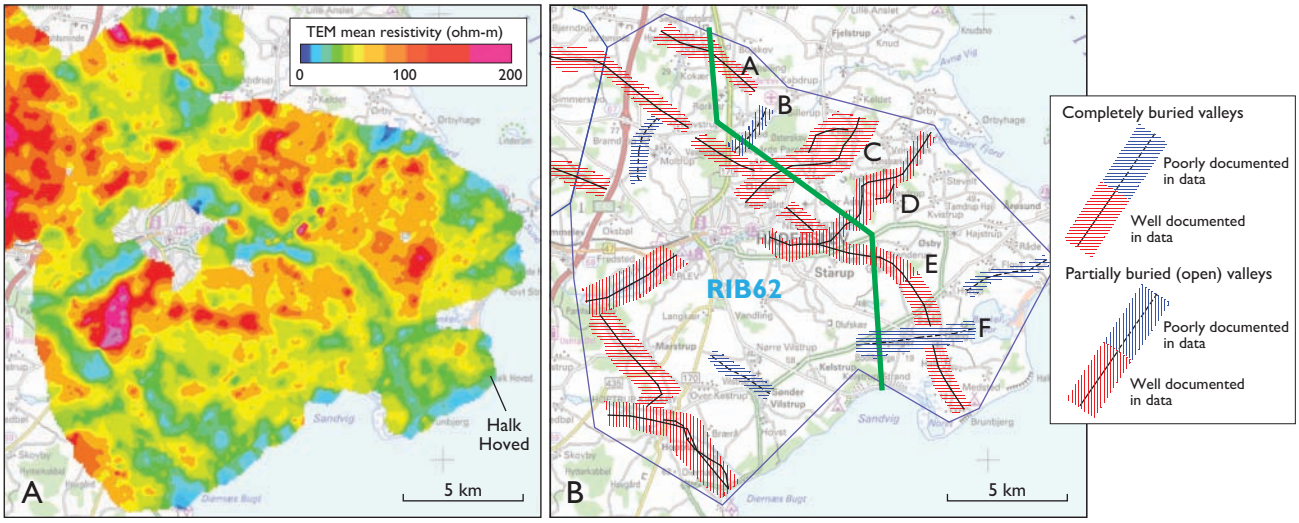

Fig. 2. Survey area RIB62 Haderslev, south-western Denmark (outlined by blue polygon). **A:** Airborne TEM resistivity data (30–35 m b.s.l.). **B**: Same map window without TEM data but with interpreted buried valleys shown as hatched polygons. Green line shows location of cross-section in Fig. 3. Tunnel valleys marked A to F corresponds to valleys shown in Fig. 3.

the mapped buried valleys are comparable with open tunnel valleys found in the present-day Danish landscape. The water seemed to flow in relatively small channels on the floors of the tunnel valleys, which gradually became ice-filled. Tunnel valleys were often re-used during repeated cycles of glaciations, producing separate valley generations and multiple internal cut-and-fill structures. The ages of individual valleys are usually difficult to assess because of the repeated erosion and the general lack of precise age determinations, but it is assumed that tunnel-valley formation has been a common phenomenon throughout the Quaternary. Relative dating of the individual generations can commonly be performed, based on the lithology of the infill and on cross-cutting relationships in the subsurface. In rare cases mapped valley generations can be related to specific ice advances (i.e. Sandersen *et al*. 2009).

Even when taking the irregular distribution of the survey areas into consideration, the mapped valleys show signs of a preferred geographical distribution (Fig. 1). For instance, the highest densities of buried tunnel valleys are typically found in areas where thick successions of Palaeogene clays occur close to the surface, and the lowest densities typically where coarse-grained sediments dominate the near-surface part of the succession. The tunnel-valley formation is thus more likely to occur in areas with impermeable substrata because the high subglacial water pressures favour channelised erosion and tunnel-valley formation. However, in areas where the permeable sediments underneath the glacier were able to drain parts of the meltwater, no or only few valleys were formed. Apparently, an important factor is whether drainage through the substrata can be sufficient to prevent tunnel-valley formation (Sandersen & Jørgensen 2012).

A map of the Pre-Quaternary surface in Denmark by Binzer & Stockmarr (1994) reveals a deep valley-network eroded into the Pre-Quaternary surface. This map was primarily based on on-shore borehole data. The interpolation of the Pre-Quaternary surface was highly interpretative and performed throughout the Danish area under the presumption that the structures were sub-aerially eroded valleys and would therefore not contain isolated depressions and blind endings. It is tempting to compare the map by Binzer & Stockmarr with the map in Fig. 1, because some of the valley structures coincide. However, the buried-valley map in Fig. 1 is made differently and is not a map of the Pre-Quaternary surface. The map shows the occurrence of buried-valley structures regardless of whether they penetrate the Pre-Quaternary surface or not and hence the map is not limited to showing valleys in the Pre-Quaternary surface, and isolated depressions and blind endings have not been avoided when making the map.

A total length of 5600 km of buried valleys has been found within the TEM-mapped areas in Denmark (*c.* 17 000 km^2) and in selected adjoining areas (*c.* 1700 km^2); in total *c.* 18 700 km^2. If the average width of the valleys is 1 km (see Jørgensen & Sandersen 2006) the valleys cover 5600 km^2.

This means that in *c.* 30 % of the mapped area, erosion of the valleys has significantly changed the lithology and architecture of the subsurface. An example where mapped buried tunnel valleys dominate *c.* one third of the area is illustrated in Fig. 2. The TEM data show that tunnel valleys in this case have been eroded through the Quaternary and Miocene deposits and in some instances deeply into the underlying Palaeogene clays (Fig. 3).

The cross-section in Fig. 3 illustrates the influence the buried tunnel valleys have on the subsurface architecture. The Pre-Quaternary succession of Miocene sands and clays have been removed and replaced with sandy and clayey infill of Quaternary age. Figure 2A shows a horizontal slice (30–35 m b.s.l.) approximately through the central part of the Miocene succession. The red to orange colours show high resistivities corresponding to predominantly sandy sediments. The buried tunnel valleys are seen as both green elongate structures where the green colours represent predominantly clayey sediments and red elongate structures consisting of predominantly sand. As seen on the cross-sec-

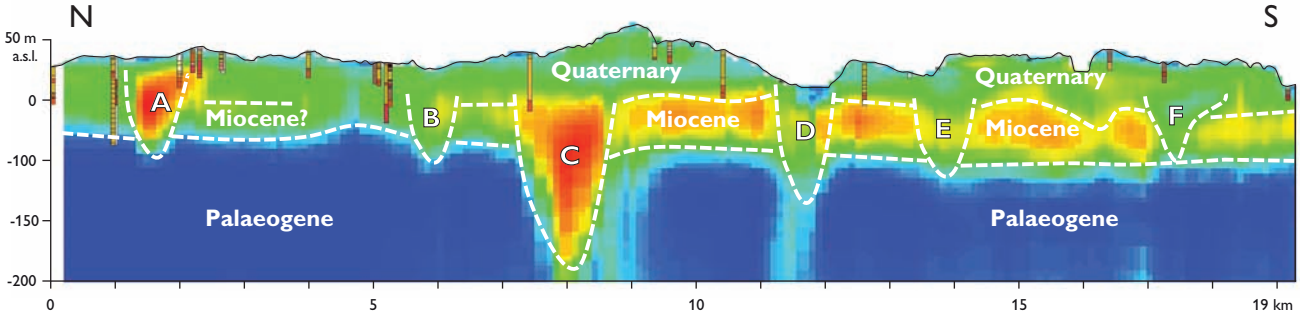

Fig. 3. Cross-section of tunnel valleys A to F in survey area RIB62 Haderslev based on 3D-gridded airborne TEM resistivity data. Vertical exaggeration 15 times. Vertical rods are boreholes included in the national Jupiter database. See Fig. 2 for resistivity legend and location.

tion (Fig. 3) valley erosions reach down to the Palaeogene clays, seen as very low resistivities in the TEM data (blue colours).

The valleys show dominant orientations of NE–SW and SE–NW, respectively (Fig. 2B). The valley infill is of Quaternary age, but the precise age of the valleys is not known. However, relative ages of the individual valley generations can be inferred from cross-cutting relationships, the terrain and the character of the overlying sediments. The buried tunnel valley D in Fig. 2B, for example, is partially buried and is expected to extend all the way to the terrain surface because it coincides with an open tunnel valley in the present-day terrain (Smed 1982). The valley obviously belongs to a young generation. The deep valley C, however, is completely buried by predominantly clay tills and apparently not reaching the surface. This valley is therefore most likely older than the adjacent valley D to the south-east. The valley E and its extension to the north-west appear to be cut by the valleys C, D and F, thus suggesting an older generation. The southern part of valley E is quite easily seen in the TEM-data from *c.* 30 to 100 m b.s.l., whereas the levels above the succession are dominated by low-resistivity clays apparently not belonging to the valley. At the nearby coastal cliff of Halk Hoved in the southeasternmost part of the area (Fig. 2), a large glaciotectonic complex formed by proglacial deformation of the NE-advance in Late Weichselian has been described by Madsen & Piotrowski (2012). This thrust-fault complex consists of stacked layers of tills and glaciofluvial sediments deposited during the Warthe glaciation in Late Saalian. According to Madsen & Piotrowski (2012), the decollement layer of the glaciotectonic complex is *c.* 20 m b.s.l. which is apparently above the level of the buried valley E farther to the south-west. The uppermost parts of the buried tunnel valley may have been deformed by the glaciotectonic event in Late Weichselian, but obviously the formation of the deep tunnel valley can be related to an earlier event.

Conclusions and perspectives

If the rough calculation above is extrapolated to cover all of the Danish onshore area, a plausible total length of buried valleys of around 13 000 km emerges. Despite the uncertainty of this calculation, the figure calls for attention when interpreting the subsurface geology of areas not at present covered by dense geophysical datasets. Mapping outside the areas with specific groundwater interests is at present sparse, but the general knowledge obtained from the mapping project can be used in areas not yet covered by dense datasets. Along with the continuously increasing knowledge of the occurrence and the origin of buried tunnel valleys in Denmark, the importance of their structures has become more and more evident. The importance for assessments of groundwater resources and their vulnerability is straightforward (i.e. Andersen *et al*. 2013; Sandersen & Jørgensen 2003), and the necessity of making the buried-valley structures play a significant role in the geological interpretations of Quaternary sedimentary sequences is unquestionable.

References

Andersen, T.R., Poulsen, S.E., Christensen, S. & Jørgensen, F. 2013: A synthetic study of geophysics-based modelling of groundwater flow in catchments with a buried valley. Hydrogeology Journal **21**, 491–503.

Binzer, K. & Stockmarr, J. 1994: Geologisk kort over Danmark. Prækvartæroverfladens højdeforhold. Danmarks Geologiske Undersøgelse Kortserie **44**, 10 pp.

Jørgensen, F. & Sandersen, P. 2006: Buried and open tunnel valleys in Denmark – erosion beneath multiple ice sheets. Quaternary Science Reviews **25**, 1339–1363.

Jørgensen, F. & Sandersen. P.B.E. 2009: Buried valley mapping in Denmark: evaluating mapping method constraints and the importance of data density. Zeitschrift der Deutschen Gesellschaft für Geowissenschaften **160**, 211–223.

Madsen, T.M. & Piotrowski, J.A. 2012: Genesis of the glaciotectonic thrust-fault complex at Halk Hoved, southern Denmark. Bulletin of the Geological Society of Denmark **60**, 61–80.

Sandersen, P. & Jørgensen, F. 2003: Buried Quaternary valleys in western Denmark – occurrence and inferred implications for groundwater resources and vulnerability. Journal of Applied Geophysics **53**, 229–249.

Sandersen, P.B.E., Jørgensen, F. Larsen, N.K., Westergaard, J.H. & Auken, E. 2009: Rapid tunnel-valley formation beneath the receding Late Weichselian ice sheet in Vendsyssel, Denmark. Boreas **38**, 834–851.

Sandersen, P.B.E. & Jørgensen, F. 2012: Substratum control on tunnel-valley formation in Denmark. In: Huuse, M. *et al.* (eds) 2012: Glaciogenic Reservoirs and Hydrocarbon Systems. Geological Society Special Publications (London) **368**, 145–157, *http://dx.doi.org/10.1144/SP368.12*

Sandersen, P.B.E. & Jørgensen, F. 2016: Kortlægning af begravede dale i Danmark. Opdatering 2010–2015. Vols 1, 106 pp. and 2, 626 pp. In Danish. Geological Survey of Denmark and Greenland, Special publication. Available from *www.buried-valleys.dk*

Smed, P. 1982: Landskabskort over Danmark, Blad 3, Sønderjylland, Fyn. Geografforlaget, Brenderup.

Sørensen, K.I. & Auken, E. 2004: SkyTEM. A new high-resolution helicopter transient electromagnetic system: Exploration Geophysics **35**, 194–202, *http://dx.doi.org/10.1071/EG04194*

Thomsen, R., Søndergaard, V.H. & Sørensen, K.I. 2004: Hydrogeological mapping as a basis for establishing site-specific groundwater protection zones in Denmark. Hydrogeology Journal **12**, 550–562.

Authors' address

Geological Survey of Denmark and Greenland, Øster Voldgade 10, DK-1350 Copenhagen K, Denmark. E-mail: *psa@geus.dk*

Nitrate transport pathways in riparian zones of the Hagens Møllebæk catchment, northern Denmark

Bertel Nilsson, Anker Lajer Højberg and Per Jensen

The Water Framework Directive (WFD) of the European Union prescribes "good ecological status" of all waters. In terms of nitrate this means, among other things, to avoid eutrophication and achieve a good ecological balance in surface water systems for the benefit of the groundwater dependent flora and fauna (Hinsby *et al.* 2012). In Denmark, the nitrate load to estuaries has been nearly halved since the first national action plan was implemented in the mid-1980s, but further abatements are required in many areas to fulfil the WFD. New approaches to regulate nitrate use are needed with measures targeted to the areas where most effect is obtained, and this is recognised at political level. Recent legislation allows farmers to increase nitrate application, but should at the same time introduce new mitigation measures and a more targeted approach to regulation. Therefore the physical system, i.e. the geological framework and topography, of the catchment has to be understood (Winter 1999). Previous studies have shown that in hydrological catchments with high geological variability, sampling of groundwater in riparian zones, the stream water itself and water in the stream bed can help to identify near-stream areas with specific nitrate problems. Detailed studies are, however, not feasible in all catchments, and development of representative typologies to guide an optimal location of mitigation measures in the catchment is thus needed. The present study is a detailed characterisation of nitrate transport and reduction in the groundwater–stream system in the river Hagens Møllebæk catchment for this purpose.

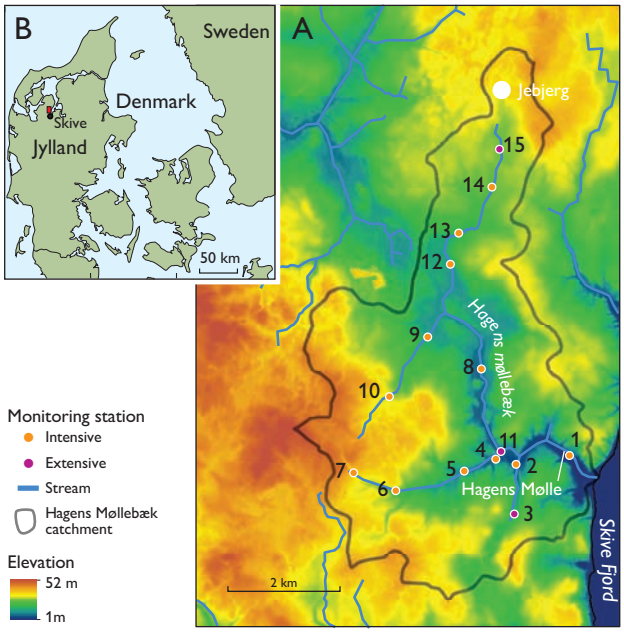

Fig. 1. **A**: Topographical map of the Hagens Møllebæk catchment with locations of nitrate-measuring stations of riparian zones, drain pipe outlets, stream and stream bed. **B**: Index map with position of study area.

Study area and hydrogeological setting

The Hagens Møllebæk catchment is located west of Skive and discharges into Skive Fjord (Fig. 1). The hydrological catchment covers 27.2 km^2. The area is relatively flat with elevations between 1–52 m above sea level (a.s.l.) and slopes near the streams. Quaternary clayey tills dominate in the west and south and glacial meltwater sand and gravel occur in the east. Holocene sand, clay and organic deposits overlie the Quaternary deposits in the stream-valley system and near the outlet of Hagens Møllebæk. In the southern part of the catchment, Oligocene clay with very low permeability is found underneath a few metres of clayey till . The primary land use is agriculture, which covers more than 80% of the area. The soil types are clay (50%), sand (47%) and organic sediments (3%).

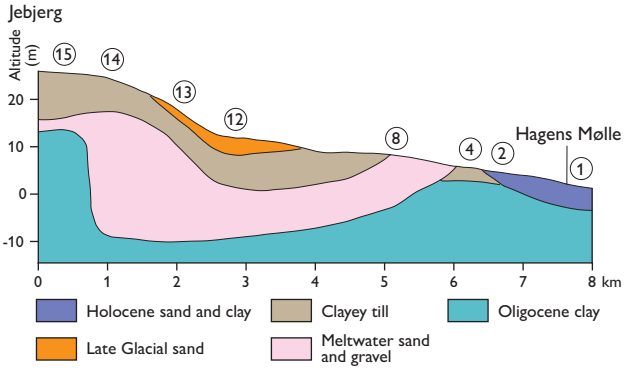

Fig. 2. Conceptual geological profile along Hagens Møllebæk with locations of numbered nitrate-measuring stations along the main stream channel.

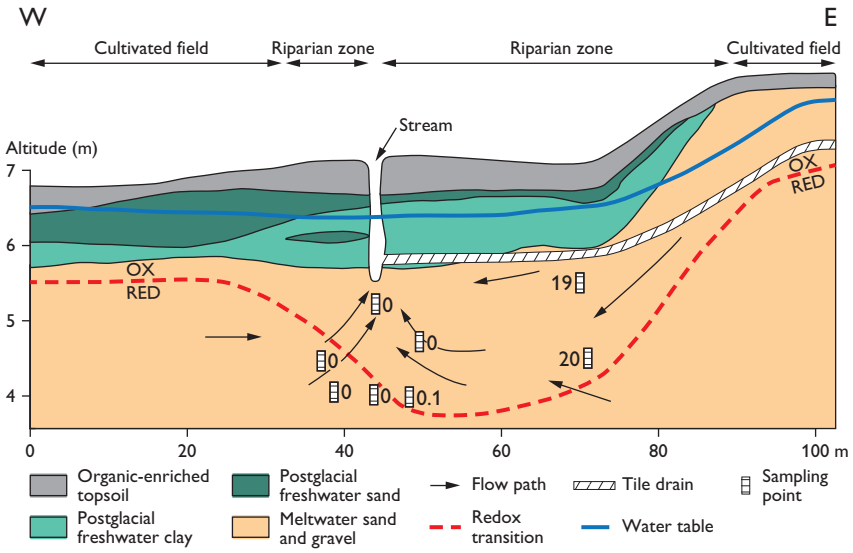

Fig. 3. Example of a cross section along Hagens Møllebæk (10 times vertical exaggeration). The profile represents a riparian hydrological type 6 of Fig. 4A. Nitrate concentrations in NO_3-N mg/l shown in groundwater, stream water and drain water. The water samples were collected in January 2017; the nitrate concentration in the submerged drain pipe outlet was about 15 mg/L, and 5–6 mg/L in the stream water.

Conceptual geological model

A conceptual geological model is presented in Fig. 2 by a profile along the main stream of Hagens Møllebæk from Jebjerg in the north (near station 15, Fig. 1A) to Hagens Mølle (station 1) near the stream outlet into Skive Fjord. The model is based on existing geological data from the Jupiter database and a Quaternary soil map on a scale of 1:200 000 (both found at www.geus.dk). From the conceptual model, a general understanding of the contact and interaction between the stream and the underlying aquifers is established on catchment scale. Between stations 4 and 5 the stream bed overlies poorly permeable clayey tills or Oligocene clay with little or no expected water exchange. Conversely, exchange of water and nitrate between the stream and the underlying aquifer is more likely where the stream bed is located directly on top of sandy aquifers.

Regional contact between aquifers and riparian zones

The local geological and hydrogeological conditions in the riparian zone of the Hagens Møllebæk catchment were characterised at 12 localities by means of geological cross-sections 10–100 m long, from the margin of the riparian zone adjacent to the cultivated field to the margin of the riparian zone on the opposite side of the stream channel (Fig. 3). In each cross-section 8–10 boreholes were hand drilled to depths of 2–4 m and the sediment described at 15 cm intervals. From this geological profiling of the riparian zones, the hydrogeological contact between the stream system and the underlying aquifer was conceptualised according to the typology of groundwater – surface water interaction (GSI; Dahl *et al.* 2007), see Fig. 4A. The hydrogeological settings adjacent to the riparian area aquifer were classified at the twelve cross-sections (Fig. 4B). Combining the regional conceptual model (Fig. 2) and the cross-sections, a preliminary delineation of local or regional sandy aquifers

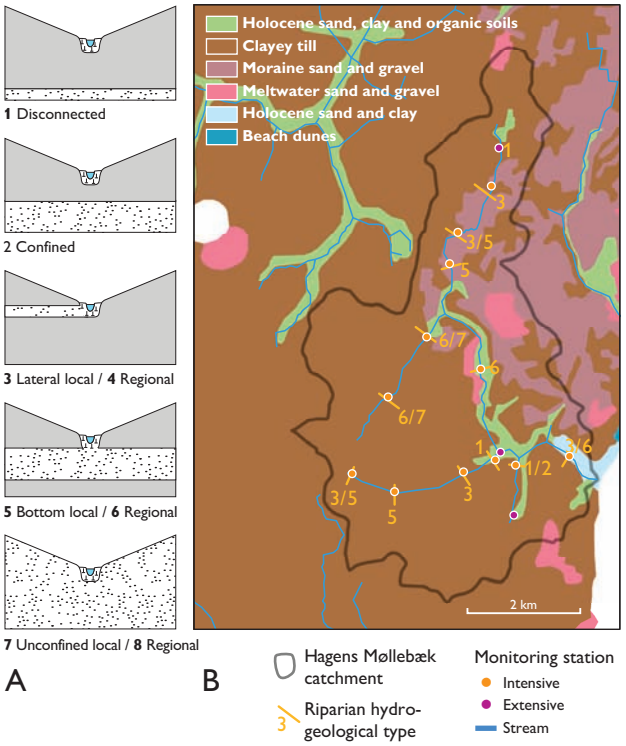

Fig. 4. Riparian zones along Hagens Møllebæk and its tributaries, divided into riparian hydrogeological types. **A**: Eight conceptual hydrogeological models of the riparian zone with different combinations of deposits with high (white-dotted) and low (grey) permeability (from Dahl *et al.* 2007). **B**: Classification of 12 cross-sections in the study area into types of riparian hydrogeological contacts (see also main text).

was obtained (Fig. 5). Further detailed field instigations are still needed at six of the locations to distinguish between local and regional aquifer characteristics. It is evident that stream reaches along the headwater of the stream system have contact to local shallow aquifers, and that the more central and down-gradient parts of the stream system have contact to a regional sand aquifer.

Observed exchange between stream water and groundwater

Stream discharges were measured on the same day in August 2016 at all stations using an OTT acoustic digital current meter (OTT Hydromet GmbH). The groundwater flux to the stream system, quantified as the so-called specific baseflow, was calculated as the change in flow (Q in L/sec) between an upstream and downstream location, divided by their distance along the stream. The specific baseflow for the summer day in August 2016 is shown in Fig. 5B. The first-order streams provide the lowest inflow rates of groundwater to the stream (0–5 L/sec/km) because of limited or no interaction between the stream system and groundwater aquifers. Higher-order (more down-gradient) stream reaches provide 5–25 L/sec/km. Along a shorter reach between stations 4 and 5 the tributary loses water through the stream bed to the underlying shallow aquifer.

At the twelve intensively monitored stations (Fig. 1A), 8–10 piezometers were installed along the cross-sections using metal or polyethylene (PEH) pipes with a screen length of 10 cm (metal) and 30 cm (PEH). The metal piezometers were pushed into the subsurface with a pneumatic hammer. The PEH pipes were manually pushed into the open boreholes for geological characterisation. All piezometers were levelled using the Trimble® R8 GPS system (vertical accuracy ±16 mm). Vertical changes in the hydraulic heads between the water table in the stream (i.e. the water stage) and the intakes of the piezometers about 0.5 m below the stream beds were measured with an accuracy of ±1 cm. Negative, vertical, hydraulic gradients indicate recharge to the groundwater aquifer, whereas positive gradients indicate discharge of groundwater into the stream. This made it possible to identify stream reaches where the exchange and direction between the stream and the aquifer can be assessed. The measurements carried out from August 2016 to January 2017 showed similar spatial distributions. This means that the vertical hydraulic gradients were positive along most stream reaches indicating groundwater discharge to the stream during the period August 2016 – January 2017.

Based on the detailed conceptual understanding of the local hydrogeological setting, the quantitative determination of baseflow and hydraulic gradients, the groundwater–stream interaction at the monitoring stations can be assessed. No or limited groundwater–stream interactions were found at stations 2–4, 6 and 15, while some or significant groundwater–stream interaction is expected to occur at stations 1 and 8–14 between the stream system and an

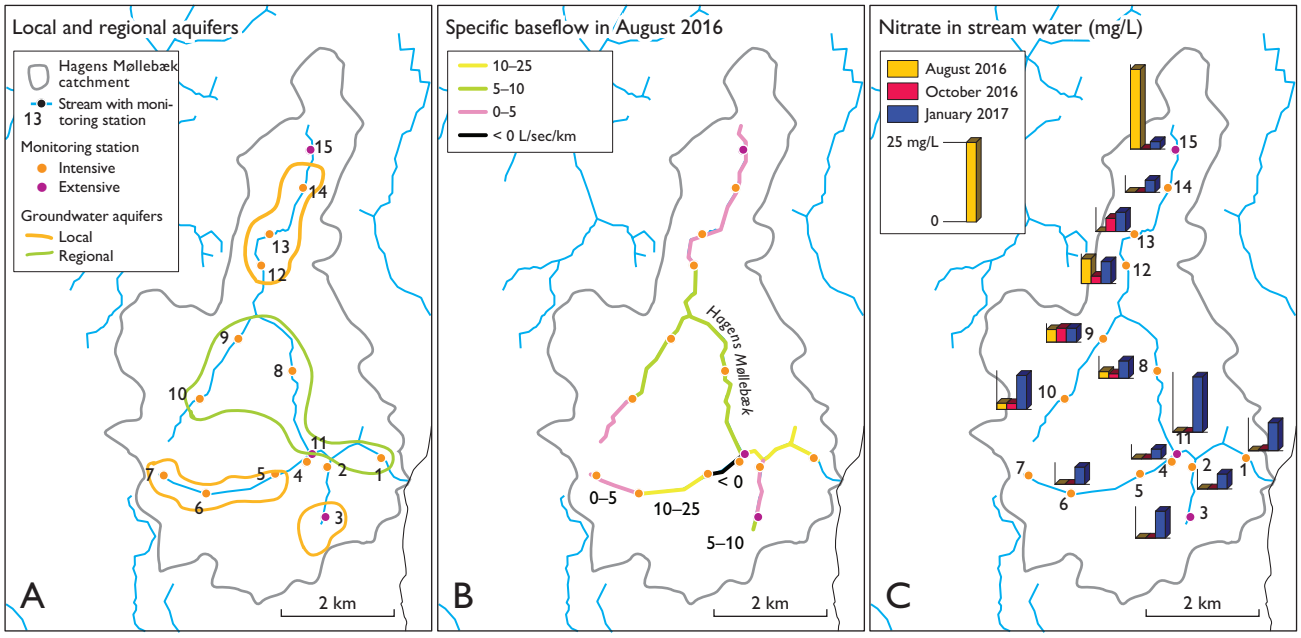

Fig. 5. Aquifers and nitrate in the Hagens Møllebæk catchment. **A**: Delineation of local and regional groundwater aquifers underneath the river system in contact with the river bed at the monitoring stations. **B**: Estimated specific base flow for individual stream reaches in August 2016. **C**: Nitrate concentrations in stream water sampled in August and October 2016 and in January 2017.

underlying sandy aquifer of local or regional extent. Further investigations of the hydraulic conditions are required at stations 5 and 7 before these can be classified.

Exchange of nitrate between groundwater, drains and stream water

The nitrate transport pathways in riparian zones were assessed by collecting water samples from groundwater in the riparian zones, in drain-pipe outlets, in the stream bed and in stream water. Groundwater samples were collected from the piezometers using 100 mL syringes. Drain-pipe outlets to the stream were only observed near five of the cross-sections (stations 4, 5, 8, 10 and 12). Water from drains having outlets above the water stage in the stream was sampled by filling a bottle directly from the outlet. Sampling of drain water from outlets below the water stage was more critical. Here a 2–3 m long, 5 mm tube was pushed into the drain pipe and a sample collected with a 100 mL syringe. The stream water itself was sampled by filling a bottle of water flowing past the monitoring station. All water samples were analysed for nitrate (NO_3-N) few hours after collection using a portable PhotoFLEX STD photometer (WTW GmbH, Weilheim).

In the cross-section of the riparian zone shown in Fig. 3, groundwater samples with nearly 20 mg/L were collected in the oxic zone 25 m east of the stream, decreasing to 0 mg/L underneath the stream bed. Normally, nitrate is not degraded in the oxic zone and the observed disappearance of nitrate in the riparian zone is likely due to the presence of microniches in the meltwater sand and gravel layer enriched with organic matter or pyrite, where nitrate degradation may occur. Moreover, it is possible that simultaneous discharge of nitrate-free groundwater into the riparian zone and stream bed may dilute the nitrate concentration in the groundwater in the riparian zone. At present we do not possess field data on a sufficiently detailed scale to support this hypothesis.

The stream water at the 15 measuring stations contained less than 5–6 mg/L of nitrate in the three sampling rounds in August 2016, October 2016 and January 2017, as expected with the highest values in January 2017 (Fig. 5C). At all the stations we have monitored, the riparian zone seems to be efficient in removing nitrate from the groundwater. However, leaching of nitrate from the nearby agricultural areas through drainage pipes can bypass the riparian zone and enter the stream system.

A river gauging station was established by the Ministry of Environment and Food of Denmark in December 2016 at the same position as station 1 in the present study. The gauging station measures the total river flow and nitrate runoff from the Hagens Møllebæk catchment to Skive Fjord. The preliminary results of this study indicate that it is useful to establish a dense monitoring system along streams to complement the new gauging monitoring station. We expect that this type of instrumentation can deliver the necessary insight to locate where nitrate-mitigation measures will be most effective.

Conclusions

After the first six-months' monitoring period (2016–2017), it seems likely that the nitrate loads to the streams in both summer and winter conditions almost entirely arise from nitrate transported by agricultural drains to Hagens Møllebæk. However, a longer monitoring period of two to three years is required to conclude this with more confidence.

In the Hagens Møllebæk catchment, riparian zones along the stream reaches with widths from a few metres to 10 m seem to be very efficient in removing nitrate from groundwater before it discharges into the stream. However, drainage pipes allow nitrate-rich water to enter directly into the stream system bypassing the riparian zone.

Acknowledgements

This work was funded by the Innovation Fund Denmark through the project Future Cropping. The authors wish to thank Bo V. Iversen and Peter K. Engesgaard for constructive comments.

References

Dahl, M., Nilsson, B., Langhoff, J. & Refsgaard, J.C. 2007: Review of classification systems and new multi-scale typology of groundwater – surface water interaction. Journal of Hydrology **344**, 1–16.

Hinsby, K., Markager, S., Kronvang, B., Windolf, J., Sonnenborg, T.O. & Thorling, L. 2012: Threshold values and management options for nutrients in a catchment of a temperate estuary with poor ecological status. Hydrology and Earth System Sciences **16**, 2663–2683.

Winter, T.C. 1999: Relation of streams, lakes, and wetlands to groundwater flow systems. Hydrogeology Journal **7**, 28–45.

Authors' address

Geological Survey of Denmark and Greenland, Øster Voldgade 10, Copenhagen, Denmark. E-mail: *bn@geus.dk*.

Structures and stratigraphy of Danian limestone, eastern Sjælland, Denmark

Peter Roll Jakobsen, Magnus Marius Rohde and Emma Sheldon

West of København, the top of the pre-Quaternary limestone is found near the terrain surface. There is only a relatively thin cover of Quaternary deposits, which makes the limestone vulnerable to pollution. Region Hovedstaden, being responsible for treating polluted sites, therefore asked GEO and the Geological Survey of Denmark and Greenland to describe the geology and hydraulic characteristics of the limestone formations (Galsgaard *et al.* 2014). During this work new information and data were collected and a revised geological model established for the area between København and Roskilde (Fig. 1). The model is based on seismic sections, a revised map of the pre-Quaternary surface, biostratigraphy, borehole information and geophysical data. This paper presents the revised geological model.

Limestone formations

The uppermost 100 m of the pre-Quaterary deposits between København and Roskilde comprises Maastrichtian chalk, bryozoan limestone (Stevns Klint Formation), the København Kalk Formation and the Lellinge Grønsand Formation (Figs 1, 2).

Cretaceous (Maastrichtian) chalk is a carbonate mudstone. It is overlain by Danian deposits in the area between Roskilde and København, but occurs at the pre-Quaternary surface in the southern part of the area.

The early and middle Danian bryozoan limestone, defined as the Stevns Klint Formation by Surlyk *et al.* (2006), usually contains 20 to 45% bryozoan fragments, but the formation also comprises mudstone or calcarenite with scattered bryozoans. Usually the bryozoan limestone is deposited in mounds, which are strongly asymmetrical in the lower mound complex and less so in the middle and upper mound complexes (Fig. 2). Flint occurs as layers between the limestone layers and lenses of coral limestone also occur. The bryozoan limestone is 53–63 m thick in the København area (Stenestad 1976).

The København Kalk Formation is of late Danian age. It is a sandy and silty carbonate mudstone defined by Stenestad (1976). It has sub-horizontal layering with pronounced flint layers parallel to the layering. A log-stratigraphy was established in the København area by Klitten *et al.* (1995; Fig. 2). The formation is 40–45 m thick.

The youngest formation, the Lellinge Grønsand Formation, is of Selandian age and consists of glauconite and carbonate-rich sand with layers and lenses of sandy limestone. Glauconite-rich marl also occurs.

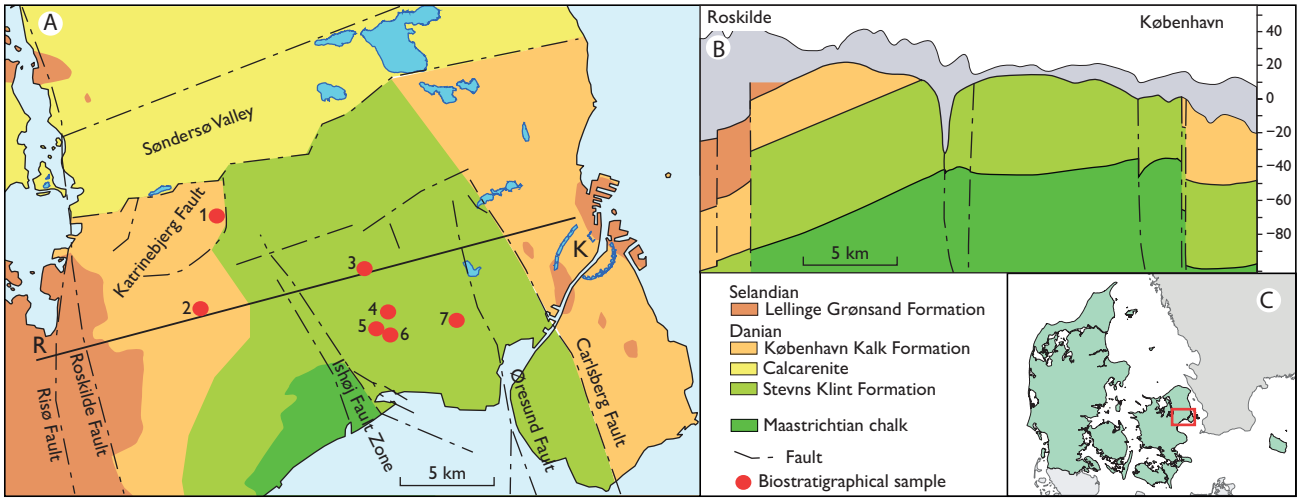

Fig. 1. **A**: A revised geological map of the pre-Quaternary surface in the København–Roskilde area. The numbered dots show the location of analysed samples. **R**: Roskilde. **K**: København. **B**: An east–west profile. **C**: Location of the study area.

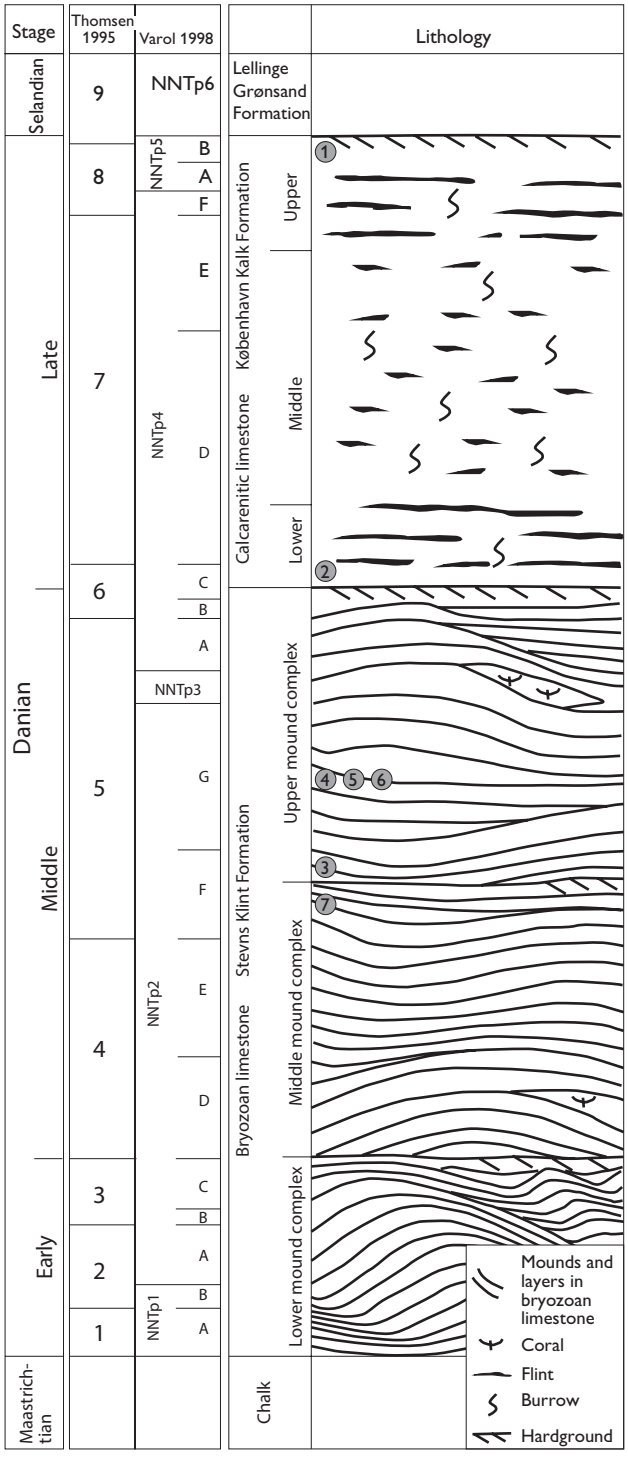

Fig. 2. Chronostratigraphy, biostratigraphy, lithostratigraphy and lithology in the greater København area (modified from Lund *et al.* 2002). Numbered dots are the numbered localities in Fig. 1A.

Biostratigraphy

Calcareous nannofossils are the main constituent of chalk deposits. Calcareous nannofossils are thought to be the remains of the principal calcareous nannoplankton group: the haptophyte algae (Bown & Young 1998). They are useful as biostratigraphic markers as they have a widespread distribution and are present globally in the photic zone of almost all marine habitats.

Table 1. Biostratigraphical results

Locality*	Nannofossil zone	Stage
1 Hove limestone pit	NNTp5B-6	Uppermost Danian – Selandian
2 Kallerup pit	NNTp4C	Early late Danian
3 Naverland 26, Glostrup	NNTp2F	Middle Danian
4 Kirkebjerg Parkvej 14	NNTp2G	Middle Danian
5 Dalager 7	NNTp2G	Middle Danian
6 Hesselager 17	NNTp2G	Middle Danian
7 Hvidovre Hospital	NNTp2F	Middle Danian

* locality numbers refer to localities marked on Figs 1, 2

The nannofossil biostratigraphic dating of the outcrops and wells from eastern Sjælland is based on the North Sea zonation scheme of Varol (1998) which, along with the Danish onshore nannofossil zonation scheme of Thomsen (1995) for comparison, is seen in Fig. 2. The zonation scheme of Varol (1998) was mainly based on North Sea wells, but sections from onshore Denmark were also used in its construction. As seen in Fig. 2, the zonation scheme of Varol (1998) allows for a higher resolution biostratigraphic breakdown than that of Thomsen (1995). Table 1 (youngest stratigraphy at the top) shows the biostratigraphic dating of samples taken from two outcrops and five wells (Fig. 1). The results show that samples from the more easterly localities are the oldest (middle Danian, subzones NNTp2F–G), and the samples become younger to the west (upper Danian–Selandian subzones NNTp4C and NNTp5B).

Faults and interpreted faults

The most pronounced tectonic feature in the subsurface of København is the SE–NW-trending Carlsberg Fault that separates the Københavns Kalk Formation from the Stevns Klint Formation (Fig. 1). The fault is one of a number of relay faults related to the Tornquist–Sorgenfrei Wrench Fault Zone. The Carlsberg Fault can be regarded as a negative flower structure with a main offset between 50 and 100 m of the hanging-wall block down to the NE (Fallesen 1995; Jakobsen *et al.* 2002). The Carlsberg Fault may still be active as terrain movements have been detected across the fault (Jakobsen *et al.* 2013) and neo-tectonic faulting of the Quaternary cover is seen (Kammann *et al.* 2016). The Carlsberg Fault is recorded on the seismic profile HGS-002 (Fig. 3) along with the Øresund Fault and the Ishøj Fault Zone. The Øresund Fault is almost parallel to the Carlsberg Fault, but they merge about 12 km north of the

seismic profile. The Ishøj Fault Zone is a *c.* 5 km wide positive flower structure with folding between the faults and an over-all inversion across the zone. The inversion has caused the Maastrichtian chalk to be present at the pre-Quaternary surface in the Ishøj area.

One of the prominent continuous reflectors in the upper part of the seismic profile is outlined in Fig. 3, and it dips *c.* 50 m from the Ishøj Fault Zone to the eastern part of the area shown in the seismic section. The same dip is seen on the seismic section HGS-001 about 10 km north of HGS-002. The Roskilde and Risø Faults are the westernmost faults presented in Fig. 1; they form part of a series of N–S-trending relay faults in the Roskilde area (Pedersen & Gravesen 2016).

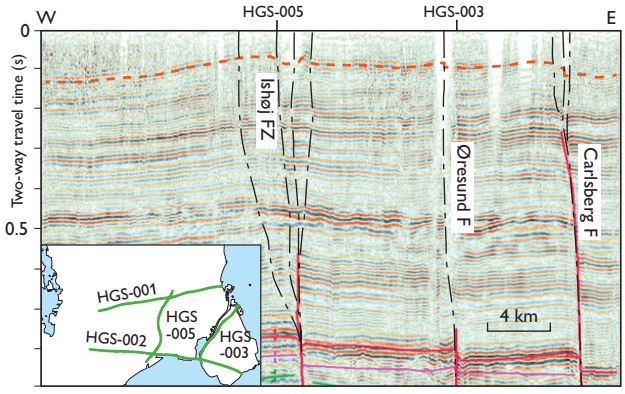

Fig. 3. Seismic section HGS-002. The inset map shows the location of the profile and some additional profiles used for the interpretation.

Pre-Quaternary surface

The Danian limestone forms the pre-Quaternary surface in eastern Sjælland and is the primary source of groundwater in the area. The large number of wells and well-logs and geological information recorded and stored in the national Jupiter database allow a detailed mapping of the limestone surface. Based on these well-logs and several geological models, a new map of the level of the pre-Quaternary surface was constructed (Fig. 4).

In the northern part of the map area, the Søndersø Valley has a valley bottom *c.* 40–30 m below sea level and strikes SW–NE. Several buried valleys have been identified and marked with red lines on the map (Fig. 4). The longest of these is the Herlev Valley that is oriented parallel with the Søndersø Valley *c.* 5 km south to the of it. Towards the west, the Herlev Valley almost intersects the smaller Katrinebjerg Valley. The general level of the pre-Quaternary surface is 5–10 m higher south of the Herlev and Katrinebjerg valleys compared with the area between these valleys and the Søndersø Valley.

Two narrow valleys, the Rådhus and Vibenhus valleys, situated below the city of København are generally well mapped based on borehole data. Several conspicuous depressions in the limestone surface are only identified from one or a few boreholes, e.g. in the northern part of Taastrup and the eastern part of the Herlev Valley. It is possible that these small depressions are un-mapped valleys similar to the clear buried valleys identified on the map in Fig. 4.

Geological model

The revised geological map and model are presented in Fig. 1. The map is based on interpretation of the map of the pre-Quaternary surface, seismic sections and biostratigraphic analyses. The biostratigraphic analysis of the middle part of the Stevns Klint Formation (Fig 1) shows that the limestone in this area, at the pre-Quaternary sur-

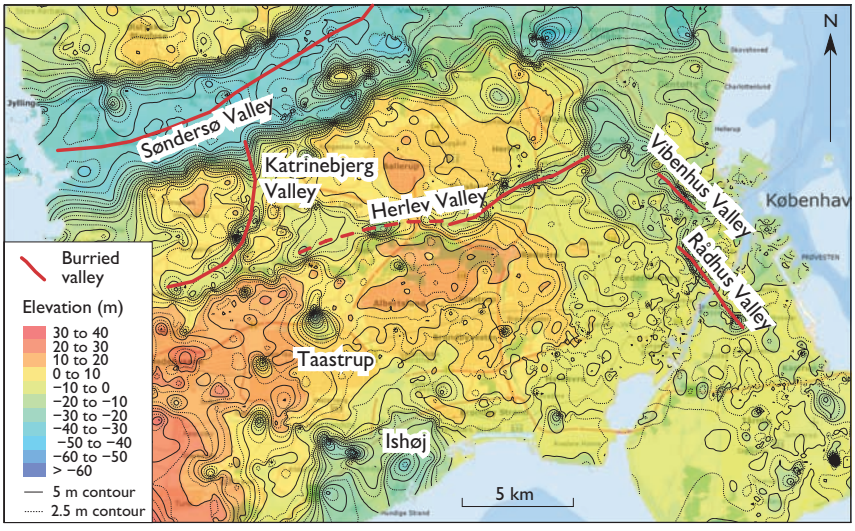

Fig. 4. Topography of the pre-Quaternary surface in the København–Roskilde area based on the latest data.

face, is of middle Danian age and belongs to the upper mound complex (Fig. 2). Compared with the depth to the Maastrichtian–Danian boundary, registered in adjacent boreholes, the thickness of the Stevns Klint Formation is fairly uniform and comparable with thicknesses known from the København area, and a uniform thickness of the limestone unit is consequently assumed. Previous maps do not show the presence of the København Kalk Formation between the Lellinge Grønsand Formation and the Stevns Klint Formation in the western part of the area (Stenestad 1976). With a dip of *c.* 50 m from the Ishøj Fault Zone to Roskilde, it is therefore expected that the København Kalk Formation is present between the Stevns Klint Formation and the Lellinge Grønsand Formation. This was confirmed by biostratigraphical analyses of samples from localities 1 and 2 (Figs 1, 2). However, the two samples representing København Kalk Formation are from the uppermost and lowermost parts of the formation, respectively. This means that the Katrinebjerg Fault (Fig.1), interpreted from the pre-Quaternary surface map, is in fact a fault, with an offset of *c.* 50 m. At Hove (locality 1, Fig. 1) a geophysical log from borehole DGU 200.5248 shows the same log pattern as it is known from the København area and shows the presence of the whole formation.

Many samples from boreholes within the western København Kalk Formation area are described as bryozoan limestone. This could represent a facies variation with a higher concentration of bryozoans than is usually seen in the København area. However, it is also possible that the tectonic conditions are more complex, with more faults than those documented so far.

Conclusions

The geological map of the pre-Quaternary surface is revised for the area between København and Roskilde. The revision is based on new seismic sections, a map of the pre-Quaternary surface and biostratigraphic analyses.

The Ishøj Fault Zone is a positive flower structure, and a prominent structural feature in this area. Between the Ishøj Fault Zone and the Roskilde Fault, the limestone dips westwards.

The Upper Danian København Kalk Formation is documented in the western part of the pre-Quaternary surface between København and Roskilde and may have a higher content of bryozoans than in the København area.

Acknowledgements

The project on geological and hydrological knowledge acquisition on Danian limestones between København and Roskilde was financed by Region Hovedstaden. Region Hovedstaden kindly allowed us to use the results from biostratgraphical analyses conducted during various projects.

References

Bown, P. & Young, J. 1998: Introduction. In: Bown, P.R. (ed.): Calcareous nannofossil biostratigraphy. British Micropalaeontological Society Publication Series, 1–15.

Fallesen, J. 1995: Stratigraphy and structure of the Danian Limestone on Amager, examined with geophysical investigations – especial with regard to the Carlsberg Fault. Unpublished MSc thesis, University of Copenhagen.

Galsgaard, J., Rohde, M., Jakobsen, P.R. & Jakobsen, R. 2014: Strømning og stoftransport i kalklagene på den københavnske vestegn. Geologisk og hydrologisk vidensopsamling og typemodel, 97 pp. Unpublished report, GEO projekt nr. 37208, Rapport 1, 2014-06-19.

Jakobsen, P.R., Fallesen, J. & Knudsen, C. 2002: Strukturer i den Københavnske undergrund – folder, forkastninger og sprækker. In: Frederiksen, J.K *et al*. (eds): Ingeniørgeologiske forhold i København. Danish Geotechnical Society Bulletin **19**, 19–29.

Jakobsen, P.R., Wegmuller U., Capes R. & Pedersen S.A.S. 2013: Terrain subsidence detected by satellite radar scanning of the Copenhagen area, Denmark, and its relation to the tectonic framework. Geological Survey of Denmark and Greenland Bulletin **28**, 25–28.

Kammann, J., Huebscher, C., Boldreel, L.O. & Nielsen, L. 2016: High-resolution shear-wave seismics across the Carlsberg Fault Zone south of Copenhagen: implications for linking Mesozoic and late Pleistocene structures. Tectonophysics **682**, 56–64.

Klitten, K., Ploug, C. & Olsen, H. 1995: Geophysical log-stratigraphy of the København Limestone. Danish Geotechnical Society Bulletin **11**(5), 5127–5134.

Lund, N.S., Nielsen, L.H. & Knudsen, C. 2002: Københavns undergrund med fokus på Danien aflejringerne. In: Frederiksen, J.K. *et al.* (eds): Ingeniørgeologiske forhold i København. Danish Geotechnical Society Bulletin **19**, 5–18

Pedersen, S.A.S. & Gravesen, P. 2016: Tectonic control on the formation of Roskilde Fjord, central Sjælland, Denmark. Geological Survey of Denmark and Greenland Bulletin **35**, 35–38.

Stenestad, E. 1976: Københavnsområdets geologi især baseret på citybaneundersøgelserne. Danmarks Geologiske Undersøgelse III. Række **45**, 149 pp.

Surlyk, F., Damholt, T. & Bjerager, M. 2006: Stevns Klint, Denmark: uppermost Maastrichtian chalk, Cretaceous–Tertiary boundary and lower Danian bryozoan mound complex. Bulletin of the Geological Society of Denmark **54**, 1–48.

Thomsen, E. 1995: Kalk og Kridt i den danske undergrund. In: Nielsen, O.B. (ed.): Danmarks Geologi fra Kridt til i dag. Aarhus Geokompendier **1**, 31–67.

Varol, O. 1998: Palaeogene. In: Bown, P.R. (ed.): Calcareous nannofossil biostratigraphy. British Micropalaeontological Society Publication Series, 200–224.

Authors' addresses

P.R.J. & E.S.,*Geological Survey of Denmark and Greenland,* Øster *Voldgade 10, DK-1350 Copenhagen K, Denmark*. E-mail: *prj@geus.dk*

M.M.R., *GEO, Maglebjergvej 1, DK-2800 Kgs. Lyngby, Denmark.*

Karst sinkhole mapping using GIS and digital terrain models

Peter Brøgger Sørensen, Holger Lykke-Andersen, Peter Gravesen and Bertel Nilsson

Danish glacial landscape elements such as basal till plains, hummocky moraine areas and outwash plains contain a variety of small and large depressions. They were probably formed in glacial, late-glacial or Holocene time and may represent dead-ice holes or degraded pingos, or sinkholes formed by interaction between pre-Quaternary chalk or limestone bedrock and the thin glacial cover. The aim of this study is to map terrain depressions that might potentially be karst sinkholes by analysing digital terrain models in the geographic information system (GIS). The incentive to apply the technique for mapping of sinkholes came from an accidental acquaintance with a farmer, Jens Kirk, whose farmland is located near Thisted. Jens Kirk told us that the front end of his tractor had suddenly sunk into the ground during routine farming work, and this incident was our inspiration to start the project described here.

Geological setting and study areas

Sinkholes have previously been registered in mainly northern Denmark where the pre-Quaternary surface consists of chalk and limestone (Feddersen 1880). In these areas sinkholes and other karst features including dolines, karst lakes, small caves, disappearing streams and karst springs are known (Nilsson & Gravesen 2017). The landforms are found at locations where Quaternary surface layers are thin and calcareous rocks are present near the surface. Sinkholes can be formed when acid groundwater dissolves and removes calcium carbonate from the calcareous sediment. Cavities are formed in the carbonate sediments, and the overlying deposits may collapse and create a surface depression. The present authors have carried out pilot studies around Limfjorden and in the northern part of Djursland in Jylland. The results from north of Thisted and in the planted wood of Svinkløv Plantage south of Svinkløv are presented here (Fig. 1). It should be noted, that Svinkløv Plantage has never been farmed, and the depressions found here are small compared to those in farmed areas. This means that even small depressions have been preserved if not covered by drifting sand.

The first study area is located 2–3 km north of Thisted (Fig. 1). The pre-Quaternary surface of Maastrichtian chalk and Danian bryozoan limestone and micritic limestone in this area is commonly covered by a thin (less than 5 m thick) Quaternary cover. Small dolines filled with Paleocene clay are found in the Danian limestone in

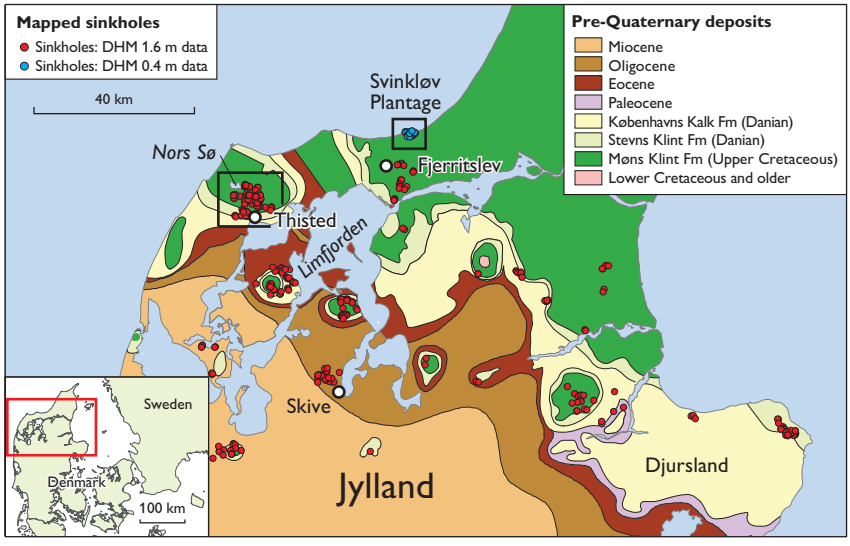

Fig. 1. Locations of mapped small depressions in northern Jylland. The surface is shown as pre-Quaternary where parts of it consists of Cretaceous chalk and Danian limestone covered by Quaternary deposits. Red and blue dots: possible sinkholes mapped with the 1.6 and 0.4 m digital elevation models, respectively. Black frames: local study areas.

Thisted town (Gravesen & Jakobsen 2016). Sinkholes are distributed over the entire area. In cliffs and limestone pits it is possible to find two types of dolines: Funnel-shaped and vertical-sided. Both types have originated as areas of intense fracturing where acid water has percolated downwards and dissolved the chalk. In the western part of the area, large karstic lakes such as Nors Sø occur along a fault zones and in the middle of a salt structure (Hansen & Håkansson 1980). Between Svinkløv and Fjerritslev on the north-west coast of Jylland many sinkholes and dolines are registered in the chalk and limestone cliffs (Gry 1979). Sinkholes also occur in the area of elevated chalk south of Fjerritslev.

Methods and data

The detailed topographic maps that became available from *c*. 1900 made it possible for Ussing (1903) and Harder (1908) to interpret the Danish glacial landscape. Since then the technological evolution has resulted in a highly detailed digital terrain model (in Danish 'digital højdemodel', DHM) with a lateral resolution of 1.6 m in the 2007 version (DHM 1.6) and 0.40 m in the 2016 version (DHM 0.4) with a vertical accuracy of a few centimetres (www.sdfe.dk). Using hill-shade versions of the DHM 1.6 model with a vertical exaggeration of 3 even the smallest vertical variations can be detected. Numerous depressions were identified, and detailed mapping was initiated, using QGIS (open source version of GIS) as a data repository. The DHM 0.4 model is delivered with hill shade but with no vertical exaggeration.

The 3D geographical information of the mapped depressions was analysed in GIS supported by other sources of spatial data such as orthophoto and topographic maps. Mobile devices such as tablets and smartphones with GPS were used in the field documentation of the depressions throughout the mapping project. Two of the authors recently demonstrated the usefulness of the combination of these techniques for identification and mapping of remnants of pingos in Denmark (Sørensen & Lykke-Andersen 2017).

More than 350 depressions supposed to be sinkholes in northern Jylland were mapped (Fig. 1); in Svinkløv Plantage sinkholes were mapped using the DHM 0.4 model. The digital terrain models were provided by the Danish Agency for Data Supply and Efficiency (www.sdfe.dk) as a digital service in raster format with and without hill shade for visual interpretation, and as a web map service for analysis and measurement.

The depression mapping was divided into three steps. Firstly, the location of each depression was found and digitised using GIS. Secondly, a profile of the depression was constructed using the QGIS profile tool and its diameter and depth measured, allowing a descriptive statistical analysis of the sinkholes and their spatial distribution. Inspection of orthophotos was sometimes helpful because the vegetation pattern can reveal differences in the topsoil. On this basis the depression was either approved or rejected. For example, a shallow depression on an inclined surface facing away from the incident light produces a significant shadow which does not represent a sinkhole. Finally, a field check was carried out for some of the proposed sinkholes, because previous studies have shown that the structural and sedimentary conditions of some of the depressions should be investigated by excavation (Zhu *et al*. 2014).

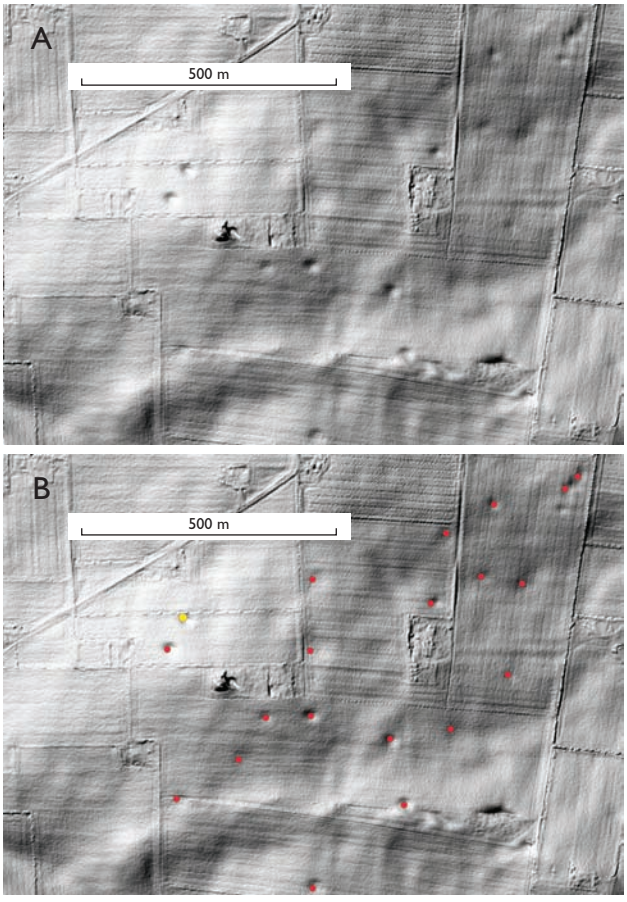

Fig. 2. Hill-shade map with 10 × vertical exaggeration showing examples of sinkholes mapped with the 1.6 m digital elevation model. **A**: Unmarked map. **B**: Mapped sinkholes (red dots). Yellow dot: location of the excavated 'Jens Kirk sinkhole' north of Thisted as shown in Fig. 3.

Results

Results from the depression mapping north of Thisted and in Svinkløv Plantage are shown in Figs 2 and 3. In the Thisted area *c.* 116 sinkholes are identified, and 20 depressions were identified on the hill shade map within the subarea measuring 1 × 1.5 km shown in Fig. 2. The diameter of the depressions in the Thisted area varies from 21 to 100 m, with depths between 0.3 and 2.5 m. To obtain information about the geometry of the depression encountered by Jens Kirk and to prove it is a sinkhole, a trench was dug (Fig. 3). The diameter of the excavated depression is 25 m. Outside the depression, the depth below the topsoil to the chalk surface was 30 cm. In the middle of the depression the chalk surface occurs about 2.35 m below the terrain surface outside the sinkhole. In the south-western part of the profile, the chalk surface is almost vertical, indicating subsidence along a fault. Stone-free topsoil, probably glacial, was found overlaying the chalk. In the middle of the depression about 40 cm above the chalk surface, a chert layer 7 m long and 5–10 cm thick was found. The geometry and structure of the depression strongly indicate that it is a karstic sinkhole. It should be noted that the diameter of the 'Jens Kirk sinkhole' (Fig. 3A) is in the lower range of those mapped north of Thisted.

In Svinkløv Plantage, 65 small sinkholes were mapped with success using the DHM 0.4 model (Fig. 4), which are not visible in the 1.6 m model; the area is partly covered by dune sand. The diameter of the small sinkholes varies from 1 to 10 m, with depths between 0.4 and 4.5 m. A survey in the Bulbjerg area has revealed a few similar small depressions that are likewise supposed to be sinkholes. The DHM 0.4 model is obviously better suited for the minor landscape elements such as the small depressions found in Svinkløv Plantage even with the absence of vertical exaggeration.

A significant difference in the diameter/depth ratio between the sinkholes in the Thisted and Svinkløv Plantage areas is seen in Table 1. The sinkholes in Svinkløv Plan-

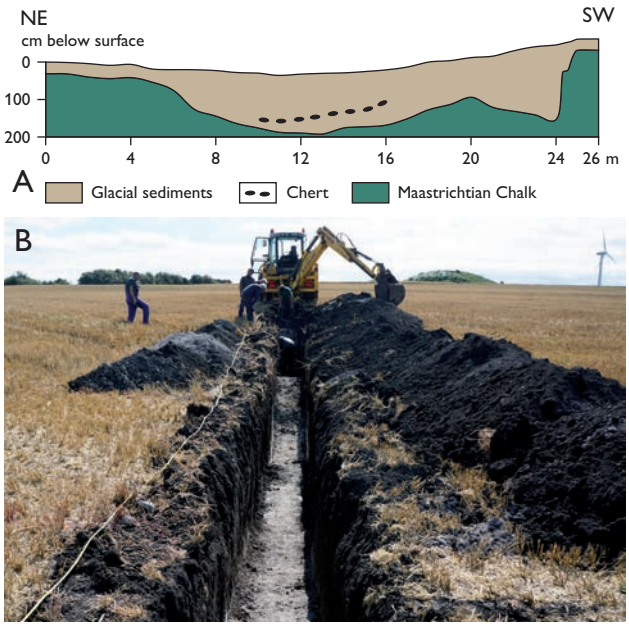

Fig. 3. **A**: Section drawn from the excavated trench through the 'Jens Kirk sinkhole' (vertical exaggeration 1.7 ×). **B**: The excavated trench with the chalk surface exposed at the bottom. UTM coordinates: 481294E, 6316209N.

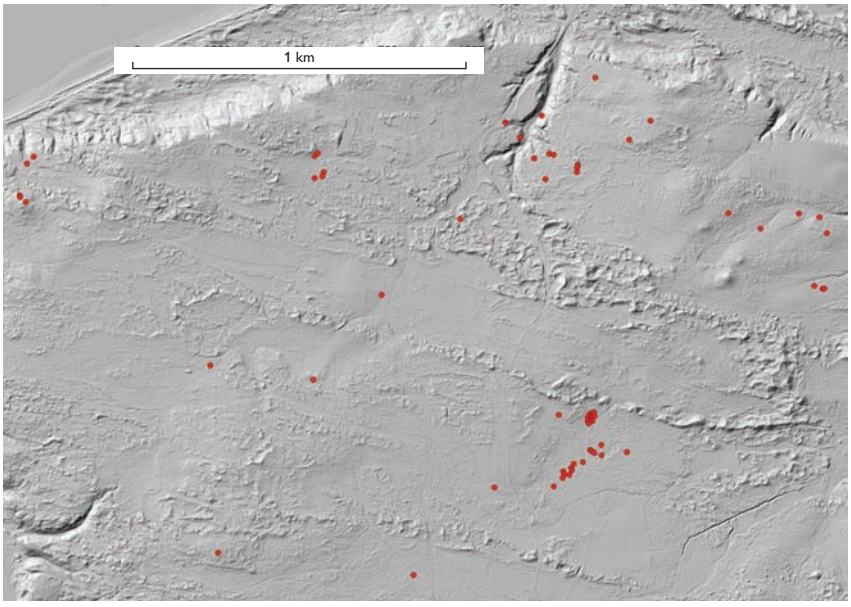

Fig. 4. Sinkholes (red dots) mapped in Svinkløv Plantage using the 0.4 m digital elevation model.

Table 1. Depths and diameters of sinkholes

	Depth, m§	Diameter, m§	Diameter/Depth
Thisted	0.3–2.5 (0.8)	21–100 (43.6)	57.4
Svinkløv Plantage	0.4–4.5	1.0–10 (4.3)	3.8

§Minimum, maximum and mean values

tage are ten times smaller but slightly deeper than those in Thisted.

Discussion

Origin of the mapped depressions

Mapping of karst sinkholes using GIS and DHM in areas with carbonate sediments underlying thin Quaternary deposits seems to be evident. However, the mapping in this study also identified depressions in areas with Palaeogene clays underneath thin glacial deposits (area west of Skive; Fig. 1). These depressions cannot have been developed due to karst evolvement. Thus, dead-ice holes or degraded pingos can be other potential origins of these depressions and have thoroughly been discussed in Sørensen & Lykke-Andersen (2017). However, it is beyond the scope of this study to collect the required structural and sedimentary documentation to classify all of the individual depressions found in northern Jylland.

Factors influencing the formation and geometry of the mapped sinkholes

Sinkholes may develop if the Pre-Quaternary surface consists of carbonate sediments such as Maastrichtian chalk or Danian limestone, which are easily dissolved and contain fractures, hollows and cavities. In order to allow the sinkhole-forming process to operate during the Neogene, the overlying sediments (mainly Quaternary deposits) must be thin. The circular shape of the sinkholes is possibly a combination of crossing fault lines and dissolution processes. The anthropogenic activity seems to be an important factor for the collapses, but also the climate with changing wet and dry conditions may influence the development. Changes in the groundwater level, abstraction of water and changing drainage patterns are other controlling factors.

Conclusions

1. The pilot study demonstrates that analysing digital terrain models in GIS is a powerful method. The DHM 1.6 model with a vertical exaggeration of 3 is very well suited for the identification of depressions with diameters greater than 20 m, while the DHM 0.4 model is better suited for the identification of small landscape elements even without vertical exaggeration.
2. The sinkholes in Svinkløv Plantage are much smaller and slightly deeper than in Thisted. One explanation for this could be that the Svinkløv area has never been farmed.
3. The structural and sedimentary conditions in other sinkholes should be investigated by excavations.

References

Feddersen, A. 1880: Nogle danske Overfladeforhold. Geografisk Tidsskrift **4**, 113–118.

Gravesen, P. & Jakobsen, P.R. 2016: Pre-Quaternary rocks and sediments with some of the highest radioactive levels in Denmark. Bulletin Geological Survey of Denmark and Greenland **35**, 31–34.

Gry, H. 1979: Description of the geological map of Denmark. Map sheet Løgstør. Quaternary deposits. 1:100 000/1:50 000 (in Danish with English summary). Danmarks Geologiske Undersøgelse I. Række **26**, 58 pp. + atlas + map vol.

Hansen, J.M. & Håkansson, E. 1980: Thistedstrukturens geologi – et 'neotektonisk' skoleeksempel. Dansk Geolologisk Forening, Årsskrift for **1979**, 1–9.

Harder, P. 1908: En østjydsk Israndslinje og dens Indflydelse paa Vandløbene. Danmarks Geologiske Undersøgelse II. Række **19**, 262 pp.

Nilsson, B. & Gravesen, P. 2017: Karst geology and regional hydrogeology in Denmark. In: White, W.B. *et al.* (eds): Karst Groundwater Contamination & Public Health. Springer International Publishing AG Switzerland (in press).

Sørensen, P.B. & Lykke-Andersen, H. 2017: Kortlægning af pingo-rester i Danmark. Geologisk Tidsskrift **2017**, 21–29.

Ussing, N.V. 1903: Om Jyllands Hedesletter og Teorierne for deres Dannelse. Oversigt over Det Kongelige Danske Videnskabernes Selskabs Forhandlinger **1903**(2) 99–152.

Zhu, J., Taylor, T.P., Currens, J.C. & Crawford, M.M. 2014: Improved karst sinkhole mapping in Kentuckey using LIDAR techniques: A pilot study in Floyds Fork watershed. Journal of Cave and Karst Studies **76**(3) 207–216.

Authors' addresses

P.B.S., *Møllepold 17, 6200 Aabenraa, Denmark*. E-mail: *peter@peterbrogger.dk*

H.L.-A., *Department of Geoscience, Aarhus University, Høegh Guldbergs Gade 2, 8000 Aarhus C, Denmark.*

P.G. & B.N., *Geological Survey of Denmark and Greenland, Øster Voldgade 10, Copenhagen K, Denmark.*

Towards a geothermal exploration well in the Gassum Formation in Copenhagen

Henrik Vosgerau, Ulrik Gregersen, Lars Kristensen, Sofie Lindström, Anders Mathiesen, Carsten M. Nielsen, Mette Olivarius and Lars Henrik Nielsen

Geothermal resources in the deep subsurface in many parts of Denmark have the potential to form a central component in the future Danish energy supply for district heating. Geothermal energy is sustainable and environmentally friendly and independent of climatic and seasonal variations, in contrast to solar and wind energy. Furthermore, geothermal plants may be integrated with other green energy supplies. The sandstone reservoirs from which the warm geothermal water is extracted may also act as temporary storage for excess heat e.g. from industrial production processes or from solar-heated water in summer periods when the demand for heating is low.

Therefore, there are many good reasons to include geothermal energy in Denmark's energy mix. Despite this, only three geothermal plants exist at present at Thisted, Copenhagen and Sønderborg (Fig. 1). Several district heating companies have, however, shown interest in geothermal energy and have taken the first step towards estimating if suitable geological conditions are present within their respective district heating areas. This has been done by analysing geological and geophysical data gathered from the nearest deep wells and seismic surveys, in some cases supplemented with new seismic data. Although these analyses generally show promising geothermal potential, hesitation prevails when it comes to drilling the actual geothermal wells. Deep drilling is complicated and expensive, but necessary in order to deduce if productive reservoir sandstones are present that can produce the required volumes of geothermal water.

In order to mitigate the geological risks and facilitate utilisation of geothermal energy, publicly supported initiatives financed by research grants have been undertaken for the last 40 years. Thereby our knowledge of the Danish subsurface and the reservoir properties of deep geothermal sandstones has considerably increased, and fundamental uncertainties regarding subsurface structures and resources have been reduced. The many promising results are publicly available via the newly established Geothermal WebGIS Portal at the Geological Survey of Denmark and Greenland (Vosgerau *et al.* 2016). Furthermore, the industry is now taking more interest in geothermal exploration and sees it as a promising business case into which it is willing to invest and share the risks associated with expensive wells. The public sector facilitates this development by supporting research projects via grants from the Energy Technology Development and Demonstration Programme of the Danish Energy Agency (EUDP) and the Innovation Fund Denmark. These projects involve research institutes, district heating companies, private companies and other stakeholders.

The present paper deals with the outcome of one of these projects called the Geothermal Pilot Hole, financially supported by the EUDP. The project elucidates e.g. how drilling can be made less expensive by focusing on geothermal sandstone reservoirs at depths shallower than *c.* 2200 m, thereby allowing the use of small rigs suitable

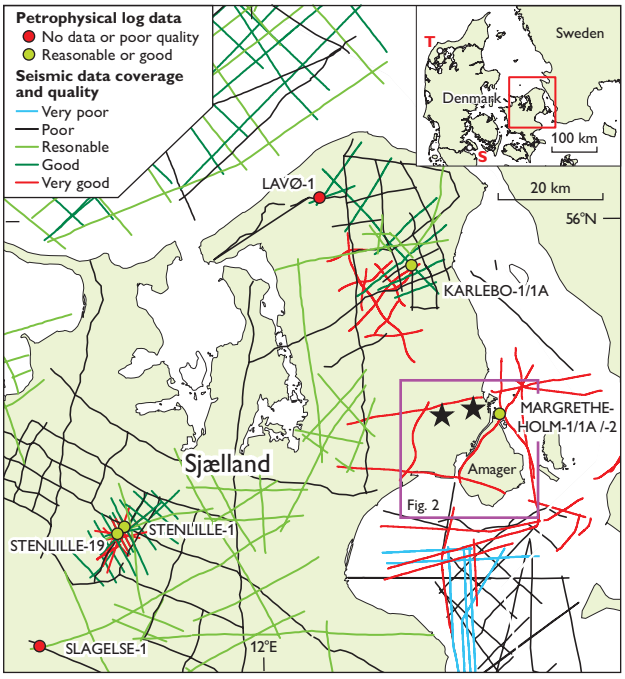

Fig. 1. Coverage and quality of seismic and petrophysical log data from deep wells in Sjælland. The quality indeces reflect to which degree the data can be used to extract information about major geothermal sandstone reservoirs in the deep subsurface. The Margretheholm wells are part of the existing geothermal plant in Copenhagen. Stars mark the approximate positions of the two areas of interest. On the inset map the locations of the Thisted (**T**) and Sønderborg (**S**) plants are shown.

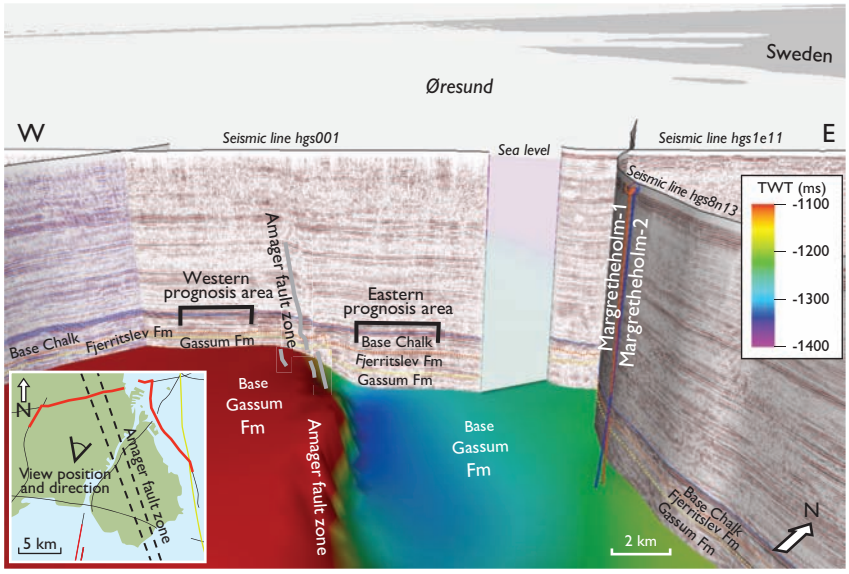

Fig. 2. Seismic lines in 3D view seen towards northern Copenhagen and Margretheholm in northern Amager. The view position and direction are shown on the inserted location map, as is the overall trend of the Amager Fault zone. The coloured surface reflects the depth and morphology of the base of the Gassum Formation, clearly illustrating the different, fault-controlled positions of the two prospect areas west and east of the fault. The thickness of the Gassum Formation, marked on the seismic profiles, increases considerably from west to east across the Amager Fault zone. Depths are shown as seismic two-way travel time, TWT.

for operation in urban areas. For comparison, the existing geothermal plant in Copenhagen utilises water from the Lower Triassic Bunter Sandstone Formation at a depth of *c.* 2.6 km. Another important part of the project is to provide a well-constrained prognosis of relevant reservoir parameters (depth, thickness, transmissivity, production capacity, temperature, etc.) of geothermal sandstone reservoirs of the Upper Triassic – Lower Jurassic Gassum Formation within two prospect areas of special interest in northern Copenhagen (Fig. 1). This activity will provide the necessary background to select the location of an exploration well in a future phase of the project yet to be granted. Previous studies have shown that the subsurface of Copenhagen contains large quantities of geothermal energy which may form a substantial contribution to domestic heating for hundreds of years to come, and the two areas in northern Copenhagen (stars, Fig. 1) have already been selected as relevant, based on suitable geological conditions and infrastructure. Copenhagen is a major city with a substantial demand for heating and like other Danish cities it has a well-established district heating network, and for these reasons it is an obvious site for geothermal energy.

The Gassum Formation constitutes the most well-known sandstone reservoir in Denmark and is exploited for geothermal energy in Thisted and Sønderborg and for gas storage at Stenlille. It is dominated by fine to medium-grained sandstones alternating with darker-coloured claystones, siltstones and thin coal seams. The sand was deposited in the Danish Basin mainly as marine shoreface sand in relatively continuous and widely distributed bodies, as well as deposits in river channels, estuaries and lagoons. In the Copenhagen area, the Gassum Formation occurs in depths of around 2000 m and has a temperature of *c.* 60°C (Balling *et al.* 2016), sufficiently high to make a district heating plant economically profitable. Furthermore, the depth is shallow enough to prevent serious diagenetic alteration under high pressure and temperature conditions which might reduce the porosity and permeability of the reservoir sandstones (Kristensen *et al.* 2016). The results of the project phases conducted so far illustrates e.g. that the subsurface geological conditions may vary considerably within a city area, thus influencing the geothermal potential.

Geological database

The critical subsurface geological information from deep wells and seismic lines in central and north-eastern Sjælland (Fig. 1) controls the reservoir prognosis for the two prospect areas in northern Copenhagen. The seismic coverage is reasonable around these two areas, especially because an E–W-trending seismic line of very good quality occurs immediately north of them. Detailed analysis of this and other nearby lines has been used to identify and estimate the depth and thickness of the Gassum Formation in the two prospect areas. The two areas are separated by the NNW–SSE-striking Amager Fault which forms part of a major regional fault zone, along which the easternmost part of Sjælland has been down-faulted (Fig. 2). The seismic mapping reveals that the Gassum Formation is thicker and occurs at a deeper level in the eastern area than in the western area.

Deep wells in north-eastern Sjælland are limited to Margretheholm-1/1A and -2, Karlebo-1/1A and Lavø-1 from which no cores of the Gassum Formation exist, and

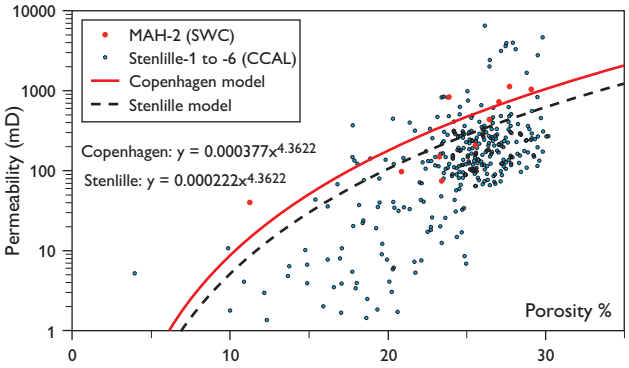

Fig. 3. Porosity–permeability models based on gas measurements on core material at laboratory conditions. The 'Copenhagen model' represents the eastern prospect area and is based on measurements on sidewall cores from the Margretheholm-2 well, whereas the 'Stenlille model' represents the western prognosis area and is based on conventional core analysis data from several Stenlille wells. The methodology for establishing local porosity–permeability models is described in Kristensen *et al.* (2016).

the petrophysical log data from Lavø-1 are of poor quality. However, a large amount of good quality petrophysical log and core data exist from the Stenlille area in the central part of Sjælland, *c.* 60 km west of the two areas of interest (Fig. 1), although not all of the well data are equally relevant for setting up a reservoir prognosis for the Gassum Formation in the prospect areas. Representative well data have been chosen based on e.g. sequence stratigraphic and biostratigraphic analysis and on similarities to the prospect areas in terms of structural setting, depositional environment, inferred distance from the palaeoshoreline, sediment sources, petrography, burial depth, diagenetic alternation, etc. In general, the data from the Margretheholm and Karlebo-1/1A wells are considered the most relevant for the eastern prospect area, as also these wells are located on the eastern, down-faulted side of the Amager Fault (Fig. 2). The locations of the Lavø-1 and the Stenlille wells west of the Amager Fault justify a higher weighting of data from these wells in the prognosticating of the western area.

Estimated reservoir values

Based on the seismic data, the Gassum Formation is estimated to be around 200 m thick with its top at *c.* 2000 m below sea level in the eastern of the project areas in Copenhagen, and around 150 m thick with its top at *c.* 1750 m below sea level in the western area (Table 1). Core and petrophysical well log data form the basis for estimating the reservoir properties of the sandstones including local porosity–permeability models (Fig. 3). The porosity and permeability values are estimated to be slightly lower in the eastern than in the western area, most likely related to its deeper burial depth and corresponding higher pressure–temperature conditions (Table 1). The reservoir transmissivity, given by multiplying the estimated thickness of potential reservoir sand with the estimated reservoir permeability, is an important parameter as it expresses the overall performance of the reservoir. As a rule of thumb, the transmissivity of a sandstone interval in the Danish subsurface should be greater than 10 Darcy-m in order to constitute a potential geothermal reservoir. Both areas fulfil this criterion as the estimated reservoir transmissivity for the Gassum Formation is 25 and 28 Darcy-m, respectively, for the two areas. Although the estimated porosity, permeability and transmissivity values are slightly higher in the western area, this does not necessary qualify this as better for geothermal exploitation. This is because the geothermal water of the Gassum Formation in the eastern area benefits from being hotter than in the western area (65°C versus 57°C, Table 1) as a consequence of its greater depth.

Table 1. Estimated reservoir values for the Gassum Formation in two potential areas§

Prospect areas in Copenhagen	western	eastern
Macro reservoir parameters		
Depth to top of formation (m below sea level)	1750	2000
Thickness (m)	150	200
Thickness, potential reservoir sand (m)	75	80
Water-conducting properties (reservoir sand)		
Porosity (%)	25	21
Gas permeability (mD)	300	250
Reservoir permeability (mD)	375	313
Reservoir transmissivity (Kh) (Dm)	28	25
Temperature (°C), middle of formation	57	65

§See Kristensen *et al.* (2016) for details.

Reservoir model simulations

Reservoir simulations in both of the prospect areas have shed further light on the suitability of the Gassum Formation for geothermal exploitation. The reservoir data and interpreted regional seismic surfaces have thus been used to simulate flow rates and the time span before cooled water from injection wells will reach the production wells. In each of the simulations, separate production and injection wells supplemented with a vertical spud well were used. Simulation runs with different well spacings show that the distance between the production and injection wells at depth can be kept as low as 900 m without cold-water breakthrough at the production well within the simulation period of 25 years. Given that the injection and production wells would typically originate from the same surface

position, short distances between the injection and production wells at the reservoir level are preferred in order to minimise the inclination of the well trajectory. This will lower the drilling risks, as drilling generally becomes more complicated with increasing inclination.

Overall, the simulations showed suitable production capacities for both locations but that the eastern location is more favourable because of higher production and injection rates for the same pressure applied to the wells, a more favourable production temperature profile, as well as thicker reservoir intervals which will delay breakthrough of cold water from the injection to the production well because the cold-water front is spread over a thicker reservoir interval.

Concluding remarks and perspectives

The various geological and geophysical analyses presented here indicate that the Gassum Formation is suitable for geothermal exploitation in both of the prospect areas. The production may be further enhanced if geothermal energy is produced simultaneously from the Gassum Formation and from sandstones in the lower part of the overlying Fjerritslev Formation. This formation largely consists of tight mudstones, but in eastern Sjælland its basal part contains several sandstones which may contribute to a geothermal production. Although the simulations point out the eastern area as being more favourable for a geothermal production, other factors must also be considered in a final selection of a borehole location, such as drilling costs related to different drilling depths and non-geological parameters such as the position of the well in relation to the district heating and other surface infrastructure.

Well data from eastern Sjælland are scarce and of varying quality. Especially the lack of cores from penetrated sandstones is a shortcoming, as such material is very valuable in estimating reservoir properties as shown by the extrapolation of core data from the Stenlille wells for the prospect areas in Copenhagen. Several packages of sandstones and intervening mudstones in the Gassum Formation have thus been correlated between the wells at Stenlille and eastern Sjælland and are therefore also expected to be present in the two prospect areas themselves. Regional seismic mapping, palynological analysis and comparison of petrophysical log data patterns furthermore indicate that the paleogeographic setting and depositional environments during the deposition of the Gassum Formation were broadly similar in Stenlille and in the prospect areas. In addition, U-Pb radiometric dating of detrital zircon grains from the Gassum Formation indicates that all of these deposits were sourced mainly from reworking of the Lower Triassic Bunter Sandstone Formation on the Ringkøbing–Fyn High, a regional basement ridge forming the southern margin of the Danish Basin.

Extrapolation of the Stenlille data as far as to eastern Sjælland inevitably implies some uncertainties. A new well in Copenhagen from which cores, petrophysical log data and hydraulic test data can be collected and analysed will considerably increase the accuracy of predictions of reservoir properties of the Gassum Formation in greater Copenhagen as well as in the Hillerød and Farum areas in northeastern Sjælland, where initial investigations have also been performed. Hence, the geological and economic risks associated with the establishment of a geothermal plant will be reduced, not only in Copenhagen but in eastern Sjælland as a whole. Furthermore, a new well will make it possible to compare existing core data (including direct porosity and permeability measurements) with petrophysical log data and hydraulic test data from intervals of penetrated reservoir sandstone, and will thus provide a unique possibility to verify to what extent traditional petrophysical log data can be used to estimate the reservoir properties of geothermal sandstones. This knowledge is important for evaluation of the geothermal potential in a specific area based on data from existing wells, and for selecting suitable log tools for estimation of the porosity, permeability and injectivity of potential reservoir sandstones in general.

Acknowledgements

The EUDP is thanked for financial support.

References

Balling, N., Fuchs, S., Poulsen, S.E., Bording, T.S., Nielsen, S.B., Mathiesen, A. & Nielsen, L.H. 2016: Development of a numerical 3D geothermal model for Denmark. Proceedings, European Geothermal Congress, Strasbourg, France.

Kristensen, L., Hjuler, M.L., Frykman, P., Olivarius, M., Weibel, R., Nielsen, L.H. & Mathiesen, A. 2016: Pre-drilling assessments of average porosity and permeability in the geothermal reservoirs of the Danish area. Geothermal Energy **4**(6), 2–27, *http://dx.doi.org/10.1186/S40517-016-0048-6*

Vosgerau, H., Mathiesen, A., Andersen, M.S., Boldreel, L.O., Hjuler, M.L., Kamla, E., Kristensen, L., Pedersen, C.B., Pjetursson, B. & Nielsen, L.H. 2016: A WebGIS portal for exploration of deep geothermal energy based on geological and geophysical data. Geological Survey of Denmark and Greenland Bulletin **35**, 23–26.

Authors' address:

Geological Survey of Denmark and Greenland (GEUS), Øster Voldgade 10, DK-1350 Copenhagen K, Denmark. E-mail: *hv@geus.dk*

Pre-drilling geothermal assessment of porosity and permeability of the Bunter Sandstone Formation, onshore Denmark

Morten Leth Hjuler and Lars Kristensen

Denmark constitutes a low-enthalpy geothermal area. Current geothermal production takes place from two sandstone-rich formations: the Bunter Sandstone and Gassum Formations. These formations form major potential geothermal reservoirs, but information about the permeability of the potential sandstone reservoirs is difficult to obtain. This may be explained by deposition in a variety of environments under different climatic conditions, and by variable diagenetic overprint (Olivarius *et al.* 2015). Thus, the sandstone characteristics and properties are diverse, and in areas where wells are scarce, the assessment of the extent and reservoir properties of sandstone layers is associated with much uncertainty. In order to reduce exploration risk it is therefore essential to develop a robust method for prediction of porosity and permeability prior to drilling.

Kristensen *et al.* (2016) presented a five-step method for predicting porosity and permeability averages of prospective geothermal formations in Danish onshore areas with low data density. The method is based on the sandstone reservoir characteristics of the Gassum Formation from geological and petrophysical data acquired in deep wells. The main purpose was to reduce the uncertainties associated with prediction of reservoir properties.

The study presented here investigates the efficiency of the five-step method when applied to the Bunter Sandstone Formation. The study area extends from the west coast of Denmark to the east coast of southernmost Sweden, and from the Danish border with Germany to just north of the Ringkøbing–Fyn High (Fig. 1). Farther north, the Bunter Sandstone Formation grades into the partly contemporary Skagerrak Formation. Eighteen wells provided well-log and core-analysis data from the formation.

The five-step method

Kristensen *et al.* (2016) developed the five-step method by integrating well log data from the Gassum Formation with porosity and permeability measurements obtained from conventional core analysis (CCAL). The main concept behind the method is that the porosity is related primarily to depth, whereas the permeability depends on a range of parameters including porosity, mineralogy, grain size and sorting. Thus, if the burial depth for a particular potential reservoir layer is known, a relatively reliable porosity estimate may be derived (step 1). A permeability estimate may then be obtained from a porosity–permeability rela-

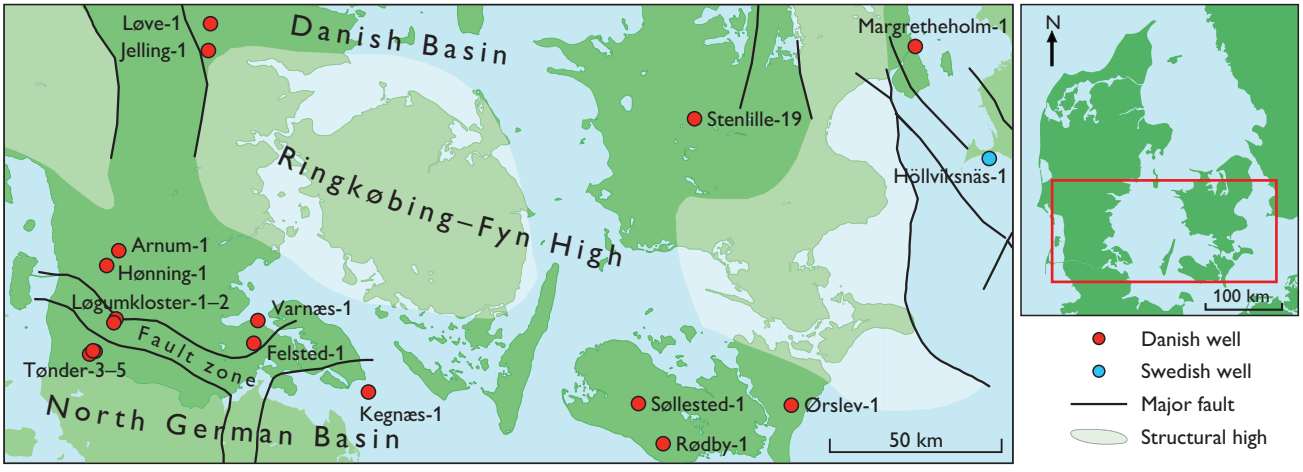

Fig. 1. The approximate extent of the Bunter Sandstone Formation in southern Denmark and adjacent areas (as delimited by the map frame), showing major structural elements and locations of investigated wells. Maps showing e.g. the extent, thickness and data sources of the Bunter Sandstone Formation are available from theWebGIS portal at the Geological Survey of Denmark and Greenland (*http://dybgeotermi.geus.dk/*).

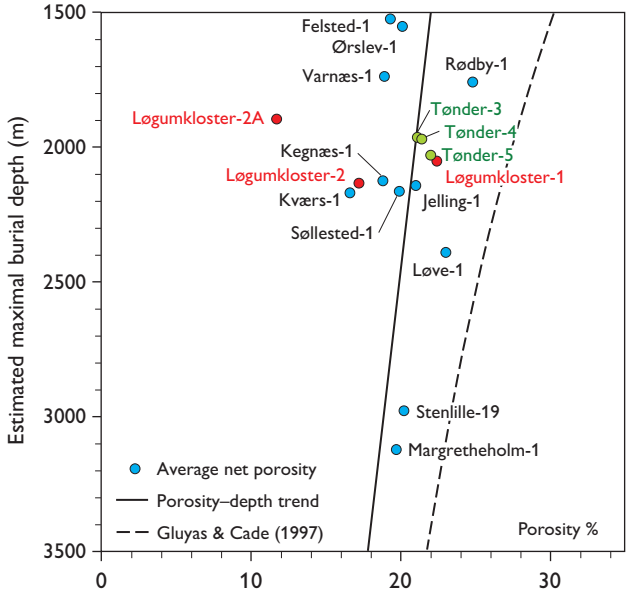

Fig. 2. Porosity–depth model (step 1) for the Bunter Sandstone Formation. The shown model (black line) is an estimate by the authors; the Løgumkloster wells were excluded from the model (see text) due to their location in a fault zone. A mechanical compaction curve (Gluyas & Cade 1997) is shown for comparison. Modified from Kristensen *et al.* (2016).

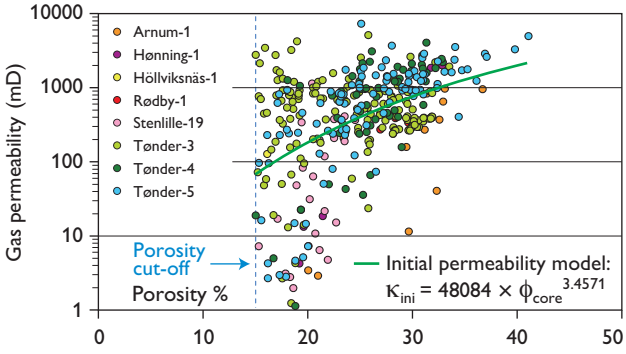

Fig. 3. Initial permeability model (step 2) for the Bunter Sandstone Formation.

tion (steps 2–4), and finally, the uncertainty can be assessed (step 5). Therefore the depth of the sandstone layer is required. In areas with no wells, the depth can only be estimated from seismic data, which therefore indirectly control whether the five-step method can be applied. Below, the main components of the five steps are defined and explained; for a detailed description of the concept, refer to Kristensen *et al.* (2016).

Step 1: Porosity–depth model. In order to predict the porosity of a formation, a regional porosity–depth relation is established. Log-derived, effective porosity data subjected to cut-off by shale content (<30%) and porosity (>15%) are averaged for each well and plotted against estimated maximum burial depth. The resulting relation, the porosity–depth model, is expressed as $\varphi_{log} = a + b \times D$ (Equation 1), where φ_{log} is the log-derived porosity, D is the burial depth and a and b are constants.

Step 2: *Initial permeability model.* An initial, basin-wide porosity–permeability relation based on core-analysis data is established in order to predict permeability. Subsequent to porosity cut-off (15%), this relation, i.e. the initial permeability model, is expressed as $k_{ini} = a \times \varphi_{core}^{\ b}$ (Equation 2), where k_{ini} is the core-gas permeability, φ_{core} is the core porosity and a and b are constants.

Step 3: General permeability model. This model uses log-derived, averaged permeabilities with the purpose of incorporating a dataset encompassing the entire formation and not only covering parts of the formation as is mostly the case with the core-based dataset used in step 2. Equation 2 is used to calculate permeability estimates from the log-derived porosity. Shale and porosity cut-offs of 30% and 15%, respectively, are applied. A cross-plot between log-derived and averaged porosity and permeability data points forms the basis for definition of a general permeability model expressed as $k_g = a \times \varphi_{log}^{\ b}$ (Equation 3), where k_g is the log-derived permeability, φ_{log} is the log-derived porosity and a and b are constants.

Step 4: Local permeability model. The general permeability model is adapted to local conditions by multiplying Equation 3 with a constant, C. Thus, the general permeability model constitutes a template for the local permeability model, which may be expressed as $k_L = C \times k_G$ (Equation 4), where k_L is the local permeability.

Step 5: Permeability-uncertainty range. A local area featuring several wells with a sufficient amount of appropriate log data is selected and a local permeability model is established. The extensive source data ensure a statistically well-restrained model and a consistent uncertainty range, which is assumed to be applicable to local models within the same formation in other parts of the Danish area. Below, the results of applying the five-step method to the Bunter Sandstone Formation in Denmark are described.

Application of the five-step method

Fourteen wells (Fig. 1) provided data for the generation of a porosity–depth model for the Bunter Sandstone Formation (Fig. 2); data from the Løgumkloster-1, 2 and 2A wells were excluded because of their location in a fault zone (Fig. 1) where tectonic activity may have altered the sandstone properties.

The porosity–depth model (step 1). Unfortunately, the scattered data distribution prevented derivation of a mathematically defined trend line, and thus a reliable poros-

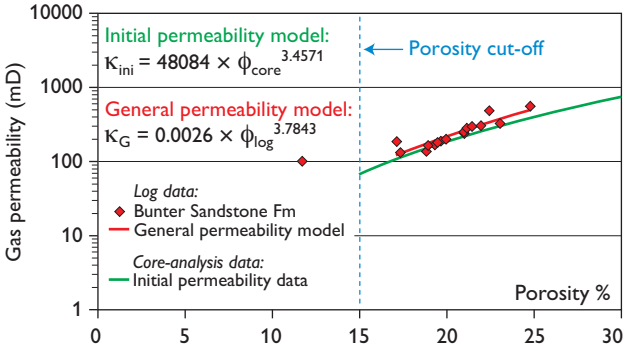

Fig. 4. Initial and general permeability models (steps 2, 3) for the Bunter Sandstone Formation after averaging the log-derived permeability and porosity.

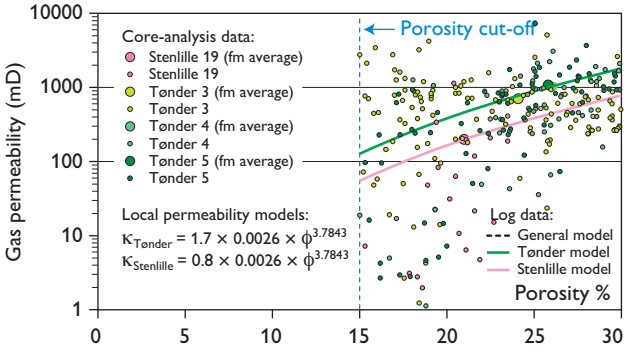

Fig. 5. Local permeability models (step 4) for the Bunter Sandstone Formation in the Tønder and Stenlille areas.

ity–depth model could not be generated. The shown trend line is the authors' best estimate based on their general experience and knowledge of petrographic characteristics and diagenetic overprints. The generation of a permeability–depth model was attempted as an alternative to the porosity–depth model, but without success as the scattered data distribution prevented establishment of a well-defined trend line.

The initial permeability model (step 2). Eight of the wells shown in Fig. 1 provided core-analysis data for the initial permeability model (Fig. 3). In order to generate a reliable porosity–permeability relation based on comparable measurements, only permeabilities obtained from cleaned, unflawed plugs of productive lithologies, measured under similar testing conditions were used. Data from uncleaned plugs and data points representing low permeabilities (<1 mD) and unproductive lithologies (claystone/shale) were removed from the dataset. Subsequently, shale and porosity cut-offs of 30% and 15%, respectively, were applied. The initial permeability model is based on 360 data points and is expressed by Equation 5: $k_{ini} = 48084 \times \varphi_{core}^{3.4571}$, where k_{ini} is in mD and φ_{core} is in per cent.

The general permeability model (step 3). The log-derived permeability was calculated for 16 wells (Fig. 1) using Equation 5 with the log-derived porosity as input. Løgumkloster-2A was discarded due to porosity cutoff. Subsequently, the log-derived permeability was averaged and a cross-plot between averaged log-derived porosity and permeability was generated (Fig. 4). The general permeability model is expressed by Equation 6: $k_g = 0.0026 \times \varphi_{log}^{3.7843}$ (Fig. 4). The introduction of the general permeability model imposes a slightly higher specific permeability estimate than that calculated from the initial permeability model, i.e., $k_g > k_{ini}$ (Fig. 4).

The local permeability model (step 4). Local permeability models were generated for the Tønder and Stenlille areas in order to demonstrate the variability of sandstone reservoirs within the Bunter Sandstone Formation (Fig. 5). For the Tønder area, the local permeability model is expressed as $k_{Tønder} = 1.7 \times (0.0026 \times \varphi^{3.7843})$ (Equation 7) and for the Stenlille area as $k_{Stenlille} = 0.8 \times (0.0026 \times \varphi^{3.7843})$ (Equation 8).

Permeability-uncertainty range (step 5). Only the Tønder area provides the data density needed for establishing an uncertainty range for a local permeability model. However, the number of data-supplying wells is limited to 3 (Tønder-3–5), and the statistical basis from the available Bunter Sandstone Formation data is insufficient to assess the uncertainty range.

Results and discussion

Porosities of the Bunter Sandstone Formation are lower than derived from the mechanical compaction curve for uncemented sandstones (step 1, Fig. 2), indicating that most of these sandstones contain clay and diagenetic cement (Kristensen *et al.* 2016). At greater depths, the sandstones preserve relatively high porosity due to microporosity within detrital clays and diagenetic iron oxide/hydroxide coatings that seemingly retard quartz cementation (Olivarius *et al.* 2015). Although a well-defined porosity–depth model (step 1) could not be created for the Bunter Sandstone Formation, the range of log-derived average porosities from 17% to 25% within the 1500–3100 m depth interval indicates favourable porosity conditions irrespective of maximum burial depth (Fig. 2). A corresponding averaged permeability range was calculated using the general permeability model (step 3, Equation 6) with 17% and 25% as porosity inputs. Within these bounds the permeability ranges from 132–557 mD (Fig. 6). From this observation, the geothermal prospectivity of the Bunter Sandstone Formation is significant, provided sufficient reservoir thickness and temperature are present.

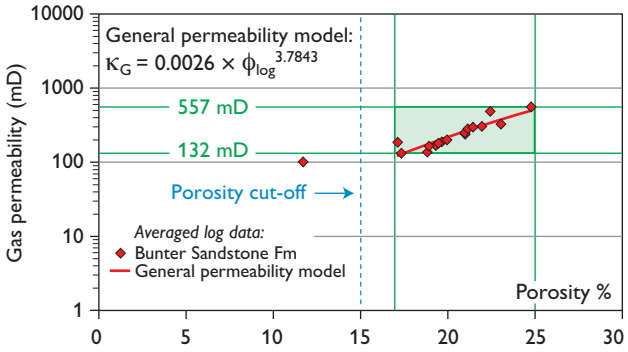

Fig. 6. Porosity and permeability range for the Bunter Sandstone Formation in the investigated wells in Denmark.

The vast majority of data behind the initial permeability model (k_{ini}, step 2) belong to the Tønder-3–5 wells. Therefore, k_{ini} represents the Tønder area rather than the entire study area. This data distribution issue was resolved by applying the averaging technique, whereby each well is represented by a single data point in the porosity–permeability plot. Thus, by using averaged data, each well becomes equally influential in the general permeability model (k_G, step 3), see Fig. 4. Further benefits of averaging the data are a dramatic reduction of the scatter of core-analysis measurements (Fig. 3) and a significant narrowing of the uncertainty band associated with average permeability estimates. In step 4, the local permeability models generated for the Tønder and Stenlille areas, $k_{Tønder}$ and $k_{Stenlille}$, demonstrate the importance of including local geological data when establishing local permeability models. At any porosity, $k_{Tønder}$ is 1.7 times higher than k_G and more than twice that of $k_{Stenlille}$. In contrast, $k_{Stenlille}$ is 0.8 times lower than k_G. These permeability variations may be explained by variations in deposition environment and maximum burial depth. At Tønder, aeolian deposition favoured the generation of well-sorted, clay-free sandstones which, subsequent to maximum burial of *c.* 2000 m, resulted in high average porosities and permeabilities (*c.* 22% and 300 mD, respectively); the presence of nitrogen gas may play a porosity-preserving role. At Stenlille, the sandstones were deposited in alluvial fan and braided river systems (Olivarius & Nielsen 2016) and maximum burial occurred at *c.* 3000 m, i.e. 1000 m deeper than at Tønder (Fig. 2), possibly causing the lower porosity (*c.* 19%) and permeability (*c.* 180 mD) due to poorer sorting and a higher degree of mechanical compaction and diagenesis.

It was not possible to establish a permeability uncertainty band for the Bunter Sandstone Formation (step 5). However, assuming that the Bunter Sandstone and Gassum Formations respond similarly to the geological factors controlling permeability variations, it is suggested that the uncertainty range derived for the Gassum Formation by Kristensen *et al.* (2016) is also applicable to the Bunter Sandstone Formation. Therefore, the uncertainty range may be expressed by multipliers of 2 and 0.5.

Conclusions

It was not possible to generate a reliable porosity–depth model (step 1) for the Bunter Sandstone Formation based on data and modelling from the Gassum Formation. However, using averaged porosities and permeabilities from all available wells (step 3), porosities from 17–25% and permeabilities from 132–557 mD can be modelled in the depth range 1500–3100 m. Local permeability models (step 4) for the Bunter Sandstone Formation in the Tønder and Stenlille areas differ significantly from the general permeability model (step 3), which emphasises the importance of using local geological data for calibration of the general permeability model. A permeability uncertainty band (step 5) could not be established for the Bunter Sandstone Formation due to insufficient data; however, the uncertainty range developed for the Gassum Formation in Kristensen *et al.* (2016) may be applied.

References

Gluyas, J. & Cade, C.A. 1997: Prediction of porosity in compacted sands. In: Kupecz, J.A., Gluyas J. & Block, S. (eds): Reservoir quality prediction in sandstones and carbonates. AAPG Memoir **69**, 19–28.

Kristensen, L., Hjuler, M.L, Frykman, P., Olivarius, M., Weibel, R., Nielsen, L.H. & Mathiesen, A. 2016: Pre-drilling assessments of average porosity and permeability in the geothermal reservoirs of the Danish area. Geothermal Energy **4:6**, 27 pp.

Olivarius, M. & Nielsen, L.H. 2016: Triassic paleogeography of the greater eastern Norwegian-Danish Basin: Constraints from provenance analysis of the Skagerrak Formation. Marine and Petroleum Geology **69**, 168–182.

Olivarius, M., Weibel, R., Hjuler, M.L., Kristensen, L., Mathiesen, A., Nielsen, L.H. & Kjøller, C. 2015: Diagenetic effects on porosity–permeability relationships in red beds of the Lower Triassic Bunter Sandstone Formation in the North German Basin. Sedimentary Geology **321**, 139–153.

Authors' address

Geological Survey of Denmark and Greenland, Øster Voldgade 10, DK-1350 Copenhagen K, Denmark. E-mail: *MLH@geus.dk*

Generation and origin of natural gas in Lower Palaeozoic shales from southern Sweden

Niels Hemmingsen Schovsbo and Arne Thorshøj Nielsen

The Lower Palaeozoic succession in Scandinavia includes several excellent marine source rocks notably the Alum Shale, the Dicellograptus shale and the Rastrites Shale that have been targets for shale gas exploration since 2008. We here report on samples of these source rocks from cored shallow scientific wells in southern Sweden. The samples contain both free and sorbed hydrocarbon gases with concentrations significantly above the background gas level. The gases consist of a mixture of thermogenic and bacterially derived gas. The latter likely derives from both carbonate reduction and methyl fermentation processes. The presence of both thermogenic and biogenic gas in the Lower Palaeozoic shales is in agreement with results from past and present exploration activities; thermogenic gas is a target in deeply buried, gas-mature shales in southernmost Sweden, Denmark and northern Poland, whereas biogenic gas is a target in shallow, immature-marginally mature shales in south central Sweden. We here document that biogenic gas signatures are present also in gas-mature shallow buried shales in Skåne in southernmost Sweden.

In south central Sweden (Västergötland, Östergötland, Närke and Öland, Fig. 1), shallow (present burial <150 m) immature to marginally mature bituminous shale has been known for decades to contain gas and is currently under exploration (see summary in Schultz *et al.* 2015). Since 2009, many deep (>800 m) exploration drillings in northern Poland (including the Lebork S-1 well, Lehr & Keeley 2016), the Vendsyssel-1 well in Denmark (Ferrand *et al.* 2016) and the A3-1, B2-1, C4-1 wells in Skåne in southernmost Sweden (Pool *et al.* 2012), have demonstrated that the Lower Palaeozoic shale succession contains gas also in these areas (Fig. 1). In Denmark and Skåne, the average gas content is 30 ft^3 gas per ton of rock in the organic-rich Alum Shale Formation (Pool *et al.* 2012; Ferrand *et al.* 2016). The equivalent shale formation in northern Poland contains up to 268 ft^3 gas per ton of rock in the Lebork S-1 well (Lehr & Keeley 2016), which is comparable to the content within the core area of North American shale gas-producing formations (e.g. Jarvie 2012).

In this study, we present empirical data on the composition and isotope signatures of gas measured in shallow (<158 m) core samples from five scientific core drillings in southern Sweden, viz. Albjära-1, Lönstorp-1, Gislövshammar-2, Hällekis-1 and Djupvik-1 (Fig. 1, Table 1). Sampling and analyses were performed in 1991–1992 as part of the *Energy Research Project EFP-1313/88-2* and the *Pre-Westphalian Source-Rocks in Northwest Europe* (PREWSOR) project (Schovsbo & Laier 2012). This paper aims at further characterising the gas composition.

Samples and analyses

The molecular composition and isotope signatures of the occurring gases were measured in 27 core samples (Table 1). The samples were selected during drilling and consist of 4–8 cm long core intervals with a diameter of 5.5 cm. The samples from Albjära-1 and Lönstorp-1 were sealed in metal containers and stored at –18°C until they reached the laboratory for analysis. The free gas was subsequently ana-

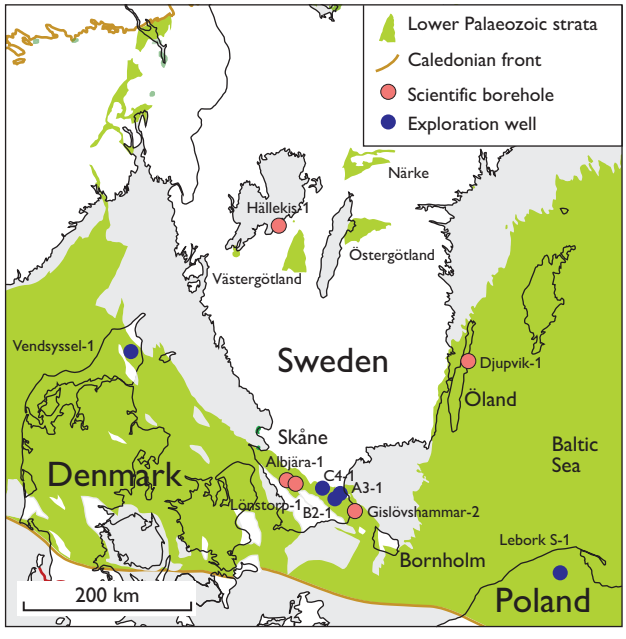

Fig. 1: Location of wells mentioned and occurrence of Lower Palaeozoic strata in southern Scandinavia. Modified from Nielsen & Schovsbo (2015).

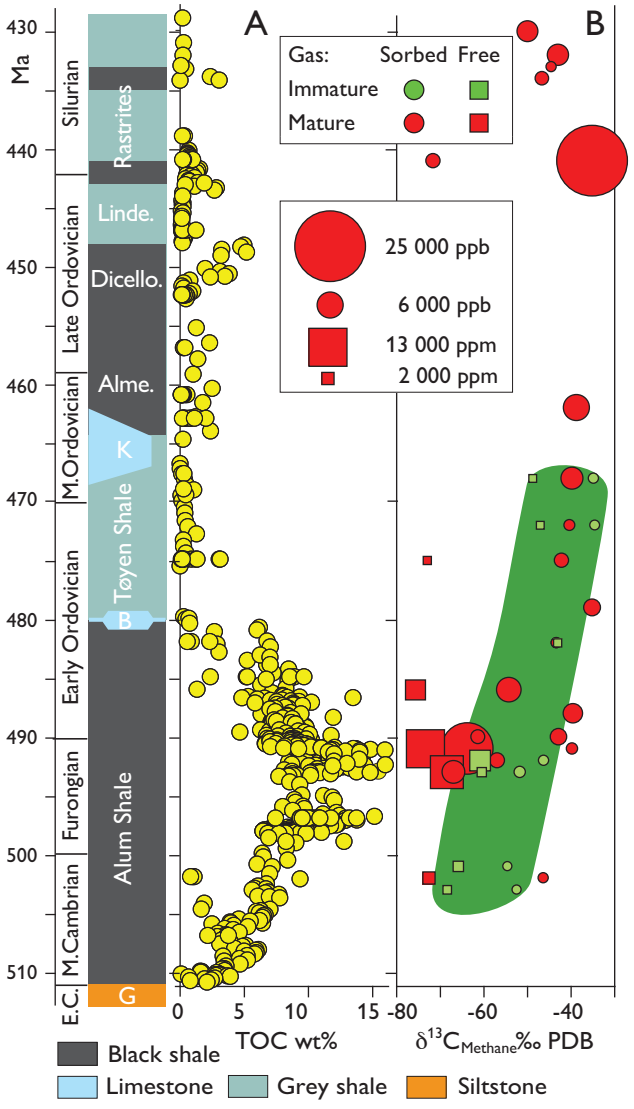

Fig. 2. Stratigraphy of the Lower Palaeozoic shales. **A**: Total organic carbon (TOC) content in shales from the Skåne–Bornholm area (modified from Schovsbo 2003). **B**: Methane isotope composition of sorbed and free gas from samples of thermally mature shale in the Albjära-1, Gislövshammar-2, and Lönstorp-1 wells and from samples of thermally immature shale in the Hällekis-1 and Djupvik-1 wells. **E.C.**: Early Cambrian. **G**: Gislöv Fm. **B**: Bjørkåsholmen Fm. **K**: Komstad Limestone. Alme.: Almelund Shale. Dicello.: Dicellograptus shale. Linde.: Lindegård Formation. Green area in **B** outlines the variation field defined by samples from the Djupvik-1 and Hällekis-1 wells.

lysed by the Geological Survey of Denmark and Greenland (GEUS) by puncturing the containers through a septum before opening. Samples from Gislövshammar-2, Hällekis-1 and Djupvik-1 were analysed by the Federal Institute for Geosciences and Natural Resources (BGR), Germany. These samples were stored at –18°C at the drill site and

Table 1. Wells and analysed samples§

Well	Formation	N	Depth range (m)
Gislövshammar-2	Tøyen S.	1	19.8
Gislövshammar-2	Alum S.	4	31.8–88.3
Djupvik-1	Alum S:	1	2.0
Hällekis-1	Tøyen S.	2	9.9–17.3
Hällekis-1	Alum S,	4	23.4–39.8
Albjära-1	Almelund	1	99.6
Albjära-1	Tøyen S.	3	114.8–134.5
Albjära-1	Alum S.	5	139.6–157.0

§Full analytical results are available on request from the first author.

subsequently transferred to a container filled with liquid nitrogen at –196°C. The free gas was measured by allowing the deep-frozen sample to equilibrate to room temperature in a sealed container. For all samples the sorbed gas in the rock matrix was liberated by treating the sample with phosphoric acid following the procedure outlined by Faber & Stahl (1983).

Gas composition

The sorbed methane concentrations range from 118 to 23867 ppb (micrograms per kg of rock) and the free gas contents from 3 to 13420 ppm (Fig. 2). The concentrations thus far exceed the level of background gas of 20–50 ppb for methane as defined by Whiticar (1994). The gas content is strongly related to thermal rank of the sampled shales. The gas-mature samples from Gislövshammar-2, Albjära-1 and Lönstorp-1 have *c.* ten times higher yields than the thermally immature samples from the Hällekis-1 and Djupvik-1 wells (Fig. 2). The gas content appears not to be related to the total organic content in the mature samples. This is exemplified by the fact that the highest yields of sorbed gas are found in the Rastrites Shale (TOC average <1%) and the lowest yields in the Alum Shale, which on average contains 9% TOC in Skåne and on Bornholm (Fig. 2).

Isotope composition and carbon isotope signatures

The gas molecule and isotopic compositions of the analysed samples plot within the bacterial to thermogenic fields in a Bernard diagram (Fig. 3A). The microbial gas is characterised by much higher negative isotope values than seen in the thermogenic-sourced methane. This signature is most clearly expressed in the free gas samples from mature shales that also have 10 to 100 times higher $C_1/(C_2+C_3)$ molecular ratios than the sorbed gas, which is also typical for biogenic gas (Fig. 3A).

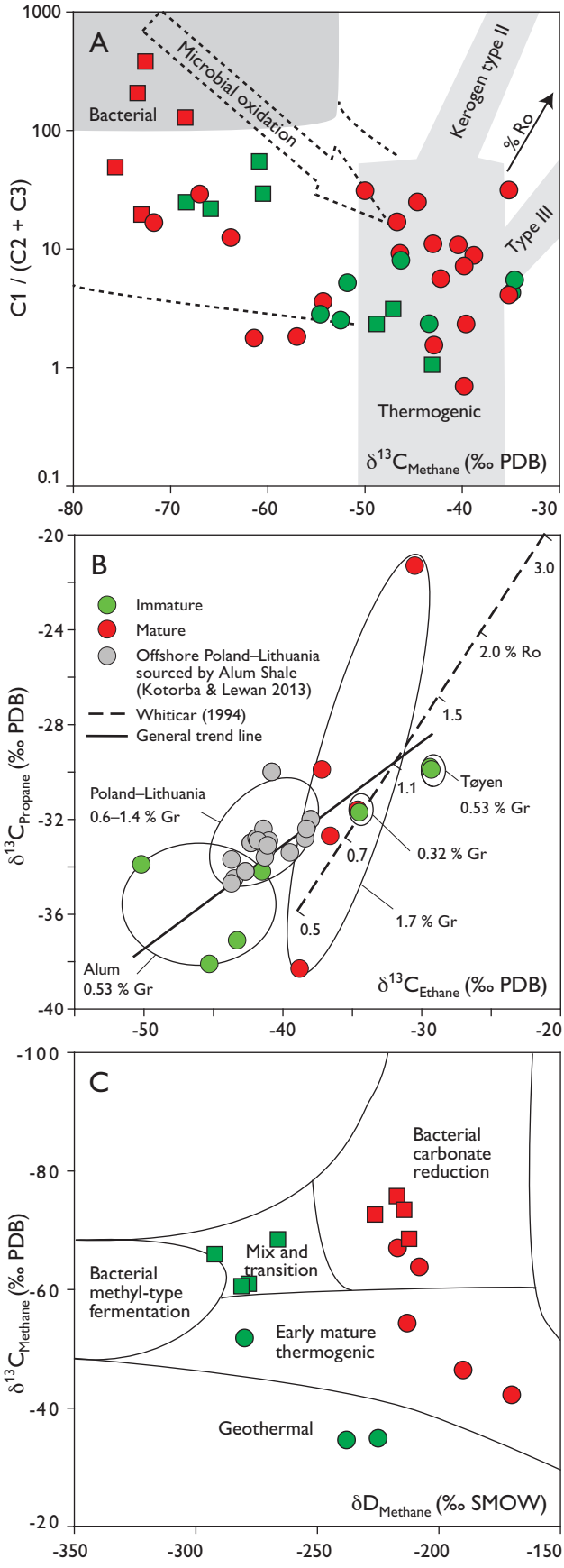

The propane versus ethane isotope gas signature is suggested to reflect the maturity of the source and this relationship can be used for a gas-to-source-rock correlation (Whiticar 1994). The analysed gas signatures follow this prediction, as immature Alum Shale samples from the Hällekis-1 well plot with relatively depleted isotope signatures of propane and ethane compared to the thermally mature Alum Shale samples (Fig. 3B). Isotope data from Lithuanian and Polish oil and gas reservoirs in Middle Cambrian sandstone, sourced by Alum Shale (Kotarba & Lewan 2013), plot with intermediate signatures (Fig. 3B).

The thermally mature samples (Gislövshammar-2 well), however, exhibit a considerable variation in propane isotope composition from –22 to –39‰ PDB, suggesting a mixture of differently derived gases. This may be caused by addition of bacterially derived ethane and/or biodegradation of a propane component (cf. Whiticar 1994). The thermally immature Alum Shale samples from the Djupvik-1 well (marked with 0.32 %Gr in Fig. 3B) and samples from Tøyen Shale from the Hällekis-1 well (marked as Tøyen 0.53%Gr in Fig. 3B) plot within an apparent gas maturity of 0.8–1.2% Ro according to the values indicated in Fig. 3B (Whiticar trend line), i.e. with much higher maturities than measured, suggesting that gas migration has occurred. In the Hällekis-1 well the migrated gas may have formed in response to intrusion of Permo-Carboniferous dikes that locally matured the shales in south central Sweden (cf. Schultz *et al.* 2015). In the vicinity of the Djupvik-1 drill site-mature shale and igneous activity are unknown and the relatively high maturity remains puzzling.

Deuterium isotopes

Measurements of deuterium and carbon isotopes in methane offer additional information on the source of the natural gases and on the processes that may have modified their composition (Whiticar 1994). Figure 3C shows the deuterium versus carbon isotope composition of methane in the analysed samples. The gas composition exhibits a

Fig. 3. Compostion and isotope signatures of organic carbon. **A**: 'Bernard diagram' showing the ratio $C_1/(C_2+C_3)$ versus $\delta^{13}C_{Methane}$ for all samples. This type of diagram is used to determine the origin of the gases and is modified from Whiticar (1994). For legend, see Fig. 2. **B**: Relationship between $\delta^{13}C_{Ethane}$ and $\delta^{13}C_{Propane}$. Tøyen and Alum 0.53% Gr denote stratigraphy and maturity of samples from the Hällekis-1 well. The graptolite reflectance (% Gr) is from Pedersen *et al.* (2013); Grönvik locality is used for Djupvik-1; estimate for offshore Poland. **C**: δD and $\delta^{13}C$ for methane. For legend, see Fig. 2. The isotope signatures of the various sources are from Whiticar (1994).

large degree of scatter, but free gas from thermally mature samples plots in the bacterial carbonate reduction field, whereas free gas from immature samples plots towards the bacterial methyl-type fermentation fields, suggesting that different processes generated the depleted methane isotope compositions (Fig. 3C). The sorbed gas compositions in general plot away from bacterial sources, indicating that a thermogenic signature is preserved (Fig. 3C).

Implications for shale-gas prospectivity

The gas-isotope composition suggests that significant post-generation modification occurred although the timing is unknown. The biogenic isotope signature of the gases in Skåne resembles similar signatures seen in Östergötland (Schultz *et al.* 2015). Here Schultz *et al.* inferred that methyl-fermenting processes contributed to the methane content. However, the gas-isotope signature was not as depleted as seen in this study, possibly owing to the mixed shale oil – biogenic nature of the Östergötland Alum Shale play. According to Schultz *et al.* (2015) the biogenic gas was generated after the Pleistocene glaciation, as modern meteoric water was able to infiltrate the shale and create the right conditions for bacterial activities. We envisage that similar conditions may have affected the shallowly buried shales in Skåne. Krüger *et al.* (2014), however, show that highly mature kerogen has a much smaller microbial generative gas potential than immature to marginally mature kerogen, since thermal maturity limits the amount of easily biodegradable organic matter that can be transformed to methane.

Conclusions

Lower Palaeozoic shales in south central Sweden and southernmost Sweden contain natural gas that exceeds the level of background gas. The gas content is strongly related to the thermal rank of the sampled shales, and mature samples have approximately ten times higher yields than the immature samples. The gas is generated by both thermogenic and bacterial processes. The microbial gas signature is most clearly expressed in the free gas samples from mature shales that also have 10 to 100 times higher molecule $C_1/(C_2+C_3)$ ratios than the sorbed gas. Migration may have occurred related to gas formation in response to intrusion of Permo-Carboniferous dikes that locally matured the shales in south central Sweden.

Acknowledgements

We thank Troels Laier (GEUS) for comments and suggestions to an earlier version of the manuscript. The authors wish to thank Mikael Erlström and Maciej Kotarba for constructive comments that improved the paper.

References

Faber, E. & Stahl, W. 1983: Analytic procedure and results of an isotope geochemical surface survey in an area of the British North Sea. Geological Society Special Publications (London) **12**, 51–63.

Ferrand, J., Demars, C. & Allache, F. 2016: Denmark – L1/10 Licence relinquishment recommendations report. Total E&P, Memo 1-9. Available from: *http://www.ft.dk/samling/20151/almdel/efk/bilag/353/1651289.pdf*. Verified 7.4.2017.

Jarvie, D.M. 2012: Shale resource systems for oil and gas: Part 1 – Shale-gas resource systems. AAPG Memoir **97**, 69–87.

Kotarba, M.J. & Lewan, M.D. 2013: Sources of natural gases in Middle Cambrian reservoirs in Polish and Lithuanian Baltic Basin as determined by stable isotopes and hydrous pyrolysis of Lower Palaeozoic source rocks. Chemical Geology **345**, 62–76.

Krüger, M., van Berk, W., Arning, E.T., Jiménez, N., Schovsbo, N.H., Straaten, N. & Schulz, H.-M. 2014: The biogenic methane potential of European gas shale analogues: Results from incubation experiments and thermodynamic modelling. International Journal of Coal Geology **136**, 59–74.

Lehr, J.H. & Keeley, J. 2016: Alternative energy and shale gas encyclopedia. 912 pp. John Wiley & Sons.

Nielsen, A.T. & Schovsbo, N.H. 2015: The regressive Early – Mid Cambrian 'Hawke Bay Event' in Baltoscandia: Epeirogenic uplift in concert with eustasy. Earth Science Reviews **151**, 288–350.

Petersen, H.I., Schovsbo, N.H. & Nielsen, A.T. 2013: Reflectance measurements of zooclasts and solid bitumen in Lower Palaeozoic shales, southern Scandinavia: correlation to vitrinite reflectance. International Journal of Coal Petrology **114**, 1–18.

Pool, W., Geluk, M., Abels, J. & Tiley, G. 2012: Assessment of an unusual European Shale Gas play – The Cambro–Ordovician Alum Shale, southern Sweden: Proceedings of the Society of Petroleum Engineers/European Association of Geoscientists and Engineers Unconventional Resources Conference, Vienna, Austria, 20–22 March, 2012, 152339.

Schovsbo, N.H. 2003: The geochemistry of Lower Palaeozoic sediments deposited on the margins of Baltica. Bulletin of the Geological Society of Denmark **50**, 11–27.

Schovsbo, N.H. & Laier, T. 2012: Composition and gas isotope signature of shale samples from 5 scientific wells in Sweden. Geological Survey of Denmark and Greenland Report **2012/17**, 1–25.

Schulz, H.-M., Biermann, S., van Berk, W., Krüger, M., Straaten, N., Bechtel, A., Wirth, R., Lüders, V., Schovsbo, N.H. & Crabtree, S. 2015: From shale oil to biogenic shale gas: retracing organic-inorganic interactions in the Alum Shale (Furongian-Lower Ordovician) in southern Sweden. AAPG Bulletin **99**, 927–956.

Whiticar, M.J. 1994: Correlation of Natural Gases with their Sources. AAPG Memoir **60**, 261–283.

Authors' addresses

N.H.S., *Geological Survey of Denmark and Greenland (GEUS), Øster Voldgade 10, DK-1350 Copenhagen K, Denmark*; E-mail: *nsc@geus.dk*

A.T.N., *Department of Geosciences and Natural Resource Management, University of Copenhagen. Øster Voldgade 10, DK-1350 Copenhagen K, DK.*

Prospectivity mapping for orogenic gold in South-East Greenland

Björn H. Heincke and Bo Møller Stensgaard

Numerous studies have proven that conceptual targeting based on integration of various geo-datasets can aid exploration companies to identify exploration targets (e.g. Joly *et al.* 2013). This is particularly true in remote, underexplored areas that are commonly just covered by airborne geophysics and remote sensing and mapped geologically only on a regional scale. Such regions are 'exploration greenfields' and may possess undiscovered economic deposits.

The ice-free coastal strip of the Archaean craton in South-East Greenland overprinted by Palaeoproterozoic orogeny (Fig. 1) is such an area due to its remoteness and arctic-alpine conditions; and deep-seated, repeatedly reactivated structures and new magmatic episodes make large parts of this region potential for orogenic Au occurrences. Although only minor Au mineralisation has been found to date, a large number of Au-bearing rock samples (Petersen & Thomsen 2014) and stream sediment anomalies suggest an elevated potential particularly in the Tasiilaq area (Fig. 1B). A large field mapping campaign (Kolb *et al.* 2016) and regional airborne magnetic surveys (Riisager & Rasmussen 2014) were conducted from 2012 to 2015, resulting in a uniform coverage of relevant geological and geophysical information, which can be combined with satellite remote sensing data. It was therefore decided to apply a fuzzy logic-based mineral prospectivity mapping (MPM) procedure (see below and Fig. 2) combined with a mineral system approach of orogenic Au (McCuaig *et al.* 2010).

However, it was a challenge to apply this approach for several reasons: (1) Strong topographical variations in this region distort some of the evidential datasets used in the MPM and their effect has to be minimised (e.g. aeromagnetic data are strongly affected by flight height). (2) Fjords, ocean and glaciers strongly limit the accessible area for prospection, lead to a non-uniform data coverage for many datasets and affect the accuracy of evidential maps associated with the MPM. (3) lack of known *in-situ* Au mineralisation limits the validation of final prospectivity maps. (4) the geological history is not fully understood, making it difficult to discard irrelevant features (e.g. magnetic anomalies may be related to insignificant Palaeogene dykes or important older faults). Such difficulties occur in many parts of Greenland, and this study gives an idea of how meaningful MPM studies might be in other regions.

Regional geology

The study area comprises the Archaean North Atlantic craton (NAC) in the south and the Palaeoproterozoic

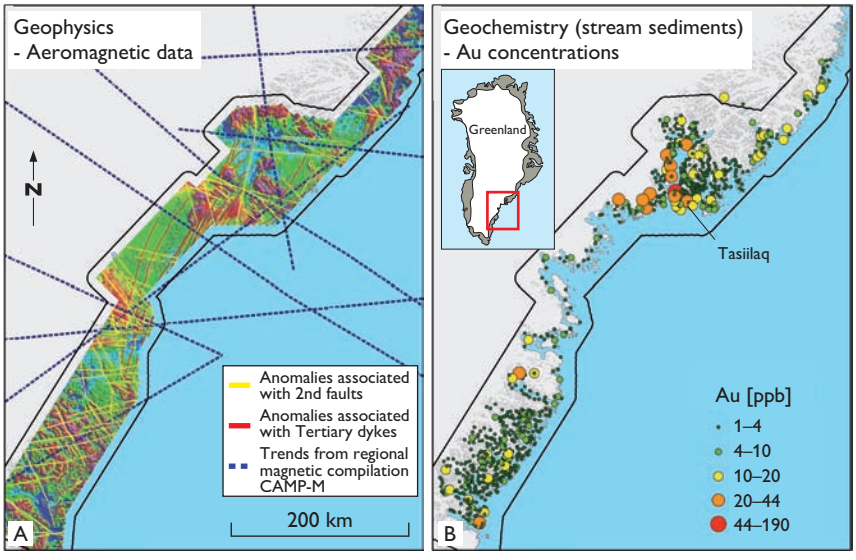

Fig. 1. Examples of data types used for the MPM study in South-East Greenland (framed area in index map). **A**: Mapped elongate anomalies from aeromagnetic data (see background map in Riisager & Rasmussen 2014) and regional magnetic compilations used as proxies for faults of 1st and 2nd order in the critical processes 'source' and 'pathways'. **B**: Stream sediment Au concentrations used as a proxy for the 'chemical scrubber'. Black lines in **A** and **B** mark the area used in the interference network.

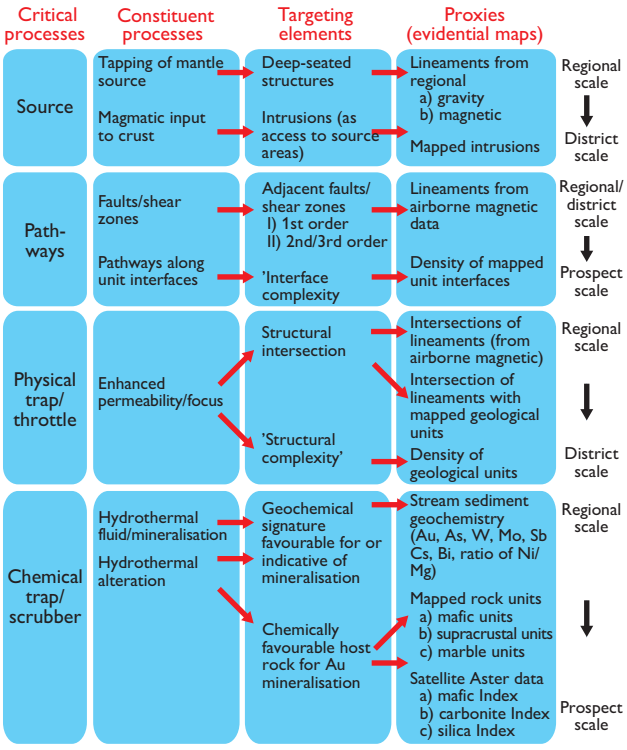

Fig. 2. The mineral system model used for the orogenic gold deposit type. The critical processes are associated with a series of constituent processes, targeting elements and proxies.

Nagssugtoqidian orogen in the north (Figs 1, 3; Kolb *et al.* 2016). To the north, the orogen includes an Archaean foreland that comprises rocks from the Rae Craton. To the south, the margin of the NAC is affected by deformation and intrusives of the Palaeoproterozoic Ketilidian orogen. The Nagssugtoqidian Orogen comprises tectonically reworked Archaean rocks subjected to high-grade metamorphism and slivers and belts of Palaeoproterozoic metavolcanic, metasedimentary and intrusive rocks. On the basis of differences in lithologies and tectono-metamorphic history, the orogen is divided into four terranes, from north to south the Isortoq terrane, the Ammassalik intrusive complex (AIC) and the Kuummiut and Schweizerland terranes. The NAC is dominated by felsic orthogneisses with subordinate supracrustal rocks, with syn- to post-tectonic alkaline intrusions in the Skjoldungen area (63°10′–63°40′N). Main deformation events within the NAC are the Timmiarmiut and Skjold-ungen orogenies.

Continental breakup in the Palaeogene led to the emplacement of coast-parallel dykes in the northern area (north of 64°N) that can clearly be identified as anomalies in aeromagnetic data (red lines in Fig. 1A).

The mineral prospectivity mapping approach

Mineral prospectivity maps used for targeted exploration highlight areas with coincident geological features that are important for a given commodity. For our mineral prospectivity mapping we use geoscience data that were selected on the basis of a mineral system approach for orogenic gold. The mineral system approach provides a holistic view of the critical geological, physical and chemical processes needed to generate a mineral deposit. For orogenic Au systems McCuaig *et al.* (2010) identified the following critical processes: (i) a source of Au in the upper mantle, (ii) active pathways allowing fluids to flow through the crust, (iii) physical traps in which fluids are throttled and focused and (iv) a chemical 'scrubber' associated with hydrothermal mineralisation and alteration (Fig. 2). Since ore-forming processes typically cannot be directly mapped, they must be inferred from geological features referred to as targeting elements. These are rarely directly measurable but are approximated from responses in geoscience data such as faults estimated from magnetic anomalies. These proxies are represented in this approach by uniform spatial grids named evidential maps (EM) that can easily be combined to build prospectivity maps.

To quantify and combine all information we use 'fuzzy logic' operations which have proven in many cases (e.g. Joly *et al.* 2013) to be suitable for building meaningful mineral prospectivity maps. First, all EMs were rescaled (i.e. transformed into maps with values ranging from 0 to 1) by employing so-called fuzzy membership functions to obtain representative maps describing how far the prospectivity is supported (0.0 = not at all; 1.0 = fully). In a multistage interference network, fuzzy OR (maximum operator equivalent to logical union) and AND (minimum operator equivalent to logical intersection) operators were then applied to combine the EMs to create first intermediate fuzzified maps representing the four critical processes and finally fuzzy prospectivity maps used to predict areas of high Au potential (electronic supplementary (ES) figure: Fig. ES1). Further details about the mineral prospecitivty mapping procedure, the underlying mineral system approach and data sets are given in Stensgaard & Heincke (2016).

Calculation of prospectivity maps

Most of the EMs associated with structural information were derived from anomalies in potential field data, either from regional data compilations (Gaina *et al.* 2011) or recent aeromagnetic surveys (Fig. 1A). A 1:500 000 scale digital geological map (Stensgaard *et al.* 2016) was used

to extract additional structural information (Fig. ES2A) and to identify geological units and other settings favourable for Au mineralisation, e.g. intersections between units and cross-cutting structural elements. Other EMs associated with preferable rock types were obtained from mineral indices of ASTER satellite data (Fig. ES2B). Finally, the contents of Au and geochemical pathfinder elements for Au mineralisation (As, Sb, Cs, W, Bi, Mo, Ni/Mg) in stream-sediment samples (Fig. 1B) were presented in EMs that reflect relevant hydrothermal mineralising fluids as well as associated alteration halos.

The non-uniform spatial data coverage made it necessary to use interpolation (kriging and natural neighbour gridding) to create the related EMs. To rescale the EMs we used fuzzy membership functions that were estimated on the basis of qualitative and quantitative knowledge (see Fig. ES3). The region used to determine the EMs and perform the interference network calculations comprises both the ice-free onshore, adjacent offshore and ice-covered areas; however, only accessible ice-free areas were considered in the evaluation of prospectivity maps (Figs 3A, B).

There are uncertainties in all steps of the mineral prospecitivity mapping procedure (McCuaig *et al.* 2010), and it is important to test how reliable the final prospectivity maps are. If known mineral occurrences that originate from the assumed mineral system are present, one option is to construct prediction-rate curves to evaluate and adapt the prospectivity procedure (Carranza 2009). However, in the absence of such mineral occurrences, we used stream-sediment locations with Au concentrations > 20 ppb as 'deposits' in such curves (see circles in Figs 3A, C). This led to a number of inaccuracies, as sample locations typically do not coincide with locations in the catchment area where gold was eroded, and where no unique and simple function generally links concentrations of Au occurrences and stream-sediment samples. Hence, conclusions based on such validation should be considered carefully.

To evaluate the robustness of the mineral prospectivity mapping and the relevance of different targeting elements,

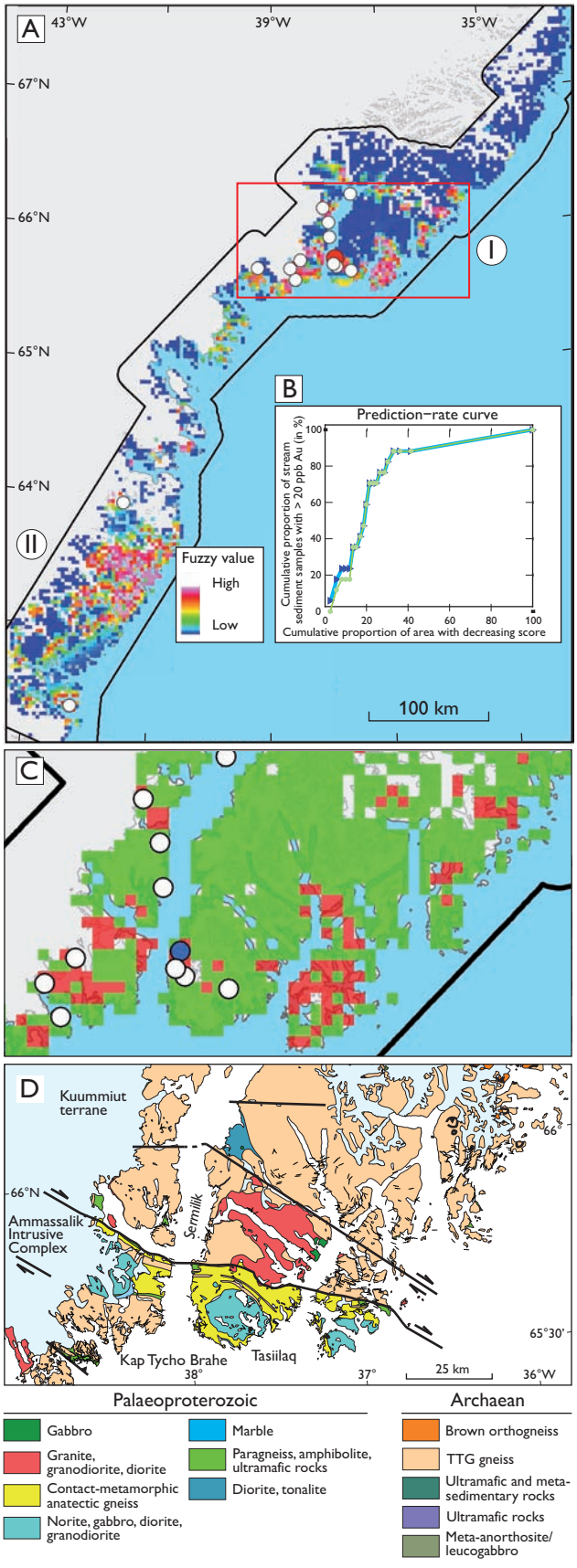

Fig. 3. **A**: Final prospectivity map obtained by using all evidential maps. White circles: Stream sediment locations with Au > 20 ppb. Red circle: the sample with highest concentration of 196 ppb. **B**: Validation curves showing the cumulative area with decreasing score versus the cumulative number of stream sediment samples with > 20 ppb Au in the same area. (In the blue and the green curves, EMs associated with stream-sediment data from Au and all elements are not incorporated). **C**: Map of the area around Tasiilaq (red rectangle in **A**). Pixels with a high fuzzy value of > 0.85 are shown in red. **D**: Geological map of the same area.

we repeated the procedure with several different combinations of EMs (e.g. all EMs, all EMs except for the one based on Au concentration from stream sediments). Irrespective of the combination of EMs, the resulting validation curves show that high fuzzy scores correlate strongly with elevated Au in stream sediment samples (Fig. 3B) suggesting that the mineral prospectivity mapping is reliable and robust.

Results and discussion

To identify areas with high orogenic Au potential, we highlighted pixels (pixel size: 3 × 3 km) in the prospectivity map with high fuzzy values > 0.85 (red colour in Fig. 3C) associated with ~8% of the total area. Particularly the Tasiilaq (I) and the Skjoldungen (II) regions are characterised by high scores (Fig. 3A). In region I, a couple of areas stand out as being anomalous in gold and its pathfinder elements; and locations of both stream sediment samples with high Au concentrations (Fig. 1B) and Au-bearing rock samples (Petersen & Thomsen 2014) coincide well with areas having elevated membership fuzzy values. The highest scores are aligned along a WNW–ESE-oriented corridor that coincides with the Ammassalik intrusive complex (AIC). In particular the boundaries of the AIC to the Kummuit and the Isortoq terranes in the north and south are identified as prospective (Fig. 3D; Kolb 2014). A major structure that likely represents a suture zone which may have acted as a mantle source-tapping feature is reported along the northern boundary of the AIC (Kolb 2014) and is confirmed by geophysics (Riisager & Rasmussen 2014). Other deep-seated structures have been suggested south of the AIC in the Isortoq Terrane (Nutman *et al.* 2008). This means that an elevated Au potential from the mineral prospectivity mapping is supported by the main geological settings. In contrast, no elevated Au concentrations from samples or other indications for Au occurrences exist within the cratonic Skjoldungen region (II). The latter area is characterised by predominant mafic granulites with thin belts of deep-crustal-formed mafic and ultramafic rocks considered unfavourable for orogenic Au mineralisation (Kolb *et al.* 2016). At this stage, the mineral system approach is set up to not exclude rock units formed at large depths, and it should be adjusted in future to take this information into account.

In summary, the results of this study suggest that modern mineral prospectivity mapping schemes based on an mineral system approach can improve the geological understanding of mineral prospectivity even in regions that are not densely covered by all data types and underexplored.

Acknowledgements

The project was jointly financed project by GEUS and the Ministry of Mineral Resources, Government of Greenland. We thank S. Weatherley and E.V. Sørensen, GEUS, for comments and contributions.

References

Carranza, E.J.M. 2008: Geochemical anomaly and mineral prospectivity mapping in GIS. Handbook of Exploration and Environmental Geochemistry **11**, 351 pp.

Gaina, C., Werner, S.C., Saltus, R., Maus, S. & the CAMP-GM group 2011: Circum-Arctic mapping project: new magnetic and gravity anomaly maps of the Arctic. Geological Society (London) Memoirs **35**, 39–48.

Joly, A., Dentith, M.C., Porwal, A., Spaggiari, C.V., Tyler, I.M. & McCuaig, T.C. 2013: An integrated geological and geophysical study of the West Arunta Orogen and its mineral prospectivity. Geological Survey of Western Australia Report **113**, 89 pp.

Kolb, J. 2014: Structure of the Palaeoproterozoic Nagssugtoqidian Orogen, South-East Greenland: model for the tectonic evolution. Precambrian Research **255**, 809–822.

Kolb, J., Stensgaard, B.M. & Kokfelt, T.F. 2016 (eds): Geology and Mineral Potential of South-East Greenland, Danmarks og Grønlands Geologiske Undersøgelse Rapport **2016/38**, 157 pp.

McCuaig, T.C., Beresford, S. & Hronky, J. 2010: Translating the mineral systems approach into an effective exploration targeting system. Ore Geology Reviews **38**, 128–138.

Nutman, A.P., Kalsbeek, F. & Friend, C.R.L. 2008: The Nagssugtoqidian Orogen in South-East Greenland: evidence for Paleoproterozoic collision and plate assembly. American Journal of Science **308**, 529–572.

Petersen, J. & Thomsen, L.L. 2014: Results in South-East Greenland from Ujarassiorit-program. Danmarks og Grønlands Geologiske Undersøgelse Rapport **2014/79**, 65–66.

Riisager, P. & Rasmussen, T.M. 2014: Aeromagnetic survey in southeastern Greenland: project Aeromag 2013. Geological Survey of Denmark and Greenland Bulletin **31**, 63–66.

Stensgaard, B.M., Kolb, J., Kokfelt, T.F. & Klausen, M.B. 2016: Digital revised 1:500 000 geologic map of South-East Greenland 62°00´N to 67°00´N and 33°00 W to 44°00 W. Copenhagen: Geological Survey of Denmark and Greenland.

Stensgaard, B.M. & Heincke, B.H. 2016: Targeting: Prospectivity mapping for orogenic gold in South-East Greenland. Danmarks og Grønlands Geologiske Undersøgelse Rapport **2016/43**, 176 pp.

Authors' addresses

B.H.H., *Geological Survey of Denmark and Greenland (GEUS), Øster Voldgade 10, DK-1350 Copenhagen K, Denmark,* E-mail: *bhm@geus.dk*

B.M.S., *EIT RawMaterials GmbH, Europa Center, Tauentzienstr. 11, 10789 Berlin, Germany. Local office: Goldschmidtsvej 23, DK-2000, Frederiksberg, Denmark.*

Inversion structures as potential petroleum exploration targets on Nuussuaq and northern Disko, onshore West Greenland

Erik V. Sørensen, John R. Hopper, Gunver K. Pedersen, Henrik Nøhr-Hansen, Pierpaolo Guarnieri, Asger K. Pedersen and Flemming Getreuer Christiansen

The onshore Cretaceous–Paleocene Nuussuaq Basin in West Greenland (Fig. 1) has long served as an analogue for offshore petroleum exploration. With the discovery of oil seeps on Disko, Nuussuaq, Ubekendt Ejland and Svartenhuk Halvø in the early 1990s, onshore exploration was also carried out. This eventually resulted in the GRO#3 wildcat exploration well on western Nuussuaq in 1996, which showed several intervals with hydrocarbons (Christiansen *et al.* 1997). Recent photogrammetric mapping of conspicuous marker horizons within the volcanic sequences of the basin shows that significant compressional structures may have developed in the latest Paleocene on central Nuussuaq and northern Disko that could be promising potential exploration targets.

Regional geological setting of the Nuussuaq Basin

The Nuussuaq Basin, central West Greenland, is a rift basin that developed during the Cretaceous–Paleocene in response to regional extension between Greenland and Canada. It is situated at the north-eastern edge of a complex system of rift basins and transfer systems that linked extension and sea-floor spreading in the Labrador Sea to the Baffin Bay (Fig. 1). The basin was formed by two major phases of extension in the Early Cretaceous and Late Cretaceous, with an intervening quiescent period of thermal subsidence, when thick successions of source-prone mudstone were deposited regionally (see Dam *et al.* 2009 for a detailed summary of the lithostratigraphy of the basin). Significant volcanism beginning in the Paleocene resulted in the deposition of a thick volcanic succession (Fig. 2, electronic supplementary (ES) figure: Fig. ES1; Larsen *et al.* 2016). The supplementary material includes a summary of the complete volcanic and sedimentary stratigraphy.

Oakey & Chalmers (2012) document significant changes in the kinematic evolution of the Baffin Bay and Labrador Sea during the latest Paleocene–Eocene (magnetic Chrons C25N–C24N) that are related to the opening of the North Atlantic Ocean. Based on seismic-stratigraphic interpretation constrained by wells, this time also marks the apparent onset of inversion in the offshore basins (Gregersen & Bidstrup 2008).

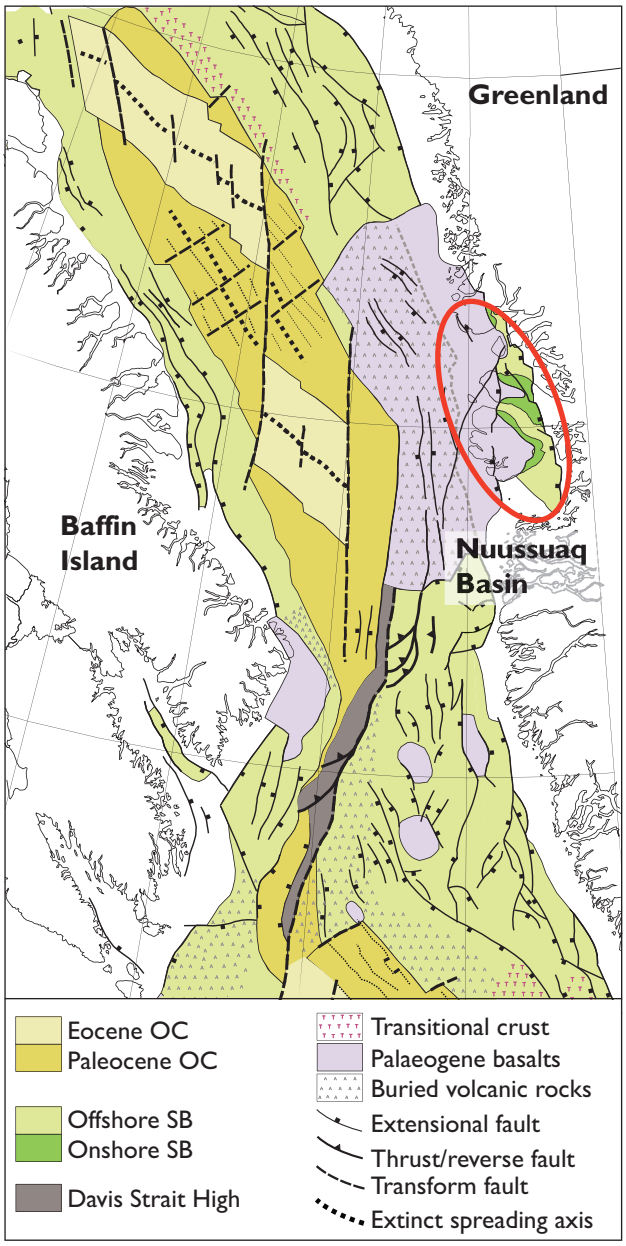

Fig. 1. Regional setting of the Nuussuaq Basin, simplified from Oakey & Chalmers (2012). **OC**: oceanic crust. **SB**: sedimentary basin.

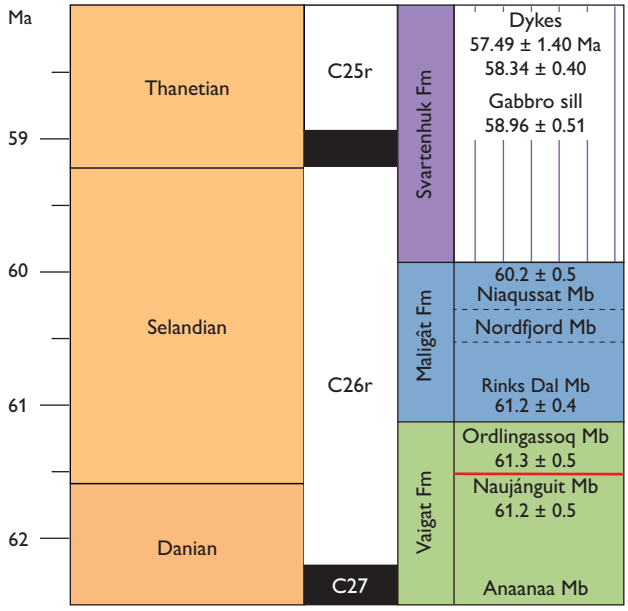

Fig. 2. Summary of the Paleocene volcanic stratigraphy of the Nuussuaq Basin from Larsen *et al.* (2016). The red line marks the stratigraphic position of the Tunoqqu surface. More complete sedimentary and volcanic stratigraphy from published material is available as an electronic supplement (Fig. ES1).

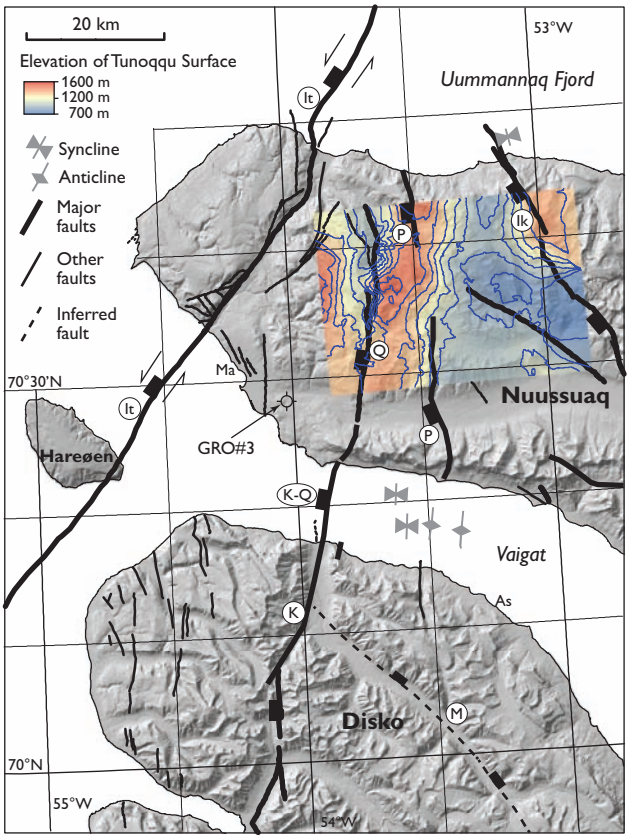

Fig. 3. Tunoqqu surface mapped by photogrammetry. **As**: Asuk locality. **Ma**: Marraat locality. **Ik**: Ikorfat Fault. **It**: Itilli Fault. **K–Q**: Kuugannguaq–Qunnilik Fault. Faults 'P' and 'M' follow the nomenclature of Chalmers *et al.* (1999). Note that fault 'M' is inferred from gravity modelling, not surface geology. Location of the GRO#3 well is also shown. Note that in the Vaigat, folding with an overall N–S trend is indicated on seismic reflection data.

Photogrammetric mapping of inversion structures

During the Danian and earliest Selandian, large volumes of picritic lava were erupted in the southern part of the Nuussuaq Basin, forming the Vaigat Formation (e.g. Larsen & Pedersen 2009). The formation is divided into three main members (Fig. 2) that primarily consist of greyish weathering, Mg-rich, picritic rocks. However, intervals of brown to light-coloured, crustally contaminated siliceous basalts to magnesian andesites that make good marker horizons also occur throughout the succession. Two marker horizons in the uppermost Nujanáguit Member (Fig. 2) are regional in extent, easily mappable, and originally formed a sub-horizontal surface, referred to as the Tunoqqu surface.

Photogrammetric mapping shows that the Tunoqqu surface is now segmented into areas of different elevation and structural trends as a result of later tectonic deformation (Sørensen 2011). This is most notable on Nuussuaq where the western part is elevated and in part highly faulted. Around the Qunnilik valley, the surface has been uplifted and faulted into many small blocks by numerous faults, so that it now forms an asymmetric anticline with a steeper dipping western limb and a gently dipping eastern limb (Fig. 3). Measured vertical displacement on faults varies from a few metres to around 100 m, whereas the amplitude of the folding, measured as the elevation difference between the axial parts of the syncline and anticline amounts to around 900 m. The limbs of the anticline are coincident with two extensional faults that pre-date the Tunoqqu surface, the Kuugannguaq–Qunnilik (K–Q) and P faults of Chalmers *et al.* (1999). The main fold axis appears to have an overall N–S trend (Fig. 4), although in detail there may be local variations. The details, however, are difficult to resolve with the mapping technique, so some caution should be used when interpreting details. Seismic data from the Vaigat show evidence that underlying strata are also folded (Marcussen *et al.* 2002). These too indicate a N–S axial trend in the folds.

The exact timing of the inversion is difficult to resolve, but must post-date the deposition of the Naujánguit Mb. It is most likely a very late Paleocene structure and thus formed at the same time as the onset of offshore inver-

sion (Gregersen & Bidstrup 2008). Guarnieri (2015) suggests an E–W-directed, compressional, palaeostress regime along West Greenland during the latest Paleocene that is consistent with the orientation of the structure. Whether the inversion was a short-lived event or took place during a longer period of time is less clear from the present data. In any case the NE–SW-trending Itilli Fault, an important strike-slip fault active during the Eocene, shows a left-lateral movement that seems to be incompatible with N–S-trending compressional folds on central Nuussuaq and northern Disko. For this reason the activity of the Itilli Fault likely post-dates the tectonic inversion, suggesting a short-lived period for the compressive event.

Distribution of potential source rocks

Hydrocarbon seeps have been mapped in the region and five distinct oil types have been identified (Fig. 4; Bojesen-Koefoed *et al.* 1999). Two oil types are particularly important for exploration: the Marraat oil and the Itilli oil. The source rock for the Marraat oil was sampled in the GRO#3 well within the marine, syn-volcanic Eqalulik Formation. The source rock for the Itilli oil has not been sampled, but is interpreted to be of Cenomanian–Turonian age or older and have a wide distribution (Bojesen-Koefoed *et al.* 1999). Although currently unproven, this interval is expected to be present in the lower Itilli Formation in the region (Bojesen-Koefoed *et al.* 1999).

Figure 4 shows inferred distribution of the two most important source-prone formations. The distribution of the Itilli Formation is regarded to be of regional extent, extending west and north-west into the Davis Strait and Baffin Bay. Based on sediment thicknesses modelled by Chalmers *et al.* (1999), it is suggested here that the lower Itilli Formation was probably sufficiently buried to have generated oil in large areas west and north-west of the Ikorfat Fault, although the timing of hydrocarbon generation is highly uncertain. The map is thus consistent with the broad distribution of the Itilli oil type observed throughout the region. In contrast, the region where the Eqalulik Formation may have been sufficiently buried to generate oil is likely more limited. Here it is suggested that the oil potential of the formation is restricted to the west of the Kuugannguaq–Qunnilik Fault and thus is not likely to migrate to areas east of the fault, consistent with the lack of Marraat oil observed in areas other than south-west Nuussuaq.

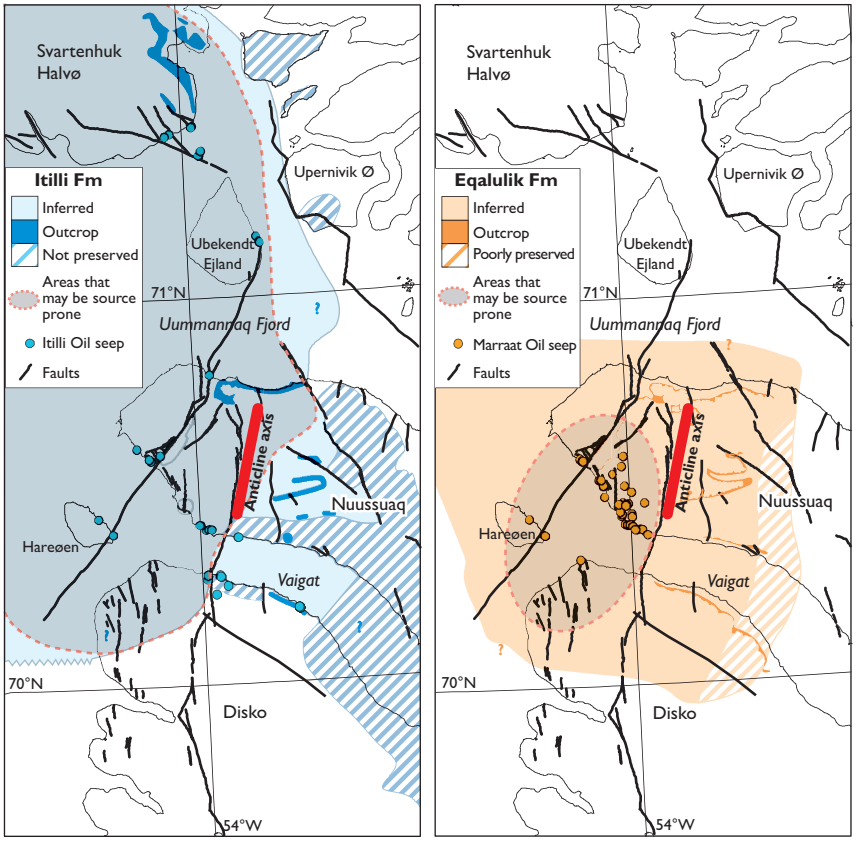

Fig. 4. Inferred distribution maps of the Itilli and Eqalulik formations. Black lines are faults (see Fig. 3). The overall trend of fold axis of the anticline mapped is shown by the red line. The maps are based on the known distributions from onshore outcrops and from offshore seismic data that indicate the presence of significant Cretaceous–Paleocene sedimentary strata (Marcussen *et al.* 2002). Also shown are the locations of Marraat and Itilli oil seeps and stains. It is notable that the Marraat oil is concentrated only on Nuussuaq between the Qunnilik and Itilli Faults whereas the Itilli oil is known regionally. The distribution of areas where there may be oil-prone intervals is shown by the grey shading. This is highly speculative and based on the locations of oil seeps and outcrops. Along southern Nuussuaq and northern Disko, the lower Itilli Formation is absent east of the K–Q Fault, but recent samples collected suggest it is present near the Ikorfat Fault along northern Nuussuaq.

Conclusions

Oil and gas shows in cores, along with numerous oil seeps, attest to the fact there is a working petroleum system in the region. Previous exploration on western Nuussuaq where seeps are most abundant failed to identify viable traps and early exploration was therefore abandoned after drilling of the GRO#3 well. However, the structural anticline defined by the Tunoqqu surface covering an area of ~250 km^2 on central-west Nuussuaq suggests that large structures could well be present in the region and in the underlying sedimentary rocks.

Previous play concepts in the region generally assume that the main source rocks are to the west or south-west of the main oil-seep areas, i.e., in the main deep marine depocentres. The areas farther east have been considered to be less prospective, since any oil would have to migrate longer distances and bypass the faulted area around the K–Q Fault. The presence of oil seeps at Asuk far to the east of this fault is thus enigmatic, raising questions about the source rock. Here, we suggest a new lead concept and propose that the central-west Nuussuaq and Uummannaq Fjord areas also hold potentially mature source rocks. This would imply that the region west of the Ikorfat Fault is prospective on Nuussuaq and possibly also in Vaigat and on northern Disko. The migration path of the oils found at Asuk could very well be from the north, rather than the west.

Acknowledgements

This contribution is partly the result of a project funded by the Ministry of Mineral Resources, Greenland. Discussions and work with Niels H. Schovsbo, Thomas F. Kokfelt, Morten L. Hjuler, Christian Knudsen, Peter Johannessen, Jim A. Chalmers, Lotte M. Larsen, Jørgen Bojesen-Koefoed, Ulrik Gregersen, Peter Japsen, Jens-Jørgen Møller, and Nina Skaarup were helpful during the course of the project.

References

Bojesen-Koefoed, J.A., Christiansen, F.G., Nytoft, H.P. & Pedersen, A.K. 1999: Oil seepage onshore West Greenland: evidence of multiple source rocks and oil mixing. In: Fleet, A.J. & Boldy, S.A.R. (eds): Petroleum Geology of Northwest Europe: Proceedings of the 5th Conference, 305–314. London: Geological Society.

Bojesen-Koefoed, J.A., Bidstrup, T., Christiansen, F.G., Dalhoff, F., Nytoft, H.P., Nøhr-Hansen, H., Pedersen, A.K. & Sønderholm, M. 2007: Petroleum seepages at Asuk, Disko, West Greenland: implications for regional petroleum exploration. Journal of Petroleum Geology **30**, 219–236.

Chalmers, J.A., Marcussen, C. & Pedersen, A.K. 1999: New insight into the structure of the Nuussuaq Basin, central West Greenland. Marine and Petroleum Geology **16**, 197–224.

Christiansen, F.G., Boesen, A., Dalhoff, F., Pedersen, A.K., Pedersen, G.K., Riisager, P., & Zinck-Jørgensen, K. 1997: Petroleum geological activities onshore West Greenland in 1996, and drilling of a deep exploration well. Geology Survey of Greenland Bulletin **176**, 17–23.

Clarke, D.B. & Pedersen, A.K. 1976: Tertiary volcanic province of West Greenland. In: Escher, A. & Watt, W.S. (eds): Geology of Greenland, 365–385. Copenhagen: Grønlands Geologiske Undersøgelse.

Dam, G., Pedersen, G.K., Sønderholm, M., Midtgaard, H., Larsen, L.M., Nøhr-Hansen, H. & Pedersen, A.K. 2009: Lithostratigraphy of the Cretaceous–Paleocene Nuussuaq Group, Nuussuaq Basin, West Greenland. Geological Survey of Denmark and Greenland Bulletin **19**, 171 pp.

Gregersen, U. & Bidstrup, T. 2008: Structures and hydrocarbon prospectivity in the northern Davis Strait area, offshore West Greenland. Petroleum Geoscience **14**, 151–166, *http://dx.doi.org/10.1144/1354-079308-752*

Guarnieri, P. 2015: Pre-break-up palaeostress state along the East Greenland margin. Journal of the Geological Society **172**, 727–739, *http://dx.doi.org/10.1144/jgs2015-053*

Larsen, L.M. & Pedersen, A.K. 2009: Petrology of the Paleocene picrites and flood basalts on Disko and Nuussuaq, West Greenland. Journal of Petrology **50**, 1667–1711.

Larsen, L.M., Pedersen, A.K, Tegner, C., Duncan, R.A., Hald, N. & Larsen, J.G. 2016: Age of Tertiary volcanic rocks on the West Greenland continental margin: volcanic evolution and event correlation to other parts of the North Atlantic Igneous Province. Geological Magazine **153**, 487–511, *http://dx.doi.org/10.1017/S0016756815000515*

Marcussen, C., Skaarup, N. & Chalmers, J.A. 2002: EFP Project NuussuaqSeis 2000: Structure and hydrocarbon potential of the Nuussuaq Basin: acquisition and interpretation of high resolution multichannel seismic data. Danmarks og Grønlands Geologiske Undersøgelse Rapport **2002/33**, 63 pp.

Oakey, G.N. & Chalmers, J.A. 2012: A new model for the Paleogene motion of Greenland relative to North America: Plate reconstructions of the Davis Strait and Nares Strait regions between Canada and Greenland. Journal of Geophysical Research **117,** *http://dx.doi.org/10.1029/2011JB008942*

Sørensen, E.V. 2011: Implementation of digital multi-model photogrammetry for building of 3D-models and interpretation of the geological and tectonic evolution of the Nuussuaq Basin, 204 pp. Copenhagen: Unpublished PhD thesis.

Authors' addresses

E.V.S, J.R.H., G.K.P & P.G., *Geological Survey of Denmark and Greenland (GEUS), Øster Voldgade 10, DK-1350 Copenhagen K, Denmark*. E-mail: *evs@geus.dk.*

A.K.P., *Natural History Museum of Denmark, Øster Voldgade 5-7, DK-1350 Copenhagen K, Denmark.*

Potential hydrocarbon reservoirs of Albian–Paleocene age in the Nuussuaq Basin, West Greenland

Morten L. Hjuler, Niels H. Schovsbo, Gunver K. Pedersen and John R. Hopper

The onshore Nuussuaq Basin in West Greenland is important for hydrocarbon exploration since many of the key petroleum systems components are well exposed and accessible for study. The basin has thus long served as an analogue for offshore exploration. The discovery of oil seeps on Disko, Nuussuaq, Ubekendt Ejland, and Svartenhuk Halvø (Fig. 1) in the early 1990s resulted in exploration onshore as well. In several wells, oil stains were observed in both the siliciclastic sandstone and in the volcanic series. An important aspect of any petroleum system is a high quality reservoir rock. The aim of this paper is to review petrophysical aspects of the reservoir potential of key stratigraphic intervals within the Nuussuaq and West Greenland Basalt groups. Reservoir parameters and porosity–permeability trends for potential siliciclastic and volcanic reservoirs within the relevant formations of the Nuussuaq Basin are discussed below.

Geological setting

The Nuussuaq Basin formed in the Cretaceous–Palaeogene as part of a complex system of linked rift basins that developed along West Greenland during the opening of the Labrador Sea and Baffin Bay (Oakey & Chalmers 2012). As a result of Neogene uplift, the sediments and overlying Palaeogene volcanic rocks are exposed on Disko, Nuussuaq, Upernivik Ø and Svartenhuk Halvø (Fig. 1, Dam *et al.* 2009). The sedimentary succession is interpreted as deposited in fluvial, delta, shelf and deep marine environments, and is divided into ten formations forming the Nuussuaq Group (Fig. 2). The overlying West Greenland Basalt Group (WGBG) includes subaerial lava flows and hyaloclastite breccias (Larsen *et al.* 2016). A companion paper to this contribution (Sørensen *et al.* 2017, this volume) provides additional information regarding the structural development and potential source rock distribution of the Nuussuaq Basin.

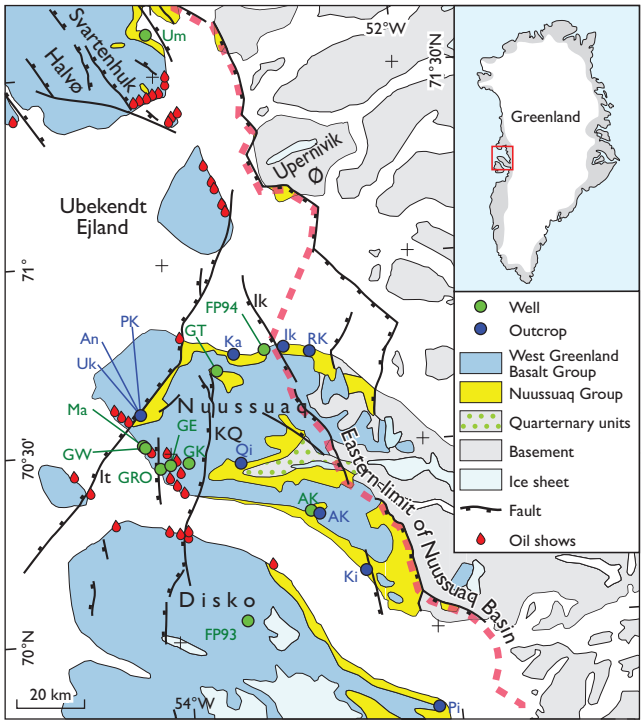

	Outcrop	Formation	Member
AK	Ataata Kuua	Kangilia	Qilakitsoq
An	Anariartorfik	Itilli	Anariartorfik
Ik	Ikorfat	Atane	Ravn Kløft+Kingittoq
Ki	Kingittoq	Atane	Kingittoq
Ka	Kangilia	Kangilia	Annertuneq Congl.
Pi	Pingu	Atane	Skansen
PK	Pingunnguup Kuua	Itilli	Anariartorfik
Qi	Qilakitsoq	Atane	Qilakitsoq
RK	Ravn Kløft	Atane	Ravn Kløft+Kingittoq
Uk	Ukalersalik	Itilli	Anariartorfik

	Well	Cores	Formation	Logs
AK	GGU247801	566 m	Atane	-
FP93	FP93-3-1	139 m	Atane	-
FP94	FP94-11-04	340 m	Itilli	-
GE	GANE-1/1A	631 m	Agatdal+Vaigat	Core logs
GK	GANK-1	364 m	Kangilia+Vaigat	-
GRO	GRO-3	-	Itilli+Kangilia+ Agatdal+Vaigat	Well logs
GT	GANT-1	891 m	Itilli+Kangilia	-
GW	GANW-1	199 m	Vaigat	-
Ma	Marraat-1	448 m	Vaigat	Well logs
Um	Umiivik-1	1200 m	Itilli+Kangilia	-

	Faults
Ik	Ikorfat fault
It	Itilli fault zone
KQ	Kuugannguaq-Qunnilik fault

Fig. 1. Geological map of the study area showing well and outcrop locations. Abbreviations of outcrop, well and fault names are explained to the right, where lithostratigraphic units occurring at outcrops and wells are also listed.

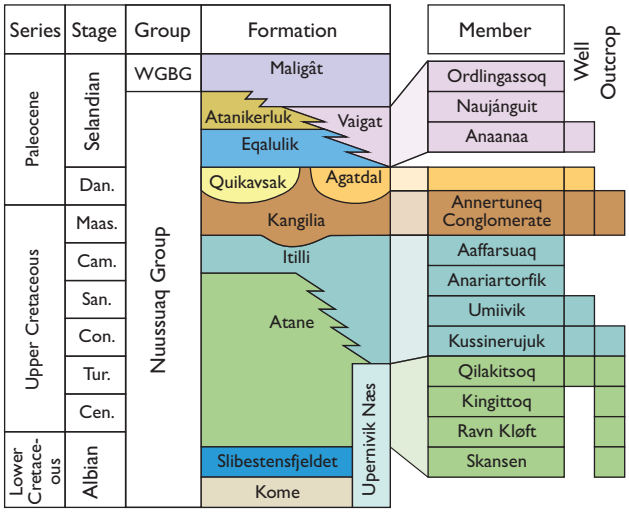

Fig. 2. Lithostratigraphic scheme of the Nuussuaq Group and the lowermost part of the West Greenland Basalt Group (WGBG). Members studied here are indicated to the far right. Modified from Dam *et al.* (2009).

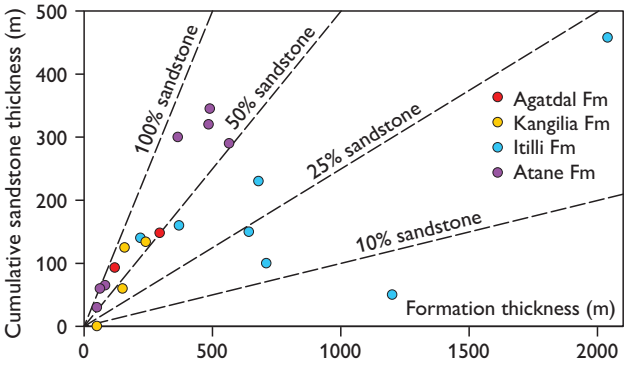

Fig. 3. Formation thickness versus cumulative sandstone thickness, data from the analysed wells and outcrops in the Nuussuaq Basin.

Lithology and distribution of relevant formations

The Atane Formation is known from the eastern part of the Nuussuaq Basin east of the Kuugannguaq–Qunnilik fault, (KQ fault, Figs 1, 2). The formation is up to 800 m thick in individual outcrops and consists of delta deposits, which include laterally extensive sandstone sheets (Dam *et al.* 2009).

The mudstone-dominated, marine Itilli Formation (Fig. 2) is known from northern and western Nuussuaq (west of the Ikorfat fault) and is more than 2.5 km thick (Sønderholm & Dam 1998). The Umiivik Member crops out in northern Nuussuaq between the Ikorfat and the Itilli faults (Fig. 1), whereas the Anariartorfik Member crops out west of the KQ fault.

The up to 438 m thick marine Kangilia Formation (Fig. 2) crops out on northern Nuussuaq between the Ikorfat and Itilli faults (Fig. 1) and has been drilled in the GANT-1 and GRO-3 wells. It has also been measured in an outcrop on southern Nuussuaq. Mudstones dominate in the outcrops while sandstones dominate in the wells. The Annertuneq Conglomerate Member mainly comprises conglomerates and sandstones (Dam *et al.* 2009).

The sub-marine to marine Agatdal Formation (Fig. 2) is known from the Agatdal area on central Nuussuaq west of the Ikorfat fault as well as from the GRO-3 well west of the K–Q fault (Fig. 1). The formation is up to 148 m thick and consists of mudstones, sandstones and conglomerates (Dam *et al.* 2009).

The volcanic Vaigat Formation (Fig. 2) is up to 1600 m thick in western Nuussuaq and northern Disko and increases to at least 5 km in thickness on Ubekendt Ejland (Larsen *et al.* 2016). The lower part of the formation is dominated by hyaloclastic breccias that are overlain by lava flows.

Methods

Ten wells and eight sedimentary outcrop successions located in the Nuussuaq Basin and described by Sønderholm & Dam (1998) and Dam *et al.* (2009) were analysed to quantify the sandstone component of the siliciclastic formations of the Nuussuaq Group. All sandstone intervals were defined as potential sandstone reservoirs and expressed as the cumulative sandstone thickness of a formation. Potential reservoir content was defined as the cumulative sandstone thickness divided by formation thickness. The cumulative sandstone thickness in outcrops and wells was estimated from sedimentological logs and core descriptions. Mudstones and heteroliths were classified as non-reservoir lithologies and included in the term 'shale'. In the uncored GRO-3 well, sandstone content was determined from wire-line logs and implies a shale content of 0–15%. Five wells containing volcanic successions of the WGBG were analysed to identify potential reservoir sections within the hyaloclastite successions. These were quantified as the cumulative thickness of hyaloclastite breccias. Lava flows were classified as non-reservoirs. Porosity–permeability trends were established for the GANE-1/1A, GANT-1 and Marraat-1 wells based on core analysis data. The porosity of the clastic formations in GRO-3 was calculated from the density wire-line log. Sandstones with porosities >10% are referred to as porous sandstones. A porosity log of the GANE-1/1A well was generated from gamma-ray and density logs obtained from core scans.

Reservoir properties of formations containing potential hydrocarbon reservoirs

Potential reservoirs were identified within sandstones of the Atane, Itilli, Kangilia, and Agatdal formations and hyaloclastite breccias of the Vaigat Formation (Fig. 2). The main reservoir parameters including cumulative reservoir thickness (CRT), potential reservoir content (PRC) and porosity–permeability data are summarised below, with details in the Electronic Supplement (ES).

Atane Formation. CRT is in the range 26–360 m corresponding to a PRC of 45–80% (Fig. 3 and ES). The reservoir quality is well developed in central Nuussuaq with sandstone porosities of 5–25% (mean 17%) and air permeabilities of 0.5–150 mD (Appel & Joensen 2014).

Itilli Formation. CRT is in the range 21–458 m corresponding to a PRC of 2–51% (Fig. 3 and ES). The relatively low content of potential sandstone reservoirs compared to the Atane, Kangilia and Agatdal formations reflects significant variations within and between the members of the Itilli Formation. In the GRO-3 well, the individual sandstone units are up to 100 m thick and average porosity is 4%.

Kangilia Formation. CRT is in the range 0–134 m corresponding to a PRC of 0–72% indicating significant lateral variation in depositional environments (Fig. 3 and ES). In the mudstone-dominated successions, the Annertuneq Conglomerate Member constitutes a potential reservoir. In the GRO-3 well, porosities range between 5–17% (average 6%).

Agatdal Formation. CRT is in the range 71–148 m corresponding to a PRC of 50–67% (Fig. 3 and ES). Porosities of 6–21% and permeabilities up to 9 mD were measured in the GANE-1 well (Fig. 4), and in the GRO-3 well, an average formation porosity of 9% was assessed.

Vaigat Formation. Several oil shows have been encountered in the hyaloclastites and lava flows. Only the hyaloclastites seem to possess the necessary permeability to constitute a reservoir despite indications of lower average porosities (6%) than the lava flows (8%). For identical porosity values, the permeability is 30 times higher for the hyaloclastites compared to the lava flows (Fig. 4). The CRT of the hyaloclastites is in the range 80–671 m corresponding to a PRC of 84–100% (Fig. 2 and ES).

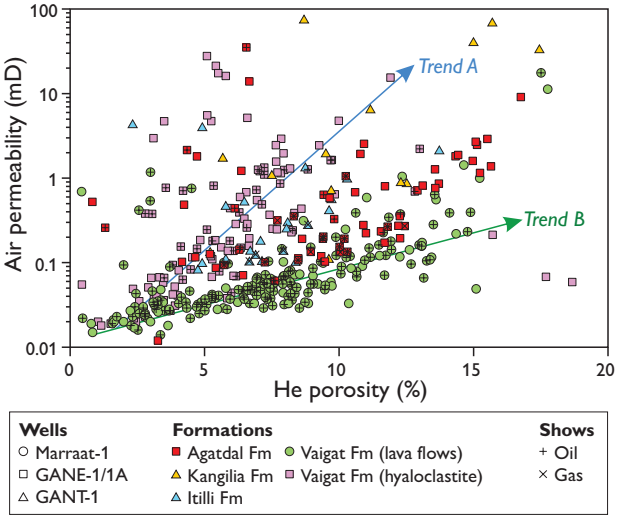

Fig. 4. Helium porosity and air permeability for selected wells. Oil shows are abundant along trend A (hyaloclastite reservoirs). Both oil and gas shows occur in the lava flows (trend B). The siliciclastic samples generally plot between the two trends.

Porosity–permeability relations of potential reservoirs

The regional distribution of porosity and permeability in the Nuussuaq Basin deposits is poorly known due to the scarcity of core measurements or studies concerned with the effects of diagenesis on reservoir quality (Kierkegaard 1998). One relatively swift way of improving the porosity database is by using core scans to generate a porosity log (Pedersen *et al*. 2013). This is shown for the Agatdal Formation in GANE-1/1A in Fig. 5. The core log-generated

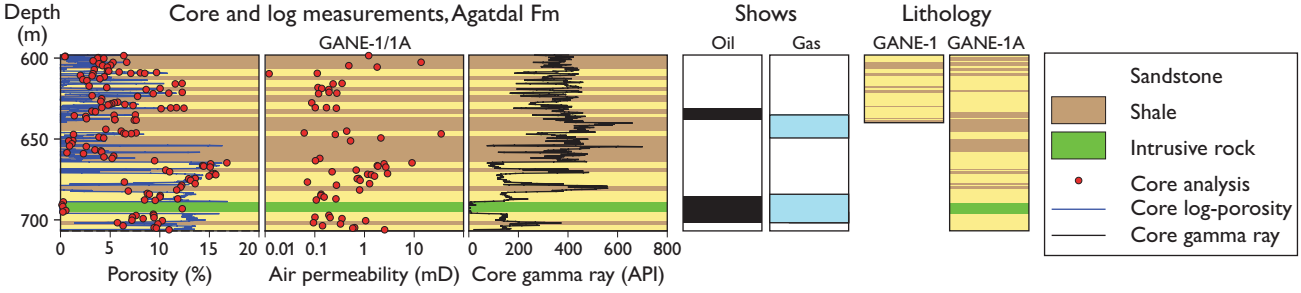

Fig. 5. Stratigraphical variation of lithology, porosity and permeability within the Agatdal Formation in the GANE-1/1A well.

porosity curve fits nicely with the core measurements and the core log-derived lithology corresponds well with the lithological log from Dam *et al*. (2009).

Core analysis data from the Marraat-1, GANE-1/1A, and GANT-1 wells were used to outline porosity–permeability trends within the siliciclastic and volcanic successions (Fig. 4). In the siliciclastic reservoirs, the porosity and permeability data show a high degree of scatter and no consistent trend can be identified. The large range in porosity and permeability values probably reflects variations in grain size and diagenesis. A large part of the porosity in the GANT-1 sandstones is secondary and related to dissolution of detrital feldspar grains (Kierkegaard 1998).

The hyaloclastite samples show a relatively high permeability–porosity ratio (trend A in Fig. 4) compared to the lava flows (trend B in Fig. 4). At 10% porosity, the expected permeability is 5 mD for hyaloclastites, but only 0.8 mD for lava flows, a tendency assumed to reflect textural control on permeability. In hyaloclastites, a network of connected pores ensures fluid or gas flow, whereas the isolated pore systems in lava flows strongly impede permeability, even at high porosity.

Conclusions

The onshore Nuussuaq Basin in West Greenland contains potential hydrocarbon reservoirs within the siliciclastic Atane, Itilli, Kangilia and Agatdal formations, and within the hyaloclastite intervals of the Vaigat Formation. The siliciclastic reservoirs occur in a wide range of geological environments from fluvial over deltaic to slope and marine settings. The potential reservoir sandstone content is generally more than 50% for the sections studied from the Atane, Kangilia and Agatdal formations, but significantly lower in the Itilli Formation. The cumulative sandstone thickness is mostly >100 m for all formations, including the Itilli Formation.

Porosity and permeability data suggest that sandstone and hyaloclastite reservoirs may be of good quality with porosities up to 20%. Permeabilities are mostly below 10 mD. However, porosity and permeability data are restricted to the western part of Nuussuaq and the diagenetic control on the reservoir quality is poorly understood regionally.

Acknowledgements

This contribution is partly the result of a project funded by the Ministry of Mineral Resources, Greenland.

References

Appel, A.U. & Joensen, I.Á. 2014: Prograderende deltaaflejringer fra øvre Kridt, Atane Formationen, Nuussuaqbassinet, centrale Vestgrønland. Unpublished Bachelor thesis, Department of Geosciences and Natural Resource Management, University of Copenhagen, 49 pp.

Dam, G., Pedersen, G.K., Sønderholm, M., Midtgaard, H., Larsen, L.M., Nøhr-Hansen, H. & Pedersen, A.K. 2009: Lithostratigraphy of the Cretaceous–Paleocene Nuussuaq Group, Nuussuaq Basin, West Greenland. Geological Survey of Denmark and Greenland Bulletin **19**, 171 pp.

Kierkegaard, T. 1998: Diagenesis and reservoir properties of Campanian – Paleocene sandstones in the GANT#1 well, western Nuussuaq, central West Greenland. Geology of Greenland Survey Bulletin **180**, 31–34.

Larsen, L.M., Pedersen, A.K., Tegner, C., Duncan, R.A., Hald, N. & Larsen, J.G. 2016: Age of Tertiary volcanic rocks on the West Greenland continental margin: volcanic evolution and event correlation to other parts of the North Atlantic Igneous Province. Geological Magazine **153**(3), 487–511.

Oakey, G.N. & Chalmers, J.A. 2012: A new model for the Paleogene motion of Greenland relative to North America: Plate reconstruction of the Davis Strait and Nares Strait regions between Canada and Greenland. Journal of Geophysical Research **117**, 1–28.

Pedersen, G.K., Schovsbo, N.H. & Nøhr-Hansen, H. 2013: Calibration of spectral gamma-ray logs to deltaic sedimentary facies from the Cretaceous Atane Formation, Nuussuaq Basin, West Greenland. Geological Survey of Denmark and Greenland Bulletin **28**, 65–68.

Sønderholm, M. & Dam, G. 1998: Reservoir characterisation of western Nuussuaq, central West Greenland. Danmarks og Grønlands Geologiske Undersøgelse Rapport **1998/6**, 36 pp.

Sørensen, E.V., Hopper, J.R., Pedersen, G.K., Nøhr-Hansen, H., Guarnieri, P., Pedersen, A.K. & Christiansen, F.G. 2016: Inversion structures as potential petroleum exploration targets on Nuussuaq and northern Disko, onshore West Greenland. Geology of Greenland Survey Bulletin **38**, 45–48.

Authors' address

Geological Survey of Denmark and Greenland, Øster Voldgade 10, DK-1350 Copenhagen, K, Denmark. E-mail: *MLH@geus.dk*

Greenland, Canadian and Icelandic land-ice albedo grids (2000–2016)

Jason E. Box, Dirk van As, Konrad Steffen and the PROMICE project team*

Albedo, Latin for 'whiteness', is a term used to describe the amount of sunlight reflected by the ground. Fresh snow albedo can exceed 85%, making it among the most reflective natural substances. Warm conditions promote snow crystal metamorphosis that, like the presence of liquid water, bring snow albedo down below 65%. With the darkening, caused by the metamorphosis, absorbed solar energy thus increases by roughly a factor of two. Seasonal snow melts over the lower reaches of a glacier leading to the exposure of bare ice with albedo below 55%. Impurities such as dust, black carbon or microbes can bring glacier-ice albedo below 30%, meaning that snow ablation gives way to impurity-rich, bare glacier ice which increases absorbed sunlight by more than a factor of three.

The thickness of the winter snow layer and the intensity of spring melt are important determinants of the annual glacier-ice melt, as the amount of snow cover governs the timing of darker ice exposure; the earlier the exposure, the more ice can melt. Because snow and ice albedo properties make it an amplifier of climate change, surface albedo has been designated as an Essential Climate Variable and a Target Requirement for climate monitoring (WMO 2011).

Polar orbiting satellites facilitate albedo mapping with Arctic coverage multiple times per day in clear-sky conditions. Satellite-based retrievals of surface albedo depend on accurate compensation of the intervening atmosphere. Thus, without ground truth, the satellite retrievals are uncertain. In Greenland, snow and ice albedo is monitored by automatic weather stations (AWSs) from The Greenland Climate Network (GC-Net; Steffen *et al.* 1996) since 1995 and after 2007 from The Programme for Monitoring of the Greenland Ice Sheet (PROMICE; van As *et al.* 2013). Using the GC-Net data, satellite-derived albedo values are compared with ground data (e.g. Stroeve *et al.* 2013).

Here, we present comparisons of daily GC-Net and PROMICE albedo data to satellite-derived albedo from the NASA Moderate Resolution Imaging Spectroradiometer (MODIS) MOD10A1 product (Hall *et al.* 1995). MOD10A1 data have been available since May 2000 and are here de-noised, gap-filled and calibrated into a daily 500 × 500 m grid covering Greenland, Iceland and the Canadian Arctic glaciers (Fig. 1).

Daily albedo from MODIS

The MOD10A1 product contains daily snow extent, snow albedo, fractional snow cover and a data quality assessment at 500 × 500 m resolution (Hall *et al.* 1995). Both NASA Terra and Aqua satellites are equipped with MODIS sensors. Here, Terra data are chosen over Aqua data as they

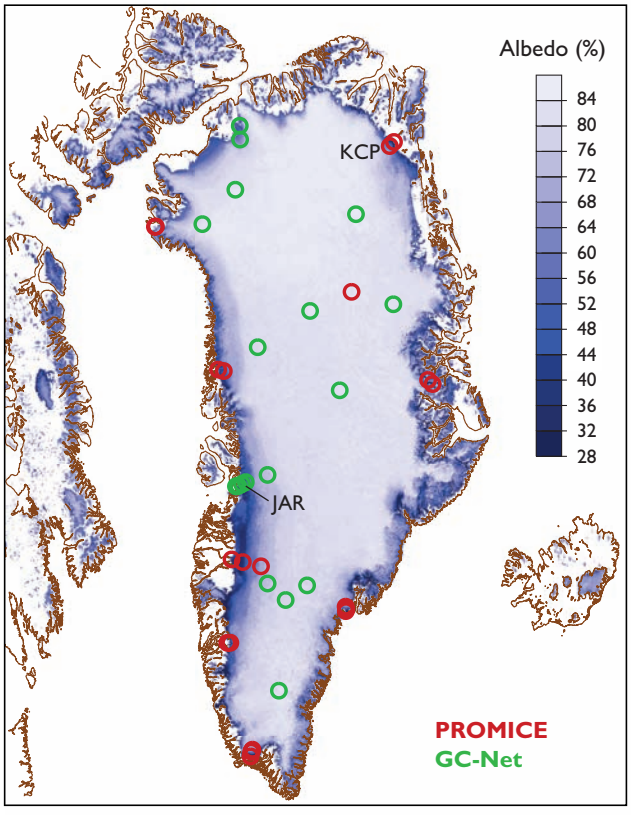

Fig. 1. An example (15 July 2016) of the daily 500 m × 500 m enhanced MOD10A1 Collection 6 albedo product presented here. The circles show positions of ground-truth observations.

* Robert S. Fausto, Andreas P. Ahlstrøm, Michele Citterio and Signe B. Andersen

give longer temporal coverage, and Aqua MODIS band 6 detectors (useful in cloud discrimination) have become degraded or non-functional (MODIS Characterization Support Team, NASA, updated February 2017). An alternative MODIS albedo product (MCD43) was not chosen due to its reduced temporal resolution of eight days. The MOD10A1 data used here span the Arctic melt season 15 March (74th day of year) to 26 October (299th day of year) for the 17 year period 2000 to 2016. The two latest MOD10A1 versions are evaluated; Collection 5 (Hall *et al.* 2011) and Collection 6 (Riggs & Hall 2015; Hall & Riggs 2016), hereafter C5 and C6.

MOD10A1 de-noising, smoothing and gap-filling

Inspection of the C5 and C6 albedo imagery reveals that, despite some cases when pixel quality is coded 'best' or 'good', cloud artifacts resembling shadows, aircraft condensation trails, thin clouds, and cloud edges can persist, often over the brightest areas presumably where there is less distinction between clouds and clean snow.

Fortunately, because the artifacts introduce abrupt temporal departures in the albedo (α) time series, it is possible to reject them on a pixel by pixel basis using temporal statistics from multi-day albedo ($\alpha_{N\text{-}days}$) samples. Here, an 11 day $\alpha_{N\text{-}days}$ sample size is selected; five days before and after each day *i*. On a pixel-by-pixel basis, statistics are computed from $\alpha_{N\text{-}days}$. The number of days *N* does not always represent 11 albedo values because some days a pixel may already be dismissed as cloudy, missing or of inadequate quality. Only cases with at least four samples per 11-day window are considered sufficient for an albedo estimate for that day and pixel. The final pixel by pixel daily albedo values are taken as the 11-day average of available values below a fractional noise threshold *(D)* value of 0.4, with *D* computed as:

$$D_i = | (\alpha_{N\text{-}days} - median(\alpha_{N\text{-}days})) / median(\alpha_{N\text{-}days}) |$$

For low albedo variability areas, for example the dry snow area, when the standard deviation $\alpha_{N\text{-}days}$ is under 0.03, then a more strict *D* threshold of 0.1 is used. The procedure has both a smoothing and a gap filling effect on the albedo time series. The resulting data product can be viewed at *https://tinyurl.com/PROMICE-albedo-Greenland.*

MODIS validation using ground-truth albedo

Daily PROMICE and GC-Net AWS albedo values are compared with the nearest 500 × 500 m resolution MOD10A1 C5 and C6 values for all stations in each of 9 or 16 years that span 2007 to 2016 or 2000 to 2015, respectively. Figure 2 provides an example for C6 data illustrating a typical result of the de-noising procedure, yielding an increased number of MODIS values, increased correlation, reduced root mean squared difference (RMSD) shifting regression slope closer to unity and no real change in bias.

Table 1 lists summary statistics for the multi-year, multi-station comparison with MOD10A1 C5 and C6. The MOD10A1 skill either improves or is stable in the C5 to C6 update. The average bias and root mean squared difference decrease and the correlation and average count of days increase. The number of compared station-years increases. From raw to de-noised, there is also a consistent improvement in agreement between the satellite and ground data (Table 2). In the de-noised product, the RMSDs are 0.08 for PROMICE stations that are concentrated in the ablation

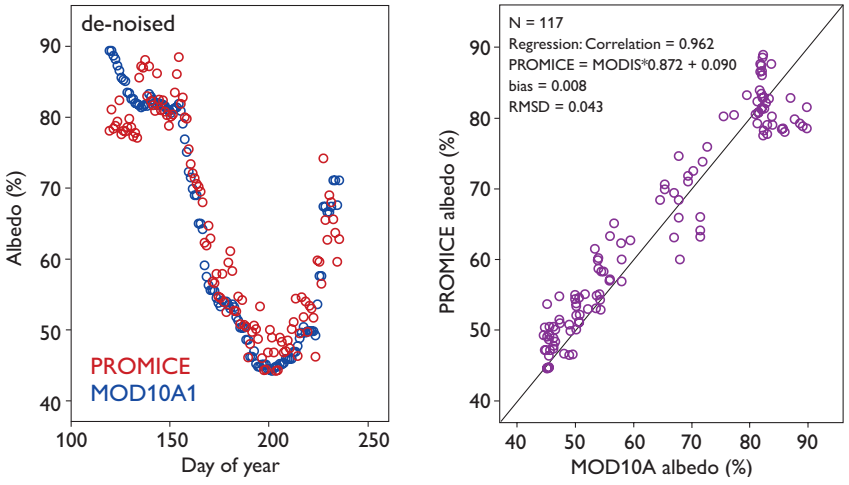

Fig. 2. Year 2013 example comparison of daily de-noised albedo from satellite (NASA MODIS MOD10A1 Collection 6 data) and the ground (PROMICE) for the KPC_L (Fig. 1) station on the north-eastern Greenland ice sheet.

Table 1. Summary statistics for comparison of $\alpha_{MOD10A1}$ Collection 5 and 6 with available $\alpha_{PROMICE}$ and $\alpha_{GC\text{-}Net}$ in the 2000–2016 period (de-noised).

$\alpha_{MOD10A1}$ versus $\alpha_{PROMICE}$	144 station years	Average	St. dev.
Collection 5	Correlation	0.838	0.182
	Bias	–0.024	0.035
	RMSD *	0.086	0.042
	Average count of days	117	37
Collection 6	Correlation	0.832	0.183
	Bias	–0.002	0.034
	RMSD	0.084	0.044
	Average count of days	124	39
$\alpha_{MOD10A1}$ versus $\alpha_{GC\text{-}Net}$	183 station-years	Average	St. dev.
Collection 5	Correlation	0.490	0.225
	Bias	-0.006	0.099
	RMSD	0.104	0.090
	Average count of days	114	33
Collection 6	Correlation	0.581	0.259
	Bias	0.006	0.038
	RMSD	0.050	0.033
	Average count of days	110	32

* Root mean squared difference.

Table 2. Summary statistics for comparison of $\alpha_{MOD10A1}$ Collection 5 and 6 with available $\alpha_{PROMICE}$ and $\alpha_{GC\text{-}Net}$ in the 2000–2016 period (de-noised minus raw).

$\alpha_{MOD10A1}$ versus $\alpha_{PROMICE}$	4 station years	Average	St. dev.
Collection 5	Correlation	0.067	0.003
	Bias	–0.001	0.001
	RMSD *	–0.022	0.003
	Count of days per year	28	13
Collection 6	Correlation	0.070	0.032
	Bias	–0.002	0.001
	RMSD	–0.029	0.003
	Count of days per year	28	13
$\alpha_{MOD10A1}$ versus $\alpha_{GC\text{-}Net}$	19 station-years	Average	St. dev.
Collection 5	Correlation	0.111	–0.048
	Bias	0.002	0.026
	RMSD	0.016	0.031
	Count of days per year	32.000	11.000
Collection 6	correlation	0.170	–0.005
	bias	–0.005	–0.042
	RMSD	–0.030	–0.037
	Count of days per year	29	12

* Root mean squared difference.

area or 0.05 for GC-Net stations that are concentrated in the accumulation area. The lower GC-Net correlation and RMSD values result from the mostly dry snow areas where albedo variability is small. For PROMICE stations which are concentrated in the ablation area (and for the GC-Net Jakobshavn Ablation Region (JAR) stations), the larger MOD10A1 pixel footprint includes a complex contribution from some combination of e.g., crevasses, snow patches and concentrated or distributed snow and ice impurities such as cryoconite. The root mean squared difference is probably more attributable to the ground data because they have a *c.* 5–10 m^2 footprint, four orders of magnitude smaller than the MOD10A1 500 m × 500 m footprint.

MODIS validation using GC-Net albedo

GC-Net albedo data, having a time coverage longer than 10 years, are compared with C5 and C6 to evaluate accuracy in year-to-year albedo changes. MOD10A1 Collection 6 (Hall & Riggs 2016) compensates MODIS sensor degradation found in Collection 5 (Lyapustin *et al.* 2014). C6 is found to compensate the temporal trend bias in dry snow areas (Fig. 3A). The trend bias is usually smaller or non-existent for darker targets such as the ablation area (Fig. 3B). The 0.02 albedo offset at the Summit site is partly attributable to the bias described in the following.

MOD10A1 sun angle bias

Whereas the adjustments to Collection 6 eliminate a spurious darkening trend concentrated over snow and in the northern part of Greenland (Polashenski *et al.* 2015), both Collections 5 and 6 MOD10A1 albedo products have a residual bias based on the angle of the sun above the horizon. The bias is evident over nearly 20° of latitude range of the PROMICE and GC-Net data. In April (days 91–120), there is no bias in southern Greenland but a *c.* 4% bright bias in the northern 2/3 of Greenland (Fig. 4A). By June (days 152–181), the pattern of the bias has shifted to a more uniform dark bias strongest in the south (Fig. 4B). The bias varies over time and latitude (see the animation: *https://tinyurl.com/bias-vs-lat*). We correct the Collection 6 bias according to the daily variation in the regression line (blue dashed line in Fig. 4A, trends in Fig. 4B). The calibration

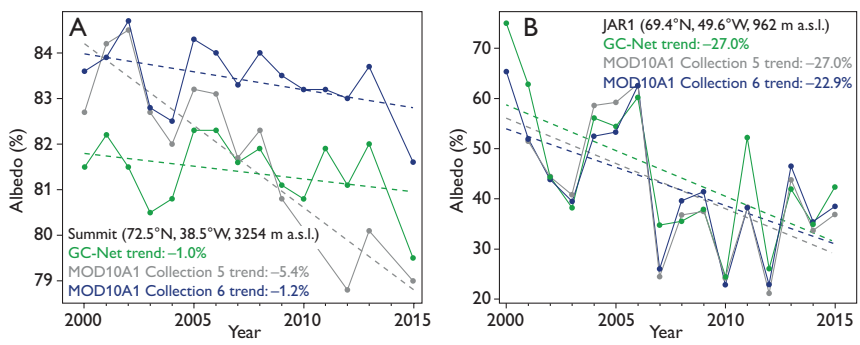

Fig. 3. Examples of July monthly average dry snow area (**A**) and ablation area (**B**) MODIS collection 5 and 6 compared with GC-Net albedo trends spanning 16 summers. **JAR**: Jakobshavn Ablation Region.

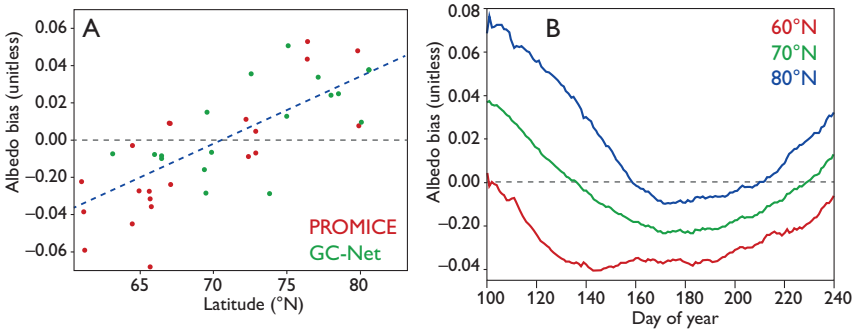

Fig. 4. **A**: Example of NASA MODIS MOD10A1 Collection 6 difference with ground data from automatic weather stations versus latitude, indicating a sun-angle-dependent bias. **B**: Bias for three latitude bands. The station names are abbreviated.

assumes there is no sun-angle-dependent bias in the PROMICE and GC-Net data.

MODIS albedo for Iceland and the Canadian Arctic

The regional product also includes albedo for glaciated areas in Iceland, Jan Mayen and the Canadian Arctic. The occurrence of clouds reduces the coverage of the product, in the case of land ice, especially at the lowest elevations often near oceans. Iceland has data coverage less than half of that of most areas of Greenland. Areas of the Canadian Arctic such as the Devon Ice Cap also have reduced time coverage compared to Greenland, which has a stronger cloud clearing effect from its high pressure areas often centered over the ice sheet.

A new PROMICE data product

The methodology developed here for de-noising, gap filling, and bias correction for the MOD10A1 albedo product yields an enhanced MODIS MOD10A1 Climate Data Record available for download through the PROMICE database via the webpage www.promice.dk

Acknowledgements

PROMICE is supported by the Danish Energy Agency through the DANCEA programme. GC-Net is supported by NASA and US National Science Foundation grants.

References

Hall, D.K. & Riggs, G.A. 2016: MODIS/Terra Snow Cover Daily L3 Global 500m Grid, Version 6. Greenland coverage. National Snow and Ice Data Center, NASA Distributed Active Archive Center, Boulder, Colorado USA. *http://nsidc.org/data/MOD10A1/versions/6*, accessed December 2016.

Hall, D.K., Riggs, G.A. & Salomonson, V.V. 1995: Development of methods for mapping global snow cover using moderate resolution imaging spectroradiometer data. Remote Sensing of Environment **54**, 127–140.

Hall, D.K., Riggs, G.A. & Salomonson, V.V. 2011: MODIS/Terra Snow Cover Daily L3 Global 500 m Grid V004, January to March 2003. Digital media, updated daily. National Snow and Ice Data Center, Boulder, CO, USA.

Lyapustin, A. *et al.* 2014: Science impact of MODIS C5 calibration degradation and C6+ improvements. Atmospheric Measurement Techniques Discussion **7**, 7281–7319.

MODIS Characterization Support Team, NASA, updated February 2017: *http://mcst.gsfc.nasa.gov/calibration/time-dependent-list-non-functional-or-noisy-detector*

Polashenski, C.M., Dibb, J.E., Flanner, M.G., Chen, J.Y., Courville, Z.R., Lai, A.M., Schauer, J.J., Shafer, M.M. & Bergin, M. 2015: Neither dust nor black carbon causing apparent albedo decline in Greenland's dry snow zone: implications for MODIS C5 surface reflectance, Geophysical Research Letters **42**, 9319–9327.

Riggs, G.A. & Hall, D.K. 2015: MODIS Snow products collection 6, User Guide. *https://nsidc.org/sites/nsidc.org/files/files/MODIS-snow-user-guide-C6.pdf*

Steffen, K., Box, J.E. & Abdalati, W. 1996: Greenland Climate Network: GC-Net. In: Colbeck, S.C. (ed.): CRREL **96-27** Special Report on glaciers, ice sheets and volcanoes, tribute to M. Meier, 98–103. Hannover: U.S. Army.

Stroeve, J.C., Box, J.E., Wang, Z., Schaaf, C. & Barrett, A. 2013: Re-evaluation of MODIS MCD43 Greenland albedo accuracy and trends. Remote Sensing of Environment **138**, 199–214.

Van As, D., Fausto, R.S., Colgan, W.T., Box, J.E. and the PROMICE project team 2013: Darkening of the Greenland ice sheet due to the melt-albedo feedback observed at PROMICE weather stations. Geological Survey of Denmark and Greenland Bulletin **28**, 69–72.

WMO (World Meteorological Organization) 2011: Systematic observation requirements for satellite-based data products for climate, Update. Global Climate Observing System, **GCOS-154**, 138 pp.

Authors' addresses

J.E.B., D.V.A. & the PROMICE team, *Geological Survey of Denmark and Greenland, Øster Voldgade 10, DK-1350 Copenhagen K, Denmark*; E-mail: *jeb@geus.dk*

K.S., *Swiss Federal Institute for Forest, Snow and Landscape Research, Zürcherstrasse 111, CH-8903 Birmensdorf, Switzerland.*

New programme for climate monitoring at Camp Century, Greenland

William Colgan, Signe B. Andersen, Dirk van As, Jason E. Box and Søren Gregersen

Camp Century was a military base constructed by the US Army Corps of Engineers (USACE) in 1959 in the near-surface layers of the Greenland ice sheet at 77.13°N and 61.03°W and 1910 metres above sea level (Clark 1965). The *c.* 55 ha base housed between 85 and 200 soldiers and was continuously occupied until 1964 (Fig.1). Camp Century primarily served as an experimental facility for the USACE to test ice-sheet construction concepts. Recent Danish scholarship has documented the political and military history of Camp Century in substantial detail (Petersen 2007; Nielsen & Nielsen 2016). To summarise, Project Iceworm, the US Army ambition to deploy offensive missiles within the ice sheet, was never realised. After three years of seasonal operation, Camp Century was finally abandoned with minimal decommissioning in 1967. The Government of Denmark has now established a GEUS-led programme for long-term climate monitoring, as well as one-time waste mapping, at Camp Century. Here, we briefly review the historical scientific activities at Camp Century and introduce the future goals of the Camp Century Climate Monitoring Programme. Finally, we discuss the challenges and outlook of climate monitoring and waste mapping at the former military site.

Scientific heritage

The USACE conducted extensive glaciological and climatological research during the operation of Camp Century (Fig. 2). Much of their glaciological research focused on characterising the strength and density of the relatively porous, near-surface ice-sheet layer known as firn. These projects included measuring the deformational closure rates of near-surface tunnels (Clark 1965), and excavating an inclined tunnel to 100 m depth to measure firn properties (Kovacs *et al.* 1969). Much of their climatological research focused on characterising spatial and temporal variability in snowfall. These projects include extensive surveys of regional snow-accumulation rates (Mock 1968), and maintaining a continuous weather station record from October 1960 to August 1964 that remains unpublished.

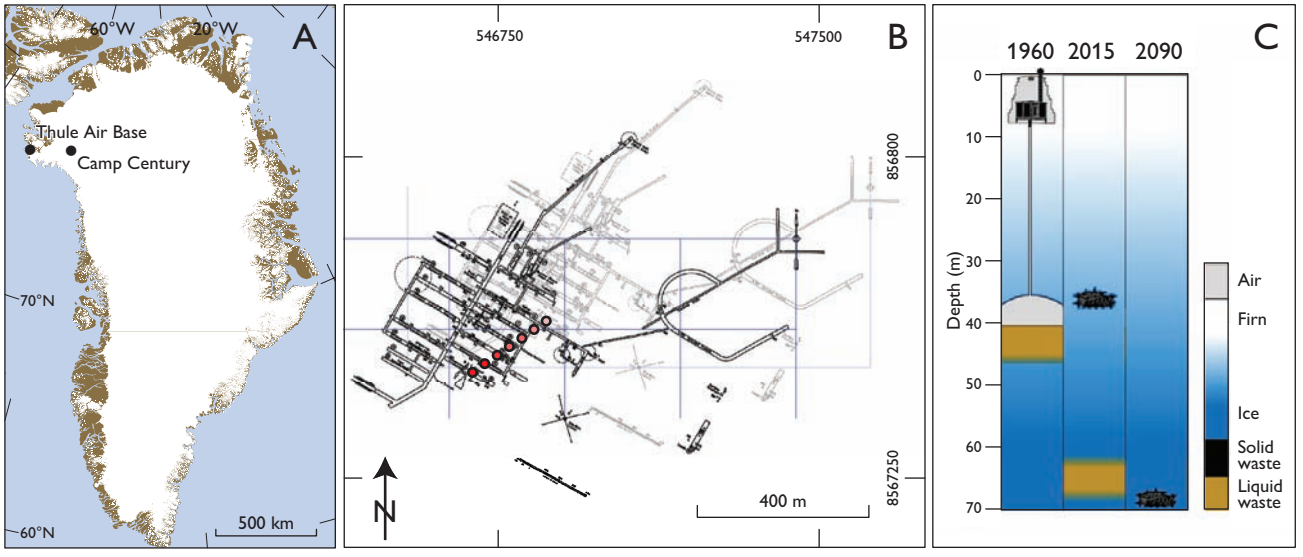

Fig. 1. **A**: Location of Thule Air Base and Camp Century in North-West Greenland. **B**: Camp Century as-built map with estimated georeferencing to 1960 (grey) and 2020 (black) locations in polar stereographic projection (EPSG 3413). Decadal borehole positions from 1960 to 2020 shown in red (Colgan *et al.* 2016). Blue lines denote a local coordinate system. **C**: Estimated depths of solid and refrozen liquid wastes in the firn and ice beneath Camp Century in 1960, 2015 and 2090 (Colgan *et al.* 2016).

Fig. 2. USACE-applied glaciology research at Camp Century. Left: Measuring the deformation of firn in 1961. Right: Measuring the compressive strength of firn in 1964. Photos: Søren Gregersen.

Today, the USACE-facilitated science at Camp Century is perhaps best known for producing the first systematic classification of ice-sheet snow facies (Benson 1962), and recovering the first ice core to the bed of the Greenland ice sheet (Dansgaard *et al*. 1969). Both the data and interpretations from these seminal studies continue to be highly cited today. After the closure of Camp Century, the US Air National Guard continued to use the Camp Century skiway, renaming it the Greenland Ice Sheet Training Site (GITS).

Aside from re-surveying the borehole position in 1977 and 1986 (Gundestrup *et al*. 1987), there appears to have been virtually no data collected at Camp Century between the abandonment of the base in 1967 and the start of NASA Program for Arctic Regional Climate Assessment (PARCA) activities at the site in 1993. PARCA activities included: deploying an automatic weather station in 1995 to record meteorology at the site (Steffen & Box 2001), drilling a 120 m deep ice core in 1996 to reconstruct snow accumulation rates (Mosley-Thompson *et al*. 2001), and measuring *in-situ* firn compaction rates in 1995–1996 (Hamilton & Whillans 2000). In 2010, a 35 m deep ice core was once again recovered at Camp Century, to further update snow accumulation and ice chemistry records since the termination of the USACE ice-core record (Buchardt *et al*. 2012). PARCA began regular airborne measurements of ice-surface elevation at Camp Century in 1993 (Krabill *et al*. 2000), with NASA Operation IceBridge regularly collecting ice-penetrating radar data over the site since 2010 (Leuschen *et al*. 2014). US National Science Foundation traverses from Thule Air Base (AB) to Summit Station, which have approximately followed the USACE trail to Camp Century since 2008, have been used as a science platform to measure accumulation rates (Hawley *et al*. 2014).

Mapping and monitoring

In 2016, GEUS participated in a multi-nation study that presented regional climate model simulations that suggested the ice-sheet surface mass balance at Camp Century may change from net snowfall to net melt by year 2100 under the UN Intergovernmental Panel on Climate Change (IPCC) RCP8.5 'business-as-usual' climate scenario (Colgan *et al*. 2016). However, under the emissions mitigation characterised by the RCP4.5 climate scenario, net snowfall would persist at Camp Century until 2100. While Colgan *et al*. (2016) also provided preliminary estimates of the non-trivial quantities of physical, chemical, biological and radiological wastes presently residing within the firn at Camp Century, at depths of between 35 and 65 m, perhaps the most socially significant outcome of this study was suggesting that the assumption that the abandoned base would be preserved for eternity by perpetually accumulating snowfall was no longer valid under the full range of IPCC climate pathways.

In response to concerns from the Government of Greenland over the potential remobilisation of contaminants from Camp Century within the next century, the Government of Denmark has now established a programme for long-term climate monitoring, as well as one-time waste mapping, at Camp Century. This Camp Century Climate Monitoring Programme will be led by GEUS and has four main goals:

1) To continuously monitor relevant climate variables, including the depth to which meltwater percolates, at the Camp Century site. This goal will be accomplished by installing an automated weather station that measures standard climatological variables controlling meltwater production (Citterio *et al*. 2015). Station measurements will be supplemented

by thermistor strings to monitor deep firn temperatures, as well as observations of firn density and compaction profiles.

2) To regularly update annual likelihoods of meltwater interacting with abandoned materials at the Camp Century site over the next century. This goal will be accomplished by using a physically-based numerical model that couples meltwater percolation and firn evolution (Charalampidis *et al*. 2016). This model will be forced by IPCC climate pathways and continuously improved using *in situ* observations, as well as novel parameterisations from community models.

3) To map the estimated spatial extent and vertical depth of abandoned wastes across the Camp Century site. This goal will be accomplished by using ice-penetrating radar and global positioning system measurements to map the Camp Century debris field during a one-time field campaign (Machguth *et al*. 2016). Delineating the present-day location of key infrastructure features will enable georeferencing of historical site maps.

4) To publicly report all findings from the Camp Century Climate Monitoring Programme in a timely manner. This goal will be accomplished by streaming the data collected by sensors deployed at Camp Century in near-real-time, maintaining an internet outreach presence of the programme, and regularly publishing GEUS reports and papers in open-access, peer-reviewed journals.

The Camp Century Climate Monitoring Programme will undertake initial fieldwork at Camp Century during the summer of 2017, to deploy automated climate and firn sensors and collect ice-penetrating radar and firn-core observations (Fig. 3). Subsequent fieldwork at Camp Century will be undertaken, as needed, to service deployed instrumentation. During subsequent site visits, additional ice-penetrating radar data may potentially be collected in more concentrated areas of the debris field. The analysis of climate measurements, including firn temperatures, as well as numerical modelling of future meltwater percolation depths, will begin during the autumn of 2017, with anticipated first public reporting in the summer of 2018. Near-real-time measurements from Camp Century, as well as programme outreach materials and publications, can be accessed at *www.campcenturyclimate.dk*.

Programme outlook

GEUS has a long tradition of applied glaciology research. Recent applied glaciology work includes operating the Programme for Monitoring of the Greenland Ice Sheet (PROMICE) on behalf of the Government of Denmark (Ahlstrøm *et al*. 2008a), consulting for the Government of Greenland on the hydropower potentials associated with ice-sheet runoff (Ahlstrøm *et al*. 2008b), and a growing involvement in private sector proglacial mining projects (Citterio *et al*. 2009). With unique applied glaciology expertise gained through these and other operations, especially in-house development of robust automated ice-sheet instrumentation and previous dedicated ice-coring and radar-acquisition campaigns, GEUS is well-suited to lead the Camp Century Climate Monitoring Programme. Indeed, GEUS involvement with Camp Century stretches from its operational period, when GEUS emeriti Anker Weidick and Søren Gregersen participated in research at the site, to contributing to the preliminary waste inventory and climate projections of the Camp Century site published last year.

While the fundamental glaciology and climatology research performed by the USACE gives Camp Century an unparalleled scientific heritage amongst Greenland research

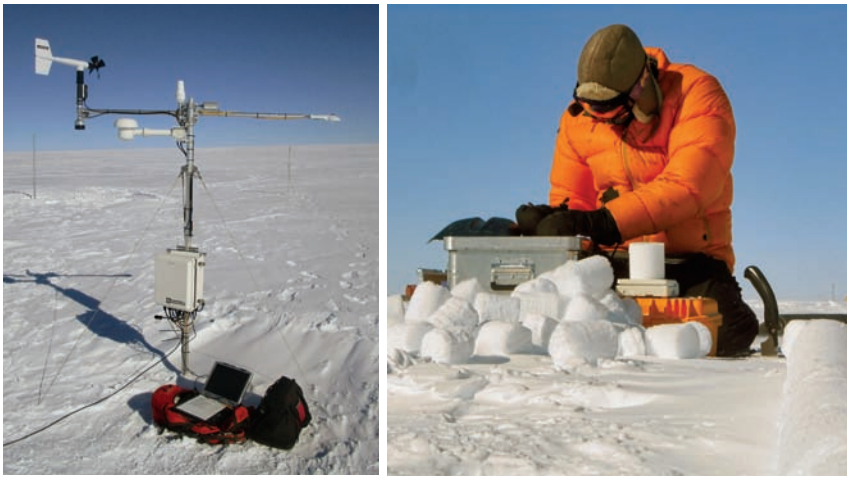

Fig. 3. Left: Servicing a PROMICE automated weather station in the ice-sheet accumulation area in 2016. Right: Measuring firn density from a shallow borehole into which thermistors were installed in 2016. Photos: Baptiste Vandecrux.

sites, the military history of Camp Century gives the site unanticipated social significance in light of climate change. Long-term climate monitoring, and one-time waste surveying, of Camp Century will provide Danish and Greenlandic stakeholders open access to relevant *in-situ* measurements and model projections. Refined knowledge of the spatial and depth distribution of different wastes, as well as the changes in firn structure and meltwater production anticipated under climate change, will facilitate a science-based discussion of the shifting fate of Camp Century. At the broadest level, a better understanding of the implications of climate change on Camp Century will perhaps provide a better understanding of the importance of mitigating greenhouse-gas emissions, and averting, rather than adapting to the consequences of business-as-usual climate change.

Acknowledgements

The Camp Century Climate Monitoring Programme is funded by the Danish Ministry for Energy, Utilities and Climate and by GEUS.

References

Ahlstrøm, A. & the PROMICE Team 2008a: A new programme for monitoring the mass loss of the Greenland ice sheet. Geological Survey of Denmark and Greenland Bulletin **15**, 61–64.

Ahlstrøm, A., Mottram, R., Nielsen, C., Reeh, N. & Andersen, S. 2008b: Evaluation of the future hydropower potential at Paakitsoq, Ilulissat, W. Greenland. Danmarks og Grønlands Geologiske Undersøgelse Rapport **2008/37**, 50 pp.

Benson, C. 1962: Stratigraphic studies in the snow and firn of the Greenland ice sheet. Cold Regions Research and Engineering Laboratory. Research Report **70**.

Buchardt, S., Clausen, H., Vinther, B. & Dahl-Jensen, D. 2012: Investigating the past and recent delta18O-accumulation relationship seen in Greenland ice cores. Climate of the Past **8**, 2053–2059.

Charalampidis, C., Van As, D., Colgan, W.T., Fausto, R.S., Macferrin, M. & Machguth, H. 2016: Thermal tracing of retained meltwater in the lower accumulation area of the southwestern Greenland ice sheet. Annals of Glaciology **57**(72) 1–10.

Citterio, M., Mottram, R., Larsen, S. & Ahlstrøm, A. 2009: Glaciological investigations at the Malmbjerg mining prospect, central East Greenland. Geological Survey of Denmark and Greenland Bulletin **17**, 73–76.

Citterio, M., van As, D., Ahlstrøm, A.P., Andersen, M.L., Andersen, S.B., Box, J.E., Charalampidis, C., Colgan, W., Fausto, R.S., Nielsen, S. & Veicherts, M. 2015: Automatic weather stations for basic and applied glaciological research. Geological Survey of Denmark and Greenland Bulletin **33**, 69–72.

Clark, E.F. 1965: Camp Century evolution of concept and history of design, construction and performance. Cold Regions Research and Engineering Laboratory. Technical Report **174**, 69 pp.

Colgan, W., Machguth, H., MacFerrin, M., Colgan, J., van As, D. & MacGregor, J. 2016: The abandoned ice sheet base at Camp Century, Greenland, in a warming climate. Geophysical Research Letters **43**, 8091–8096.

Dansgaard, W., Johnsen, S.J., Møller, J. & Langway, C.C. 1969: One thousand centuries of climatic record from Camp Century on the Greenland ice sheet. Science **166**(3903), 377–380.

Gundestrup, N.S., Clausen, H.B., Hansen, B.L. & Rand, J. 1987: Camp century survey 1986. Cold Regions Science and Technology **14**(3), 281–288.

Hamilton, G. & Whillans, I. 2000: Point measurements of mass balance of the Greenland Ice Sheet using precision vertical Global Positioning System (GPS) surveys. Journal of Geophysical Research **105**, 16,295–16,301.

Hawley, R.L., Courville, Z.R., Kehrl, L.M., Lutz, E.R., Osterberg, E.C., Overly, T.B. and Wong, G.J. 2014: Recent accumulation variability in northwest Greenland from ground-penetrating radar and shallow cores along the Greenland Inland Traverse. Journal of Glaciology **60**(220), 375–382.

Kovacs, A., Weeks, W.F. & Michitti, F. 1969: Variation of some chanical properties of polar snow, Camp Century, Greenland. USA Cold Regions Research and Engineering Laboratory, Research Report **276**, 33 pp.

Krabill, W., Abdalati, W., Frederick, E., Manizade, S., Martin, C., Sonntag, J., Swift, R., Thomas, R., Wright, W. & Yungel, J. 2000: Greenland Ice Sheet: High-Elevation Balance and Peripheral Thinning. Science **289**, *http://dx.doi.org/10.1126/science.289.5478.428*

Leuschen, C., Gogineni, P., Hale, R., Paden, J., Rodriguez, F., Panzer, B. & Gomez, D. 2014, updated 2016: IceBridge MCoRDS L1B Geolocated Radar Echo Strength Profiles, Version 2, [indicate subset used]. Boulder, Colorado USA: National Snow and Ice Data Center. *http://dx.doi.org/10.5067/90S1XZRBAX5N*

Machguth, H., MacFerrin, M., van As, D., Box, J., Charalampidis, C., Colgan, W., Fausto, R., Meijer, H., Mosley-Thompson, E. & van de Wal, R. 2016: Greenland meltwater storage in firn limited by near-surface ice formation. Nature Climate Change **6**, 390–393.

Mock, S. 1968: Snow accumulation studies on the Thule Peninsula, Greenland. Journal of Glaciology **7**, 59–76.

Mosley-Thompson, E., McConnell, J., Bales, R., Li, Z., Lin, P., Steffen, K., Thompson, L., Edwards, R. & Bathke, D. 2001: Local to regional-scale variability of annual net accumulation on the Greenland ice sheet from PARCA cores. Journal of Geophysical Research **106**, 33,839–33,851.

Nielsen, H. & Nielsen, K. 2016: Camp Century – Cold War City Under the Ice. In: Doel, R., Harper, K. & Heymann, M. (eds): Exploring Greenland: Cold War Science and Technology on Ice, 195–216. Palgrave Studies in the history of science and tehcnology, Palgrave Macmillan US.

Petersen, N. 2007: The iceman that never came. 'Project Iceworm', the search for a NATO deterrent, and Denmark, 1960–1962. Journal of Scandinavian History **33**, 75–98.

Steffen, K. & Box, J. 2001: Surface climatology of the Greenland ice sheet: Greenland Climate Network 1995–1999. Journal of Geophysical Research **106**, 33,951–33,964.

Authors' address

Geological Survey of Denmark and Greenland, Øster Voldgade 10, DK-1350 Copenhagen K, Denmark; E-mail: *wic@geus.dk*

Asynchronous ice-sheet development along the central East Greenland margin: a GLANAM project contribution

Lara F. Pérez and Tove Nielsen

The sedimentary record of the glaciated margins of the North Atlantic holds evidence of past ice-sheet activity, and reflects spatial and temporal variations in the ice–ocean–climate interaction as well as the influence of tectonic processes. Furthermore, the record of cross-shelf ice sheets provides a direct link between the continental ice cover and the deep ocean, a relevant issue in the context of climate research.

With a four-year funding period, a Marie Curie Initial Training Network on the Glaciated North Atlantic Margins (GLANAM) was started in the spring 2013. The network involved international partners from both academia and industry and enrolled 15 young scientists working in different areas of the North Atlantic margins.

The Geological Survey of Denmark and Greenland was partner in the network, leading the Greenland margin research and hosting three fellows. One of the main topics of the GLANAM project was to investigate the impact of the ice sheets on the large-scale evolution of the East Greenland margin. The present work summarises some new insights into the glacial history of the central East Greenland margin gained through a study within this project (Fig. 1).

The glaciated East Greenland margin

The dynamic evolution of the Greenland ice sheet is related to the glacial history of the Northern Hemisphere (e.g. Thiede *et al.* 2010). Despite evidence of glaciated hinterland and tidewater glaciers in Greenland during the Eocene and Miocene (e.g. Thiede *et al.* 2010), the onset of large-scale glaciations in the Northern Hemisphere, where ice expanded onto the continental shelf, has been suggested to date between 5 and 2.5 Ma based on a marked decrease in global benthic $\delta^{18}O$ values and the presence of ice-rafted debris deposits (e.g. Bailey *et al.* 2013). Since the Mid-Pliocene the oscillation of the ice sheets of the Northern Hemisphere, and thus of the East Greenland margin, is considered to have followed the glacial–interglacial cycles (e.g. Sarnthein *et al.* 2009).

Major tectonic events related to the Miocene–Pliocene uplift of the East Greenland margin have been pointed to as instigators of the eastwards glacial advance across the shelf (Døssing *et al.* 2016). Furthermore, the build-up of the North Atlantic ice sheets has also been influenced by the oceanographic circulation which, along East Greenland, is mainly controlled by the East Greenland Current (EGC; Fig. 1; Sarnthein *et al.* 2009). The EGC is a southward-flowing current formed by a complex system of branches and different water masses (Våge *et al.* 2013).

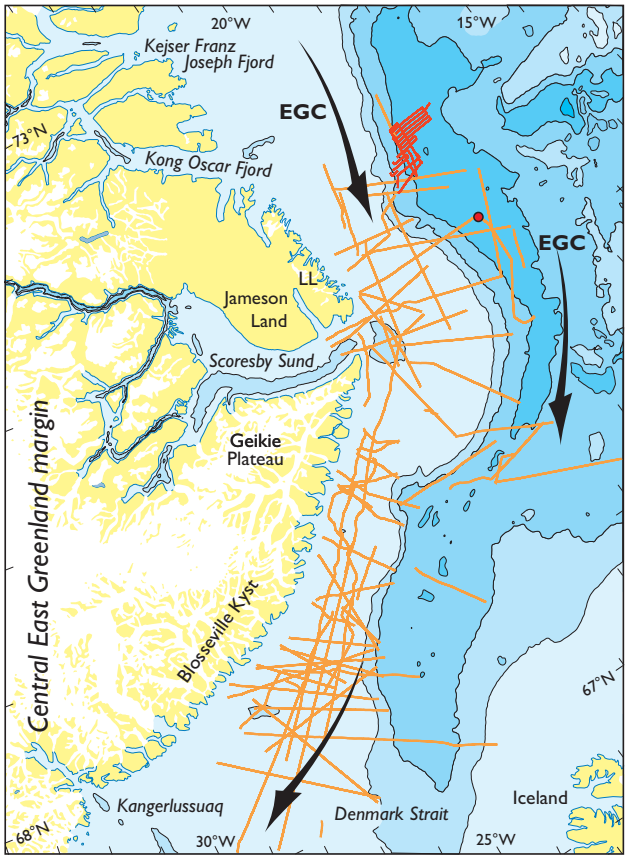

Fig. 1. Bathymetric map of the study area based on the International Bathymetric Chart of the Arctic Ocean (IBCAO; Jacobsson *et al.* 2012). Contour interval: 500 m. Orange lines: reflection seismic profiles. Red lines: sub-bottom and multibeam data. Red dot: ODP site 987. Black arrows: general circulation of the East Greenland Current (**EGC**). **LL**: Liverpool Land. Note the outwards bulging of the shelf edge off the major fjords.

It is an important component of the Atlantic Meridional Overturning Circulation (AMOC) and therefore has implications for the global climate system (De Schepper *et al.* 2015). The contribution of the EGC to the AMOC has been partly controlled by tectonic pulses of the Denmark Strait (Parnell-Turner *et al.* 2015), a 600 m deep threshold located around 67°N (Fig. 1). The Denmark Strait is part of the Greenland–Scotland Ridge and constitutes a natural boundary that divides the East Greenland margin into a northern and southern part, which have experienced different ice-sheet dynamics. Our study focuses on the glacial history of the margin section that lies just north of the Denmark Strait, i.e. the central East Greenland margin (Fig. 1).

Database and interpretation procedure

Based on a large database of 2D seismic reflection profiles (Fig. 1), we have divided the sedimentary record into major seismic sequences, which show evidence of various sedimentary processes (Pérez *et al.* unpublished data). A local dataset of high-resolution reflection seismic, sub-bottom profiles and swath bathymetry allowed for a detailed breakdown of the recent stratigraphic and morphological features (Pérez *et al.* unpublished data). The ages of the major seismic sequences have been assessed by a direct tie to site 987 of the Ocean Drilling Program off Scoresby Sund (Fig. 1; Pérez *et al.* unpublished data). Seismic-stratigraphic analyses of these datasets made a large-scale reconstruction of key stratigraphic events possible, revealing several stages of the Greenland ice sheet dynamics along the central East Greenland margin from late Miocene to Present.

Evidence for cross-shelf ice sheets and ice streams

Central East Greenland is characterised by large fjords, many of which are connected with cross-shelf troughs that are up to 300 m deep and 35 km wide (Fig. 1). These troughs were formed by erosion of ice streams that passed from the fjords across the shelf, delivering a concentrated accumulation of sediments to the shelf edge (e.g. Batchelor & Dowdeswell 2014). From there the sediments were transported down the slope as glacigenic debris flows that build up to form large prograding wedges called trough-mouth fans. The presence of a trough-mouth fan is often revealed in the seabed morphology as an outwards bulging of the shelf edge (Fig. 1), and the youngest debris flows are often observed on the present-day seabed. Ice streams are recognised as one of the most important controls on ice-sheet configuration and stability (e.g. Stokes *et al.* 2016). Therefore the study of palaeo-ice stream behaviour and dynamics by mapping buried cross-shelf troughs and trough-mouth fans is a useful tool in reconstructing former ice-extent and palaeoclimate variability (e.g. Batchelor & Dowdeswell 2014). In addition, submarine glacial forms outside the cross-shelf troughs hold clues of the existence of more steady, grounded ice. Notable features are grounding-zone wedges up to 160 m high identified along the central East Greenland shelf. These ridge-like sedimentary features mark a temporary position of the ice margin on the shelf (Dowdeswell & Fugelli 2012).

Discussion

Prograding deposits off Blosseville Kyst dating back to the late Miocene constitute the first evidence of cross-shelf glaciations on the central East Greenland margin (Fig. 2). The oceanward glacial advance continued during the early Pliocene, where cross-shelf troughs and trough-mouth fans off Blosseville Kyst and Scoresby Sund denote ice-sheet growth with ice streams occasionally reaching the palaeo-shelf edge (Fig. 2). This glacial intensification coincided with the first large-scale glaciation reaching to the palaeo-shelf edge along the south-western Greenland margin (Nielsen & Kuijpers 2013).

During the middle Pliocene (3.65–2.90 Ma), the seismic-stratigraphic analysis denotes a period of glacial retreat along the central East Greenland margin. As the ice retreated, the oceanic current took over the control of the depositional environment, indicated by a predominance of current-generated wavy facies. The observed glacial retreat is coeval with the global Mid-Pliocene Warmth (3.3–3.0 Ma; e.g. Robinson 2009) and a supposed enhancement of the EGC along the East Greenland Margin (e.g. Raymo *et al.* 1996).

Thick trough-mouth fan deposits led to a major oceanward advance of the shelf edge off Scoresby Sund, providing evidence of multiple cross-shelf glaciations during the Quaternary (Fig. 2). The ice-sheet extension was largest during latest Pliocene – earliest Pleistocene (2.90–2.33 Ma), revealing a slightly older age for the onset of margin progradation off central East Greenland than observed farther north off North-East Greenland (*c.* 76°N), where the first margin progradation began *c.* 2.5 Ma (Berger & Jokat 2009). The large progradation of the central East Greenland margin coincided with the proposed onset of major Northern Hemisphere cooling at 2.7 Ma (e.g. Bailey *et al.* 2013) and the suggested full-scale glaciation of Greenland at 2.9 Ma (Sarnthein *et al.* 2009).

In addition to the cross-shelf troughs off Blosseville Kyst and Scoresby Sund, grounding-zone wedges are identified on the shelf off Liverpool Land within the Quaternary sequences, providing evidence of steady, grounded ice. Thus, repeated glacial advances over the shelf, occasionally reaching the shelf edge, are inferred along the entire central East Greenland margin during the Quaternary (Fig. 2).

However, the study of glacigenic debris-flow deposits observed on the high-resolution dataset of the Liverpool Land margin (Fig. 1) indicates that the Quaternary glacial advances to the shelf edge were not synchronous along the margin. The glacigenic debris-flow deposits identified within the early Pleistocene sequences in the southern part of the Liverpool Land dataset suggest a distal downslope input from the Scoresby Sund ice stream, in agreement with higher sediment supply to the north of the Scoresby Sund trough-mouth fan between 1.77 and 0.78 Ma (Laberg *et al.* 2013).

An upward increase of glacigenic debris-flow deposits within the upper seismic section indicates an intensification of glacial control on the sedimentation during the middle Pleistocene. This scenario matches the increase in global ice volume that accompanied the Mid-Pleistocene transition *c.* 0.9–0.8 Ma (Head & Gibbard 2005) and gave rise to the growth of larger ice sheets in the Northern Hemisphere (e.g. Dowdeswell *et al.* 1997; Stokes *et al.* 2016). The internal distribution of the middle Pleistocene glacigenic debris-flow deposits points to a changing sediment source through time. Whereas the oldest glacigenic debris-flow deposits are most abundant in the southern part of the Liverpool Land area, pointing to an ice-stream source in Scoresby Sund, the youngest glacigenic debris-flow deposits are more abundant in the northern part of the study area and thus are likely feed by an ice stream from Kong Oscar Fjord (Fig. 2). This northern-sourced pattern continued during the latest Pleistocene and Holocene, in agreement with the presence of ice-rafted debris trapped inside Scoresby Sund during the last 10 ka (Stein *et al.* 1993) and the southward-pointing, cross-shelf trough off this fjord observed in the present-day seafloor (Dowdeswell *et al.* 1997). Farther north, moraines related to the maximum extent of the Greenland ice sheet during the Last Glacial Maximum have been identified off Kejser Franz Joseph Fjord (Evans *et al.* 2002).

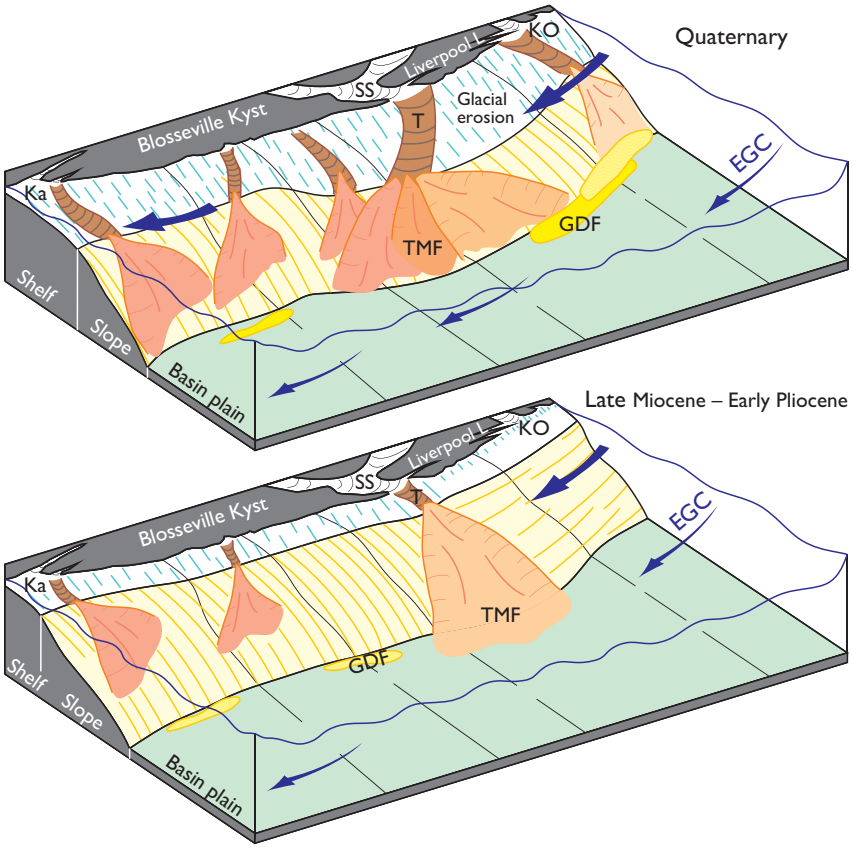

Fig. 2. 3D sketch of the central East Greenland Margin development during the late Miocene – early Pliocene and the Quaternary showing the main morphological features and key depositional processes. Within the same age range, darker colours represent older processes or deposits. **T**: trough. **TMF**: trough-mouth fan. **GDF**: glacigenic debris-flow deposit. Blue lines on shelf: predominantly glacial erosion. Orange lines on slope: predominantly progradation. Blue arrows: **EGC**: East Greenland Current. **Ka**: Kangerlussuaq. **SS**: Scoresby Sund. **KO**: Kong Oscar Fjord.

Concluding remarks

Our data indicate an early cross-shelf glaciation off Blosseville Kyst during the late Miocene and early Pliocene followed by major cross-shelf glaciations off Scoresby Sund during the early Quaternary and off Liverpool Land in the late Quaternary. Higher resolution of the Quaternary data off Liverpool Land indicates that the activity of the Scoresby Sund ice-stream system was gradually taken over by the Kong Oscar Fjord ice-stream system during the Pleistocene. Overall, our study reveals an asynchronous growth of the ice sheet across the shelf, with a marked northward progradation of ice-stream activity from the late Miocene to the Present along the central East Greenland margin.

Acknowledgements

The research leading to these results received funding from the People Programme (Marie Curie Actions) of the EU FP7 programme FP7/2007-2013/ under REA grant agreement no. 317217. The research forms part of the GLANAM (GLAciated North Atlantic Margins) Initial Training Network. For further information on the GLANAM project visit www.glanam.org.

References

Bailey, I., Hole, G.M., Foster, G.L., Wilson, P.A., Storey, C.D., Trueman, C.N. & Raymo, M.E. 2013: An alternative suggestion for the Pliocene onset of major northern hemisphere glaciation based on the geochemical provenance of North Atlantic Ocean ice-rafted debris. Quaternary Science Reviews **75**, 181–194.

Batchelor, C.L. & Dowdeswell, J.A. 2014: The physiography of High Arctic cross-shelf troughs. Quaternary Science Reviews **92**, 68–96.

Berger, D. & Jokat, W. 2009: Sediment deposition in the northern basins of the North Atlantic and characteristic variations in shelf sedimentation along the East Greenland margin. Marine and Petroleum Geology **26**, 1321–1337.

De Schepper, S., Schreck, M., Beck, K.M., Matthiessen, J., Fahl, K. & Mangerud, G. 2015: Early Pliocene onset of modern Nordic Seas circulation related to ocean gateway changes. Nature Communications **6**, 8659, *http://dx.doi.org/10.1038/ncomms9659*

Døssing, A., Japsen, P., Watts, A.B., Nielsen, T., Jokat, W., Thybo, H. & Dahl–Jensen, T. 2016: Miocene uplift of the NE Greenland margin linked to plate tectonics: Seismic evidence from the Greenland Fracture Zone, NE Atlantic. Tectonics **35**, 257–282.

Dowdeswell, J.A. & Fugelli, E.M.G. 2012: The seismic architecture and geometry of grounding-zone wedges formed at the marine margins of past ice sheets. Geological Society of America Bulletin **124**, 1750–1761.

Dowdeswell, J.A., Kenyon, N.H. & Laberg, J.S. 1997: The glacier-influenced Scoresby Sund Fan, East Greenland continental margin: evidence from GLORIA and 3.5 kHz records. Marine Geology **143**, 207–221.

Evans, J., Dowdeswell, J.A., Grobe, H., Niessen, F., Stein, R., Hubberten, H.W. & Whittington, R.J. 2002: Late Quaternary sedimentation in Kejser Franz Joseph Fjord and the continental margin of East Greenland. Geological Society Special Publications (London) **203**, 149–179.

Head, M.J. & Gibbard, P.L. 2005: Early-Middle Pleistocene transitions: an overview and recommendation for the defining boundary. Geological Society Special Publications (London) **247**, 1–18.

Jakobsson, M. *et al.* 2012: The international bathymetric chart of the Arctic Ocean (IBCAO) Version 3.0. Geophysical Research Letters **39**, L12609.

Laberg, J.S., Forwick, M., Husum, K. & Nielsen, T. 2013: A re-evaluation of the Pleistocene behavior of the Scoresby Sund sector of the Greenland Ice Sheet. Geology **41**, 1231–1234.

Nielsen, T. & Kuijpers, A. 2013: Only 5 southern Greenland shelf edge glaciations since the early Pliocene. Scientific reports **3**, 1875.

Parnell-Turner, R., White, N.J., McCave, I.N., Henstock, T.J., Murton, B. & Jones, S.M. 2015: Architecture of North Atlantic contourite drifts modified by transient circulation of the Icelandic mantle plume. Geochemistry, Geophysics, Geosystems **16**, 3414–3435.

Raymo, M.E., Grant, B., Horowitz, M. & Rau, G.H. 1996: Mid-Pliocene warmth: stronger greenhouse and stronger conveyor. Marine Micropaleontology **27**, 313–326.

Robinson, M.M. 2009: New quantitative evidence of extreme warmth in the Pliocene Arctic. Stratigraphy **6**, 265–276.

Sarnthein, M., Bartoli, G., Prange, M., Schmittner, A., Schneider, B., Weinelt, M., Andersen, N. & Garbe-Schönberg, D. 2009: Mid-Pliocene shifts in ocean overturning circulation and the onset of Quaternary-style climates. Climate of the Past Discussions **5**, 269–283.

Stein, R., Grobe, H., Hubberten, H., Marienfeld, P. & Nam, S. 1993: Latest Pleistocene to Holocene changes in glaciomarine sedimentation in Scoresby Sund and along the adjacent East Greenland Continental Margin: preliminary results. Geo-Marine Letters **13**, 9–16.

Stokes, C.R., Margold, M., Clark, C.D. & Tarasov, L. 2016: Ice stream activity scaled to ice sheet volume during Laurentide Ice Sheet deglaciation. Nature **530**, 322–326.

Thiede, J., Jessen, C., Knutz, P., Kuijpers, A., Mikkelsen, N., Nørgaard-Pedersen, N. & Spielhagen, R.F. 2010: Millions of years of Greenland ice sheet history recorded in ocean sediments. Polarforschung **80**, 141–159.

Våge, K., Pickart, R.S., Spall, M.A., Moore, G.W.K., Valdimarsson, H., Torres, D.J., Erofeeva, S.Y. & Nilsen, J.E.Ø. 2013: Revised circulation scheme north of the Denmark Strait. Deep Sea Research Part I. Oceanographic Research Papers **79**, 20–39.

Authors' address

Geological Survey of Denmark and Greenland, Øster Voldgade 10, DK-1350 Copenhagen K, Denmark; E-mail: *lfp@geus.dk*

The rescue of seismic field data from exploration activities in the Danish North Sea

Marianne M. Hansen and Nicolai Rinds

In 2009, the Danish Energy Agency informed the Geological Survey of Denmark and Greenland (GEUS) that a new legal act (Lov om fordring/Forældelsesloven) would become effective in 2011. The new act introduced a limitation period of three years on the government's right to request data from licensees' oil and gas activities in Denmark (www.retsinformation.dk 2007), and it became the catalyst for a major change in the standard procedure for licensees' submission of seismic data related to exploration activities to GEUS. A consequence of the new legal act was that the Danish authorities would have to request data from the licensee (following the Consolidated Act of the Use of the Subsoil) from the licensee no later than three years after their generation or publication; otherwise the authorities would have no legal right to the data. It was emphasised by the Danish Energy Agency that GEUS would have to submit all requests for outstanding data to the licensees no later than 1 January 2011.

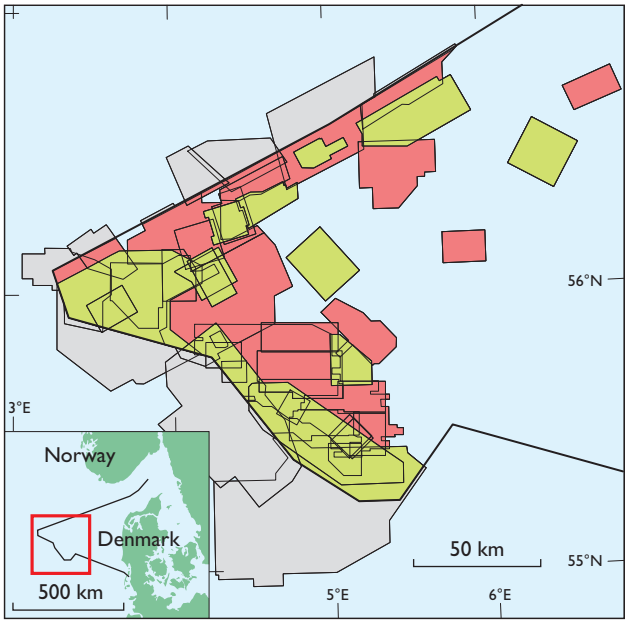

Fig. 1. 3D seismic field data status prior to the rescue project. Green polygons: field data in GEUS' archive. Red polygons: field data not in GEUS' archive. Grey polygons: parts of seismic surveys outside the Danish sector.

During the 1980s and 1990s the standard procedure for data requests from GEUS did not include pre-stack seismic data, e.g. raw field data. A search in GEUS database showed that field data had been received from only a small percentage of existing 2D and 3D surveys (Fig. 1). Being the national data bank for geological data, GEUS had to respond to this risk of losing access to valuable data, and immediate action was needed.

The National Well Data and Subsurface Archives

GEUS and its Danish predecessor the Geological Survey of Denmark (DGU) have systematically collected and stored geological data from Denmark for more than a 100 years. The idea of establishing a national data bank for geological data arose in the 1920s when Danish law made it mandatory for everyone drilling in search for water to register certain geological information encountered during drilling and deliver it to DGU. The Well Data Archive was established in 1926 to fulfil this purpose (Troelstrup 1992). The search for oil in Denmark began onshore in 1935. Until the beginning of the 1980s data submitted to DGU from oil and gas activities were stored in the Well Data Archive. For many years only few companies searched for oil in the Danish sector. In 1962, the Danish company A.P. Møller A/S was granted exclusive rights to explore the Danish subsoil according to the Sole Concession of 8 July 1962 (North

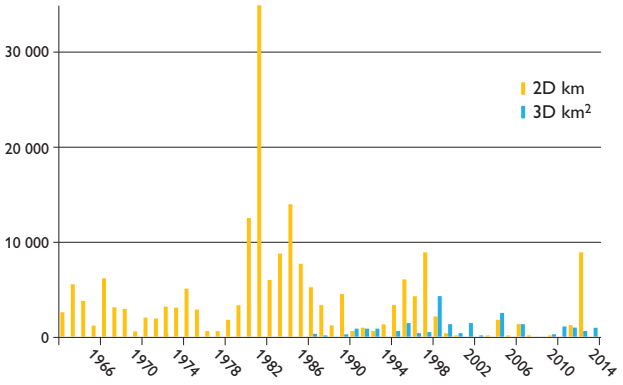

Fig. 2. Annual seismic survey activities in Denmark 1962–2014.

Sea Fund 2012). This was renegotiated in 1981, and a large concession area was relinquished. In 1984 the first competitive licensing round resulted in an increased search for oil, and the submission of data to DGU increased (Fig. 2, extracted from GEUS' database).

In the beginning of the 1980s, it was decided that a separate archive should be established – the Subsurface Archive – to store oil- and gas-related data (Kristoffersen 1995, 2017). The decision was made in order to fulfil increased requirements for a secure data environment and to control the strict confidentiality regulations applying to exploration and production data.

Data usage

Until 1980, DGU did not request digital seismic data from, the companies as part of its standard procedure. This was primarily due to the fact that only paper copies of seismic sections were used for in-house interpretation. Furthermore, space for in-house storage was very limited, and the data owners themselves were obliged to store their digital field data for a period of time and to offer the data to DGU if they decided to discard them. At that time the data were stored on vast numbers of 9-track tapes. In general, the oil companies did not use digital data either, and if such data were requested it was often on a single line basis.

By 1990, workstations had become a standard tool for interpretation and geophysical mapping in the oil industry, and access to the digital data became necessary. Therefore digital processed seismic data were added to DGU's standard data request, but their handling was a huge and time-consuming task. Licensees or companies were asked only to submit specific digital seismic data when they were needed for in-house interpretation, or if a specific request arrived from an external customer. As a consequence, DGU did not have a complete collection of digital processed seismic data at the time.

Until the 1990s, most of the seismic field data submitted to DGU came from relinquished or expired licences. In these cases, the data holders could decide to keep the seismic field data themselves or offer the data to DGU. Although the authorities have always been able to request copies of the seismic field data this was not listed as a mandatory requirement until 2002 (Danish Energy Agency 2002).

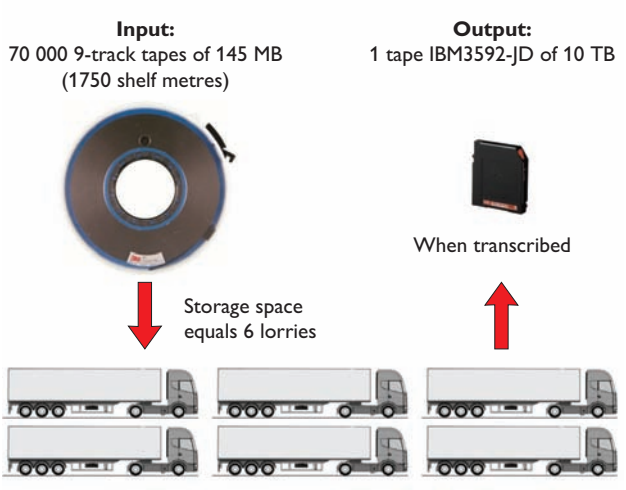

Fig. 3. Space reduction with the use of modern tapes media. Source: OvationData 2017.

Data media and volumes

The development of 3D data acquisition methods in the late 1980s resulted in an increasing amount of tapes being submitted to DGU. During the last 20 years, digital seismic data have regularly been submitted to the Subsurface Archive and maintenance of these data has been a constant challenge. The long-term use of the digital data can only be secured by keeping the data from degrading, by rewinding the 9-track tapes or transcribing the data to a new media on a regular basis.

The oil industry has frequently changed their 'standard tape media', in order to secure the very expensive collected data and to reduce the storage space needed on board vessels and in archives. The most commonly used storage medium in the 1980s and 1990s was 9-track tapes. In the mid-1990s, more compact types appeared such as Exabyte, DAT and various versions of IBM tapes, which were smaller and could contain much more data per volume. This had a tremendous impact on the number of shelf metres needed for storage. For instance, one modern IBM3592-JD tape contains the same amount of data as 70 000 high-capacity 9-track tapes, which would require 1750 archive shelf metres (Fig. 3).

Fig. 4. Seismic data and tape drives at GEUS.

Over time, GEUS has purchased various kinds of tape drives to be able to read the data and (on a small scale) make backup copies. In 2000, the Subsurface Archive contained data stored on up to 10 different tape media types, but mostly on *c.* 15 000 9-track tapes, including both seismic and well data, as well as data acquired in Greenland waters. The archive also contained 3000 Exabyte, DAT and LTO tapes and 5000 IBM tapes of various kinds.

At GEUS tape copying is considered a specialist job since up-to-date equipment and specialised treatment of deteriorating 9-track tapes are required, and the task is very time consuming, expensive and never-ending. Furthermore, vintage tape drives are difficult to maintain and acquisition of spare parts almost impossible. Since 2002, GEUS has used an external company for all tape copying jobs. A few in-house tape drives are still being used and maintained for internal purposes (Fig. 4).

The data rescue project

After GEUS was made aware of the new Act and its consequences, it was decided in 2010 to start a project to rescue older seismic field data. The aim was to rescue i.e. locate, receive and store either the original or a copy of the seismic data from all oil- and gas-related activities in Denmark. The plan was within the first year to contact all companies which had been operators or had acquired data in the Danish sector between 1980 and 1999. The plan for the following two years was to perform quality control of the submitted data, with completion of the project within three years.

The following priorities were set up: field data were considered more important than processed data. 3D data were considered more valuable than 2D data. Finally, onshore 2D data were considered more important than offshore 2D data, and data acquired from 1990 to 2000 were considered to be more valuable than older data. A search in GEUS' database showed that almost no field data from before 1995 had been received, and that some field data had been received between 1995 and 2002.

Worst-case scenario

A worst-case scenario in terms of expenditure and workload for GEUS was considered, assuming that all the companies chose to give up all their original field tapes and submit them to GEUS. It might be expected from the age distribution that most data might still be stored on the original 9-track tapes. If GEUS had to accept these directly, the Subsurface Archive would need large additional resources to cover the costs of external storage or for transcription to an in-house, modern storage medium. A rough calculation showed that if all the missing field data were submitted, GEUS could receive more than 190 000 tapes, out of which 170 000 were likely to be 9-track tapes. The cost of transcription was estimated to *c.* DKK 23 million (Table 1). Alternatively, if all the 170 000 9-track tapes were to be stored in-house the Subsurface Archive would need 4350 additional shelf metres.

Table 1. Estimated copying cost – worst-case scenario†

Survey type	Total km in Denmark	No. of tapes	DKK per tape	DKK total
2D	3405	3405	140	476 700
3D	156 234	156 234	140	21 872 760
Total cost				22 349 460

†Assuming: All field data from 1995 and earlier are located. All data are stored on 9-track tapes. Data are 60-fold. There is 1 km of data per tape.

After making a list of 2D and 3D surveys from which the seismic field data had not been submitted, a priority list consisting of 48 3D surveys and 40 2D surveys was made. The next step was to contact the companies involved, but it proved difficult to locate some of the companies and relevant contact persons. In 2002, GEUS had sent requests for data to all licensees in the Danish sector, typically to the company headquarters without a specific contact person. The outcome of this campaign was unfortunately almost

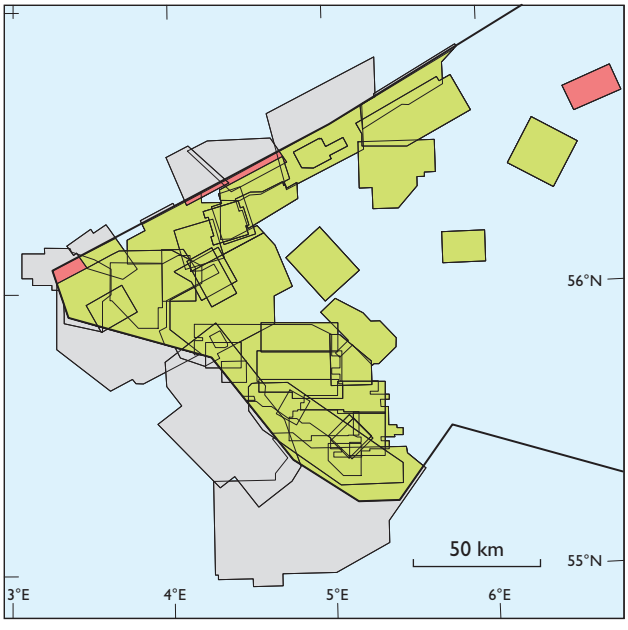

Fig. 5. 3D field data status after the rescue project. For location and polygon colours, please see Fig. 1.

nill. The oil industry is a rapidly changing business, and some of the companies which had been active in the Danish sector in the 1970s or 1980s no longer existed or had been taken over by or merged with other companies. Keeping track of a company can be strenuous and time consuming, and the subsequent search for a relevant contact person was even more difficult.

Results and achievements

As part of the data rescue project, 17 companies were contacted during 2010 and 2011. In general their responses to locate and deliver the missing data have been positive and cooperative. The project benefitted from the fact that two of the older oil companies are still operating in the Danish sector, since both Mærsk Olie og Gas A/S (Mærsk) and DONG Energy E&P A/S (DONG) have been in charge of, or involved in, data acquisition for many years. The most time-consuming part of this project turned out to be the quality control of the received data due to insufficient documentation, e.g. erroneous transmittals or missing acquisition and processing reports.

The recovery process was initiated in 2010 by meetings with the two companies, whereby a large number of surveys from the priority list could be ticked off, and the focus then shifted towards contacting the owners of the remaining data.

Mærsk and DONG decided to transcribe their original data themselves to modern media types. Given the large quantities of data and tapes, this task was very time consuming. It took several years before the copying jobs were finalised and tapes could be submitted to GEUS, but it had the benefit that GEUS received all data on modern media types (IBM 3592 tapes or USB disks). Initially, high-priority 3D field data from 34 of the 48 3D surveys on GEUS' priority list were missing; to date GEUS has located 82% of the missing surveys and received data from 74% of them (Fig. 5). GEUS has also received some missing processed data. Because of the above-mentioned complications, the recovery project lasted six years instead of the anticipated three, with a time consumption of *c*. 1600 man hours at GEUS. Over a six-year period GEUS has spent *c*. 1 million DKK on external copying.

Lessons learnt and conclusions

In hindsight, the timing of the rescue project was optimal. Between 2010 and 2014 the world experienced high oil prices (www.macrotrends.net 2017), which is likely to have encouraged the oil companies, especially Mærsk and DONG, to transcribe their original field tapes to modern media. The companies took the opportunity to recover their vintage data and thereby also save future storage costs. If the project was to be started today, the companies might have had other priorities and it might not have been possible for GEUS to keep the copying costs at a relatively low level compared to the worst-case scenario.

To rescue seismic field data is both a cumbersome and potentially expensive task. However, seismic field data represent a valuable asset for evaluation of the hydrocarbon potential of a given area. New companies in the Danish sector, especially smaller companies, commonly request field data from both 2D and 3D seismic surveys in order to reprocess existing data prior to committing themselves to acquisition of new seismic data. The access time to the field data is optimised, since the rescue project has provided GEUS with most of the field data requested by the companies. The data can also be used in future scientific studies. It is therefore an important task for a geological survey like GEUS to secure these data by making it a high priority to request and secure all data which are acquired from the Danish subsurface.

References

Danish Energy Agency 2002: Danish Executive Order No. 56 of February 4, 2002 Executive Order on Submission of Samples and Other Information about the Danish Subsoil. Danish Executive Order No. 56. [Unofficial translation]. *https://ens.dk/sites/ens.dk/files/OlieGas/submission_samples_other_info_danish_subsoil.pdf*

Kristoffersen, F.N. 1995: DGU's undergrundsarkiver [DGU's Subsurface archives]. In: Binzer, K. (ed.): Annual report 1994. Copenhagen: Geological Survey of Denmark, 102–105 [in Danish].

Kristoffersen, F.N. 2017: Undergrundsarkiv - fra kaos til moderne databank [The Subsurface Archive – From chaos to modern data bank]. Hundested, 1 p. [Unpublished report in Danish].

North Sea Fund 2012: Brief History of Danish Oil & Gas Exploration 1984 – 2011 – Licensing Rounds 1–6. Renewed Interest in Hydrocarbon Exploration in Denmark. Ahead of the 7th Round in 2013, 14 pp.

Troelstrup, S. 1992: The national geological databank. In: Binzer, K. (ed.): Annual report 1991. Copenhagen: Geological Survey of Denmark, 45–47.

www.macrotrends.net 2017: *http://www.macrotrends.net/2516/wti-crude-oil-prices-10-year-daily-chart*

www. retsinformation.dk 2007: LOV nr 522 af 06/06/2007 (Forældelsesloven) – Historisk. *https://www.retsinformation.dk/Forms/R0710.aspx?id=2655* [in Danish – no translation available].

Authors' address

Geological Survey of Denmark and Greenland, Øster Voldgade 10, DK-1350 Copenhagen K, Denmark. E-mail: *mmh@geus.dk*.

An integrated public information system for geology, groundwater and drinking water in Denmark

Martin Hansen and Charlotte Toftemann Thomsen

Denmark has a long tradition for having central geological databases, including a systematic collection and storage of geological and hydrological information from all surficial boreholes which was initiated in 1926. Since the mid-1970s such data have been stored digitally. A large variety of users access a central Danish, geological database: the public, for information about their local drinking water quality, environmental employees in municipalities, regions and the state for using, entering and updating data as well as consultants and drilling companies working for public administration and local water works.

The local Danish administrative system previously consisted of 14 counties and 248 municipalities. The counties were responsible for groundwater mapping, drinking water management and activities concerning contaminated soil, as well as for harmonisation and transfer of data to the central database. With effect from 1 January 2007, this administrative system was replaced by five regions, seven environmental centres and 98 municipalities, which required major changes in the administrative handling of borehole data at the local and regional levels. For this, a public and shared central database was established and a countrywide harmonisation of data, transfer and storage was initiated and all geological, groundwater and drinking water data were transferred to this central database at Geological Survey of Denmark and Greenland (GEUS).

In an updated database system, public authorities were set up to access the central database to store their relevant borehole data and almost all data were made publicly available. The database is maintained by GEUS. It is directly connected to other public databases at GEUS including the shallow geophysical database GERDA, where e.g. borehole loggings are stored, and to the Model Database where simple geological models are stored (Fig. 1).

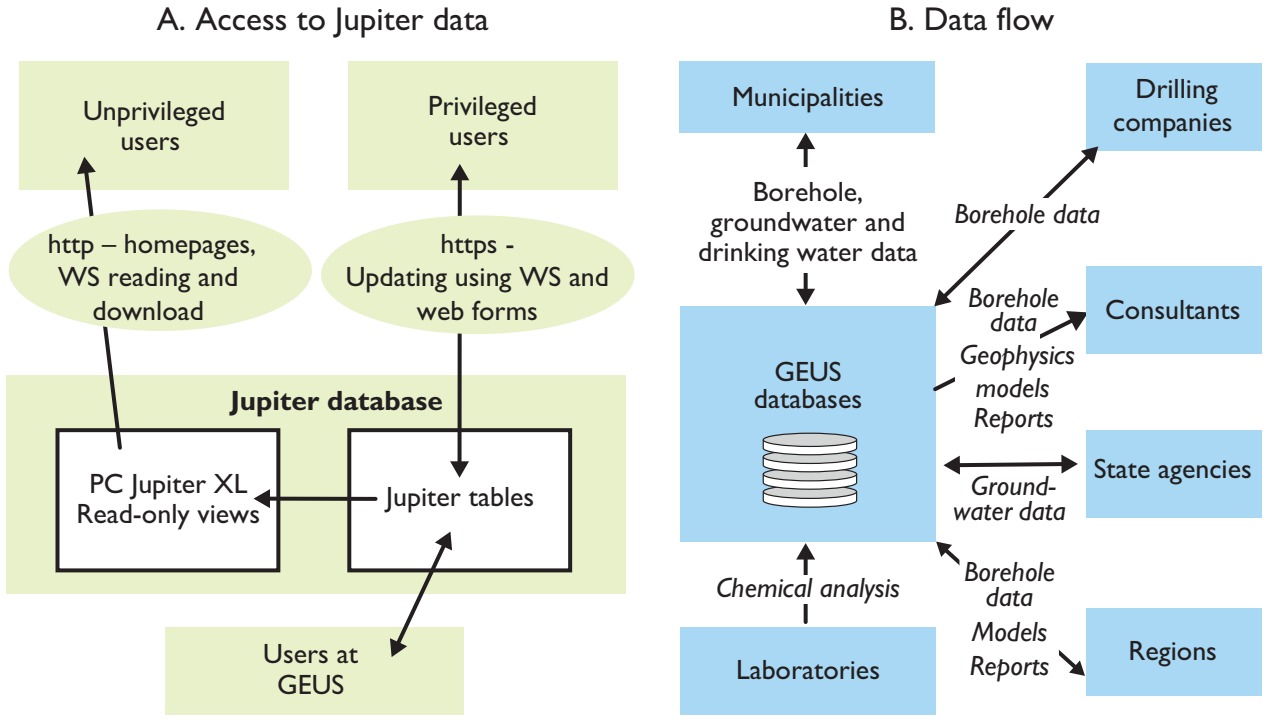

Fig. 1. Diagram showing **A**: The access to data in the Jupiter database from different users and **B**: How data flow to and from the database. **WS**: web services.

Table 1. User roles and privileges

Name of user role	Privileges and use
Laboratory	For entering and editing samples and chemical analyses. For laboratories to add data to the system.
Borehole write	For entering and editing information about boreholes including location, geology/lithology and borehole construction. For consultants and local authorities to enter new boreholes.
Borehole read	For reading publicly available data about boreholes, water, soil and air samples and analysis.
Drinking water approval	For approving new drinking water samples with analyses. For users from the authorities to quality control new drinking water data and by approving the data, making them publicly available.
Groundwater approval	For approving new groundwater samples with analysis. For users from the authorities to quality control the new groundwater data and by approving the data, making them publicly available.
Water level	For entering and editing water-level measurements. For users from the authorities to enter and edit water-level measurements.
Sample approval	For approving new water, soil and air samples with analyses from surface samples. For users from the authorities to quality control the new water, soil and air analyses from surface samples and by approving the data, making them publicly available.
Water resources	For entering and updating information about water works. These data include water well fields, treatment plants, permits, annual volumes of extracted water, sampling sites and volumes of water shared between different water works. For the municipalities that survey the drinking water to create and update their drinking water structure.

This updated system is used by the municipalities to manage their water supply data (e.g. water supply structure, permits, groundwater and drinking water quality data), by state agencies to manage groundwater data from the groundwater mapping and by the regions to maintain their soil pollution data. The system has gradually been expanded since 2007 and now local authorities can store and maintain a wide range of their own data in the central database.

The database system

The database system currently consists of the following components:

1. A central database;
2. A public data model, agreed upon by a committee under the The Danish Natural Environment Portal;
3. A user-management system, managed by the The Danish Natural Environment Portal, providing direct access to the central database;
4. A suite of Simple Object Access Protocol (SOAP) web services – an interface that allows computer-to-computer communication. This enables local authorities to manage their own data in the central database through their own applications;
5. Applications that can access the database utilising the components above.

The central database

The central database is based on GEUS' Jupiter database and run on an Oracle database. It has been under development during the last 40 years. The extensions made since 2007 include full public online access to read data and write access for public authorities to almost all data types. The public part of the database is made available through a view layer exposing the public data model.

The public data model

The public data model can handle:

- Borehole data, including: localisation and administrative data, construction data, abandon data, geological description using common methodology, hydraulic head measurements, samples and analyses from soil, water and air;
- Surface soil and water sample data;
- Water supply data for water plants, agriculture and industry, including: extractions wells, well fields, water treatment plants, extraction permits, water quality data, water extraction, water use data, exchange of water between water works, ownership and contact persons;
- Soil pollution data: projects; soil, water and air chemistry data from boreholes, surface samples and remediation plants.

The data model is being developed and maintained by GEUS, but all extensions and alterations have to be agreed upon by the Groundwater Group under the Danish Natural Environment Portal (DNEP). This is a common public partnership between the Ministry of Environment and Food of Denmark (45%), the Danish municipalities (45%) and the Danish Regions (10%), and it acts as an independent portal across boundaries of authority. Its major goal is to ensure continued access to harmonised, updated, natural environmental data. The Groundwater Group itself consists of members appointed by the municipalities,

the Danish Environmental Protection Agency , the Danish Regions, DNEP and GEUS. The public data model consists of more than 90 data tables.

Data responsibility agreement

The data responsibility agreement determines which organisations are responsible for producing and maintaining which data, and for making the data available to the public. The various responsibilities are defined partly by legislation and partly through agreements signed by the participating partners and by voluntary reporting. At any time, any data set in the public database has one and only one responsible owner organisation.

Data ownership

The ownership of data can be defined either by the user who enters the data or by the location of the data point. In this way, the municipality or region in question, a state agency and GEUS can own water-level measurements in the same well. Each data owner is responsible for entering their own data and secure their quality.

The analysing laboratory carrying out the quality control of drinking water is responsible for entering its data, and it owns the data until the data entry and quality control have been completed. After this step, the ownership is transferred to the municipality to which the water works belongs. The municipality has to release the data before it becomes publicly available. Apart from quality control of the data sets, the new owner cannot alter the data. If errors are found during the quality control, the municipality must reject the water sample and all of its analyses, and the laboratory has to resubmit a corrected data set.

User management

The Danish Natural Environment Portal has a central user-management system which enables the user to use the same login credentials to access and update data in different systems. The users and their rights are managed locally by user administrators who define the user rights through a set of roles. Each role defines to which part of the database the user shall have access. In this way it is the local administrator who decides who should be allowed to access the different public systems or obtain privileges to enter and edit data. The different roles in the Jupiter system are presented in Table 1. In addition to these roles, the system gives the users access to data according to their geographical location. For example, all users can access water works

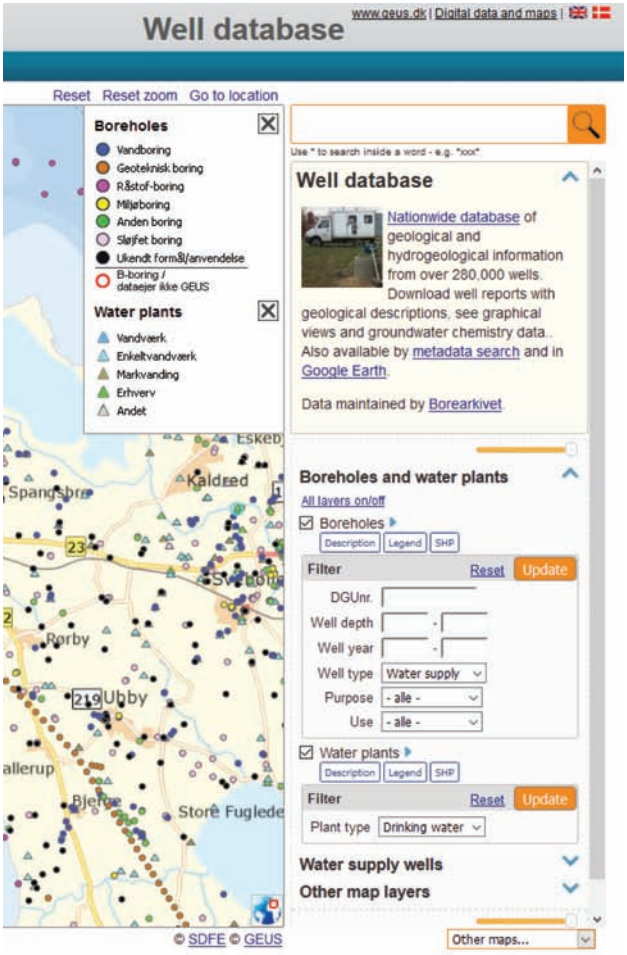

Fig. 2. Screen shot from the web map interfaces to Jupiter showing boreholes and water plants from central Sjælland.

but only users from the municipality, where the water works is situated, can update the information (provided the user has the right role).

Data interface

The data are available in several ways. Most of the data are available through:

Jupiter's homepage: This entry is read-only and mainly used by municipalities and members of the public to look up specific data (Fig. 2).

SOAP web services: These services give read-and-write access to different parts of the data model and have been under development since 2007. With this interface private companies can write applications for administrative units for their data management. These services constitute

the main entry outside GEUS for update of data. See for example: *http://webs.geus.dk/miljoeportal.groundwater.boring.2.0.0/B-Boring?wsdl* for updating borehole data.

WMS/WFS: Several of the data themes are exposed through web map services (WMS) and web feature services (WFS). Web map services deliver maps as bitmaps while web feature services can deliver the same data as geographical objects (point, lines and polygons) that can be used for spatial queries in a GIS. These are used to support the map interface on the Jupiter homepage, are available for end users, and can also be imported into local GIS. These services are used mainly in systems made for the different administrating units. See for example the WMS publishing borehole information *http://data.geus.dk/geusmap/ows/25832.jsp?SERVICE=WMS&VERSION=1.1.1&REQUEST=GetCapabilities&LAYERS=jupiter_boringer_ws%2cjupiter_anlaeg_ws*

Database download: Advanced users can download data as database exports. In this way it is possible to export all available data to a local hard drive (excluding water quality control data not yet approved by the data owner and information about owners and contact persons). This function is meant for advanced users for e.g. geological modelling or complex calculations on groundwater chemistry. It is even possible to install a scheduled application that keeps the local database updated on a nightly basis with changes made in the central database. Such local copies of the database are mainly used by consulting companies and large administrative units.

Discussion and conclusions

Nearly all data in the database must be publicly available. Therefore, the access has been divided into two packages of services since the first version of the Web Services was developed up to January 2007. One set contains all the read-only functionality without any user management systems, while the other package contains functions for updating the data. However, due to very frequent use the read-only services will have to be revised in the near future. Not all users comply with the rules set up for the use of the services, and since they are anonymous, it is difficult to identify those who break the rules. For example, users are not allowed to use the services in batch mode or create a local copy of the database.

We can, however, see from the logs, that one or more read-only users behind a single ip-address make up to tens of thousands of calls on a daily basis and thus obviously do not comply with the rules set-up for the services. An increase from *c.* 200 000 to 12 000 000 calls per month in the last few years causes a heavy and increasing system load. If a login with user name and password was to be required to enter the read-only services, it would be possible to contact directly the users who use software that does not comply with the rules of use. The access would still be free of charge.

A public, shared database like Jupiter gives access to a very broad use, where the data can be combined with other public data or with private, non-public data. Also the many different ways in which the data are available, such as web, web GIS, different types of web services or download in database format, make the data highly usable. The user gets a coherent dataset containing geology, groundwater and drinking water data, where the water can be followed all the way from the borehole to the water plant. In recent years, the database has been used for analysis of public health in combination with drinking water quality. The free access to the publicly available data has greatly increased the value of the data. The authors do not know of any other publicly available, combined geology – groundwater – drinking water database systems like Jupiter. As the system is based on a data model that has been agreed upon between different stakeholders from municipalities, regions, state agencies and the geological survey, the model can most probably be used as a good starting point for development of similar systems by other organisations and countries.

References

Gerda database: *http://data.geus.dk/geusmap/?lang=en&mapname=gerda#layers=gerda_projects%2cgerda_data*

Jupiter database: *http://data.geus.dk/geusmap/?mapname=jupiter&lang=en*

SAML 2.0: *https://en.wikipedia.org/wiki/SAML_2.0*

SOAP web services: *https://en.wikipedia.org/wiki/SOAP*

The Danish Natural Environment Portal: *http://www.miljoeportal.dk/English/Sider/default.aspx*

The Model Database: *http://data.geus.dk/geusmap/?lang=en&mapname=modeldb*

Authors' address:

Geological Survey of Denmark and Greenland, Øster Voldgade 10, DK-1350 Copenhagen K, Denmark. E-mail: *mh@geus.dk*

Arctic geopolitics and the beginning of earthquake monitoring in Denmark and Greenland

A. Lif Lund Jacobsen

Where there scientific or political reasons behind Denmark's decision to establish its first seismological stations for earthquake monitoring? In a nation where earthquakes are few and of small magnitude, it is remarkable that since 1927 the Geological Survey of Denmark and Greenland (GEUS), and its predecessors back to the Danish Geodetic Institute have recorded seismological events from permanent stations in Denmark and Greenland and shared data through international data centres.

As early as 1907, on private initiative by E.G. Harboe, a seismological station was established in Godhavn, West Greenland (Harboe 1911). However, with time it became clear that the phase readings from the instruments lacked precision (Fig. 1), and in 1912 monitoring was discontinued due to lack of funding (Geodætisk Institut 1978). Having never officially joined the International Seismological Association, or suffered destructive earthquake within their territory, Danish authorities did not at the time have any vested interest in operating expensive seismological stations.

The origins of Denmark's seismological monitoring programme

Historians of science have argued that scientific knowledge of Greenland equalled sovereignty (Ries 2012; Doel *et al*. 2016). Inspired by their approach, I suggest that theformation of a network of Danish and Greenlandic seismological stations could be understood as an expression of national geopolitical strategy rather than a display of scientific vigour. By examining historical records from public institutions like the Ministry of Education, Ministry of Foreign Affairs, Ministry of War and the Danish Geodetic Institute as well as letters from Erik Nørlund and Inge Lehmann, kept at the Danish National Archives and GEUS, it is possible to assess to what degree geopolitical considerations were a factor in establishing a seismological monitoring programme in Denmark.

Fig. 1. Seismograms from the old station in Godhavn kept at GEUS. These seismograms from 1907–1912 are among the oldest seismological records in existence. Photo: Danish National Archives.

In 1923, Denmark became a full member of the International Union of Geodesy and Geophysics (IUGG), but it was not until October 1924 after the second IUGG General Assembly in Madrid that (lack of) seismological monitoring from its territory became an issue for Denmark. Before the Assembly, a national committee for seismology had hastily been formed under the leadership of Niels Erik Nørlund, professor of mathematics at Copenhagen University and director of the Danish Geodetic Service (*Den Danske Gradmaaling*). After the Assembly, Nørlund reported to the Ministry of Education that there had been considerable pressure on Denmark to record and share geophysical data from Greenland. So substantial was the pressure that Nørlund warned that unless Denmark initiated a programme of general geodetic research, in particular seismological monitoring and international data sharing, other nations would question Denmark's authority in Greenland (Danish National Archives (DNA) 1).

It was a potent threat, since the Danish government rightfully feared that their claim to sovereignty over Greenland could be contested by their neighbours. For example, a stipulation of the 1917-treaty between Denmark and the USA regarding the sale of the West Indies to the USA was, in addition to paying DKK 25 million, that the USA also acknowledged Denmark's sovereignty over Greenland. Norway on the other hand made counterclaims to parts of eastern Greenland in 1924 and 1931 (Kragh *et al.* 2008).

Over the next months, Nørlund worked on securing support for his envisioned network of seismic stations. As

director of the Danish Geodetic Service, Nørlund was appointed to reorganise national geodesy, including triangulation efforts which traditionally had been a key interest area of the army's Department of Topography (*Generalstabens Topografiske Afdeling*). Using his position, he added seismology to the list of intended activities.

In order to secure the necessary political backing and financial support from private funds, Nørlund employed several different arguments. In addition to demonstrating sovereignty over Greenland, he argued that Denmark needed seismological stations because all cultural and refined nations in Europe had a least one. Also scientifically, seismological data constituted a valuable source of information for geodetic research. Finally, he argued that international data sharing was a means to maintain international peace and collaboration.

During the winter 1924/25, enough political and financial support was mustered that Nørlund and the Danish Geodetic Service could begin building the network.

Establishing seismological stations from 1925 to 1927

From early on, it was clear that while the Danish government was willing to authorise the construction of seismological stations, much of the funds to build stations and buy scientific instruments had to come from private donations.

In the spring of 1925, orders for a variety of different seismographs and other instruments were placed at international suppliers in England, Germany, Russia and the USA. Not knowing which seismic frequencies they could expect and at a time where no standards for performance and accuracy exsisted, orders were for state-of-the-art seismograph models of different mechanical or electrical designs. The costly instruments were all paid for by the Carlsberg Foundation which also made significant contributions towards the construction costs of the stations. In addition, Carlsberg also agreed to provide an annual grant to cover operating costs for two of the three stations, a practice that continued until the 1950s.

Without any practical knowledge about the working of seismological instruments or how they would react to the extreme climate of Greenland, it was decided that a station in Denmark should act as a testing and comparison site for the different instruments. At the same time negotiations began to secure space for stations both in Copenhagen and Greenland. Historical records show that geopolitical and strategic considerations played a significant role in where to locate the three planned stations (e.g. DNA 2).

Fig. 2. In COP's Caponiére XIII, the purely mechanical Wiechert Horizontal seismograph is still in its original location. Photo: Casper Brogaard Højer.

Being relatively close to the city, the permanent station in Copenhagen (COP) was the first to be completed. In the spring of 1925, the Army handed over two caponieres located in the old fortifications of Copenhagen (*Vestvolden*) to be used as a seismological station. Still being part of the military defense system, access to the station was restricted until well after the Second World War.

Installations began in the autumn of 1926. By 17 February 1927 all instruments were in place and monitoring began, but due to occasional failure of the timing, the working of the station was not considered satisfactory before March. Hereafter publication of the records began in a seismological bulletin. By then COP was equipped with the following seismographs: A Wiechert 1000 kg Horizontal (Fig. 2), a Wiechert 1300 kg Vertical, three Galitzin instruments (two horizontal and a vertical), a 2-component Milne-Shaw. Later a 2-component Wood-Anderson seismograph was added.

Today historical bulletins and log book from all the stations can be found at *http://seis.geus.net/seismic_service.html*. As the largest of the three seismological stations in the network, COP had a fulltime caretaker to do daily maintenance and recording, paid by the Carlsberg Foundation and living in a nearby cottage.

Establishing and installing Denmark's first permanent seismological station was not an easy task for the untrained personnel hired by Nørlund, and in recognition of their valuable contribution, Inge Lehmann and two students received a bonus worth nearly two months' salary (DNA 3). By all accounts, this was also the later so famous seismologist Inge Lehmann's first encounter with seismological work, which principles she first began to study in earnest later that year.

The station in Ivittuut (IVI), South West Greenland, was the second to be completed (Fig. 3). With the help

Fig. 3. The entrance to the seismological vault in Ivittuut is next to the old tennis court. Today (2014), the court is unkempt and Ivittuut largely deserted.

Fig. 4. Inge Lehmann (second from the left) inspects SCO presumably in the summer of 1928. Photo: From Inge Lehmann's private archive at the Danish National Archives.

of the Danish mining company *Kryolith Mine og Handelsselskabet,* a seismological vault was blasted into the bedrock about 250 m from the mine's main blasting sites (!) To determine the effect of blasting on the seismological instruments tests were made with a portable seismograph during the summer of 1926, but it was not before the summer of 1927 that the intended seismographs, a Wiechert Vertical and a Wiechert Horizontal seismograph, were installed (DNA 4). Operated, for an extra fee, by the local radio-telegraphist employed by the mining company, the station began recording on 24 August 1927 (Bulletin Ivigtut 1929).

When the third and final station in the Danish network was constructed, it became clear that that geopolitical arguments worked both ways between Arctic nations.

In September 1925, Nørlund wrote to the Danish Ministry of Foreign Affairs that the Danish Geodetic Service was considering a permanent seismological station on Jan Mayen because the island had an active volcano. It was a delicate subject since Norway's Meteorological Institute had annexed part of the island on behalf of Norway. Denmark had refused to officially state its position on the matter but maintained that some buildings within the Norwegian-claimed area were owned by Denmark. With the aid of the Ministry of Foreign Affairs, an agreement was made with Norway in March 1926 to the effect that the Danish Geodetic Service could place a station on the Norwegian part of Jan Mayen. However, shortly afterwards in July, Norway announced that their Meteorological Institute would expand its activities to the whole island and claim it on behalf of Norway (DNA 5).

In the summer of 1926, initial seismological tests were carried out on Jan Mayen by the Danish Geodetic Service, but results were poor and it was decided to establish the station at the newly founded colony of Scoresbysund (*Ittoqqortoormiit*). Founded in 1925, one of the colony's purposes was to establish a Danish presence in East Greenland where Norway also had made claims.

Construction of the station (SCO) began in the summer of 1927, also here funded by the Carlsberg Foundation. By then the Danish Geodetic Service had enough experience with construction and installation to proceed relatively quickly. A cellar was blasted into the bedrock, and on top of that a low building was constructed. To protect the instruments from variations in temperature the cellar was covered by 80 tons of rock and access restricted to a low corridor one could only crawl through. A second building housed the radio station and electronic recording instruments (Geodætisk Institut 1930).

The installation of the seismological instruments went smoothly, as the station was equipped with two Galitzin horizontal seismographs and a Galitzin vertical seismograph transferred from COP (Den Danske Gradmaaling 1928). Fully funded by the Carlsberg Foundation the station began operation on 12 January 1928, with the local radio-telegraphists in charge of daily recordings (Fig. 4). In the beginning the paper seismograms were sent annually to the Geodetic Institute by ship, but later it became practice that results from large events were radioed immediately to Copenhagen.

After 1928

In 1928 the Danish Geodetic Service and the Department of Topography of the Army General Staff (*Generalstabens Topografiske Afdeling)* merged to become the Danish Geodetic Institute (*Danmarks Geodætiske Institut).* Inge Lehmann, who had been the principal figure in setting up the Copenhagen station and analysing data from all the

stations, was appointed chief of the Geodetic Institute's new Seismic Section.

The value of the Greenlandic seismological stations as evidence of sovereignty was soon tested. In 1931, Norway claimed parts of East Greenland, Denmark opposed the claim and the matter was put to the Permanent Court of International Justice in The Hague. In preparation for the trial, the Ministry of Foreign Affairs asked the Danish Geodetic Institute to prepare a series of reports about their scientific activities in Greenland. In July 1932, Inge Lehmann forwarded a special report about the seismological station in Scoresbysund to the Ministry (DNA 5) which was submitted as part of the evidence supporting the Danish claim. In April 1933, the Court decided against Norway, recognising Danish sovereignty over all parts of Greenland.

Scientifically, the three stations also soon proved valuable by providing quality seismic records from remote, low-noise Greenland, with efforts put into timing records and adjustment of instruments in the challenging environment. It was partly data from the seismological stations in Ivittuut and Ittoqqortoormiit that in 1936 enabled Inge Lehmann to deduce the existence of the Earth's inner core (Lehmann 1936).

Today GEUS records seismological data from about 25 locations in Denmark and Greenland, including the original stations in Copenhagen, Ivittuut and Ittoqqortoormiit, now equipped with modern digital instruments.

Conclusions

Historical documents from the Danish National Archives and GEUS clearly show that international geopolitics and strategic considerations played a significant role in the location of the seismological stations. Especially Denmark's need to express its sovereignty over Greenland played a pivotal role. It was by invoking arguments of power, culture, science and international peace the director of the Danish Geodetic Service, Erik Nørlund, was able to gain the necessary political and financial support for establishing a network of seismological stations, and in 1928 establish a permanent Danish seismological monitoring authority under the Danish Geodetic Institute.

As the Danish government's main interest was the strategic value of the seismological stations, it fell to private donations to unlock the scientific potential of the stations. It was therefore the logistic support of the *Kryolith Mine og Handelsselskabet* and the long-term financial commitment of the Carlsberg Foundation that made it possible to equip and operate the stations at a high scientific standard.

Acknowledgements

This study is part of a project on Inge Lehmann and the history of modern seismology 1925–1970, funded by the Carlsberg Foundation and Danish National Archives. The author wishes to thank Trine Dahl-Jensen, Tine B. Larsen and Peter Voss for help and access to material kept at GEUS.

References

Bulletin of the Seismological Station, Ivigtut 1929. Copenhagen: Geodetic Institute, *http://seis.geus.net*

Den Danske Gradmaaling 1928: Aarsberetning 1. April 1927 – 31. marts 1928. Seismisk Arbejde, *http://seis.geus.net*

Danish National Archives (1): Niels Erik Nørlund (1885–1981): Mat. Vedr. Union Géodésique et Géophysique Int. (1924–1936). Box 116.

Danish National Archives (2): Krigsministeriet 4. kontor, Indkomne sager 1868–1950, 1895–1950. Geodætisk Institut 50.2. Box A373.

Danish National Archives (3): Niels Erik Nørlund (1885–1981): Regnskabet 1933/1934, Regnskabsmateriale vedr. Carlsbergfondet (1925–1955). Box 52.

Danish National Archives (4): Generalstabens Topografisk Afdeling (1842–1928). Vedr. etablering og drift af Seismisk Station Ivigtut, 1924–1953. Sagsarkiv (1801–1978). Box 50.

Danish National Archives (5): Geodætisk Institut. Journalsager (1925–1988): 3 1 Udenrigsministeriet 1925 – 3 1 Udenrigsministeriet 1961. Box 1.

Doel, R.E., Harper, K.C. & Heymann, M. 2016: Exploring Greenland's Secrets: Science, Technology. Diplomacy, and Cold War Planning in Global Context, 1–22. In: Doel, R.E., Harper, K.C. & Heymann, M. (eds): Exploring Greenland. Palgrave Studies in the History of Science and Technology, New York: Palgrave Macmillan.

Geodætisk Institut 1930: The seismological stations København and Scoresbysund Copenhagen: Geodetic Institute.

Geodætisk Institut. 1978: Geodætisk Institut 1928–1978. Copenhagen: Geodetic Institute.

Harboe, E.G. 1911: Das Erdbebenobservatorium auf der Disko-Insel. Leipzig: Wilhelm Engelmann, *http://seis.geus.net*

Kragh, H., Kjærgaard P.C., Nielsen N. & Nielsen K.H. 2008: Science in Denmark, a thousand-year history. Aarhus: Aarhus University Press.

Lehmann, I. 1936: P'. Publications du Bureau Central Seismologique International. Serie A: Travaux scientifique **14**, 3–31.

Ries, C.J. 2012: Armchairs, Dogsleds, Ships, and Airplanes. Field Access, Scientific Credibility, and Geological Mapping in Northern and North-Eastern Greenland 1900–1939. In: Harbsmeier, M. *et.al.* (eds): Scholars in the Field. Studies in the History of Fieldwork and Expeditions, 329–361. Aarhus: Aarhus University Press.

Author's addresses

A.L.L.J., *Danish National Archives, Rigsdagsgården 9, DK-1218 Copenhagen K, Denmark and Geological Survey of Denmark and Greenland, Øster Voldgade 10, DK-1350 Copenhagen K, Denmark*. E-mail: *LLJ@sa.dk*.